Received: 30 September 2020 | Revised: 29 December 2020 | Accepted: 5 January 2021

DOI: 10.1002/nano.202000162

REVIEW

Nano Select WILEY

Recent progress of magnetic nanoparticles in biomedical applications: A review

Muzahidul I. Anik[1] | **M. Khalid Hossain**[2,3] | **Imran Hossain**[4] | **A. M. U. B. Mahfuz**[5] | **M. Tayebur Rahman**[6] | **Isteaque Ahmed**[7]

[1] Chemical Engineering, University of Rhode Island, Kingston, Rhode Island 02881, USA

[2] Interdisciplinary Graduate School of Engineering Science, Kyushu University, Fukuoka 816–8580, Japan

[3] Atomic Energy Research Establishment, Bangladesh Atomic Energy Commission, Dhaka 1349, Bangladesh

[4] Institute for Micromanufacturing, Louisiana Tech University, Ruston, Louisiana 71270, USA

[5] Biotechnology and Genetic Engineering, University of Development Alternative, Dhaka 1209, Bangladesh

[6] Materials Science and Engineering, University of Rajshahi, Rajshahi 6205, Bangladesh

[7] Chemical Engineering, University of Cincinnati, Cincinnati, Ohio 45221, USA

Correspondence
M. Khalid Hossain, Interdisciplinary Graduate School of Engineering Science, Kyushu University, Fukuoka 816–8580, Japan.
Email: khalid@kyudai.jp; khalid.baec@gmail.com

Abstract

Magnetic nanoparticles (MNPs) offer tremendous potentialities in biomedical applications for a long while. Since these materials' interactions in biological media largely rely on their crystal structures, sizes, and shapes, detailed studies on their synthesis mechanism for medicinal aspects are crucial. Despite many review reports that have already been published on MNPs, they mainly have focused either on their perspective in biomedical applications or their synthesis and characterization along with functionalization mechanisms as individual entities. For this reason, this review uncovers a comprehensive insight into the ongoing improvement of fabrication processes, surface functionalization of MNPs for biomedical applications together. Besides, various magnetic nanocomposite (MNCs) for smart drug delivery, recent hyperthermia treatment, lab-on-a-chip, and magnetic bio-separation, and some of the recent emerging imaging techniques using MNPs are discussed. A detailed analysis of toxicity, challenges, and recent progress of clinical trials of MNPs is sketched out to open numerous entryways for advanced research on MNPs for biomedical applications.

KEYWORDS

clinical trial, CRISPR-Cas9, drug delivery, lab-on-a-chip, magnetic bioseparation, magnetic hyperthermia, toxicity of magnetic nanoparticles

1 | INTRODUCTION

Nano-platforms have been proven to be excellent agents for biomedical applications.[1–4] Of them magnetic nanoparticles (MNPs) have received increased attention due to their unique structural, behavioral, and diversified applicable attributes such as their unique magnetic properties along with tunable size, high chemical stability with enhanced surface area, functionalizable surface with different molecules, and biocompatibility with various cell types.[5,6] Furthermore, they have been applied in custom research fields due to particular aspects such as superparamagnetism, high magnetic susceptibility, and inductive magnetic moment that can be controlled using an external

magnetic field, which is crucial for immobilization near targeted physiological system.[6] Their significance has been manifested in various applications, including drug delivery systems, magnetic hyperthermia treatment, contrast agents for magnetic resonance imaging (MRI), tissue engineering, gene delivery, cell separation and selection, magnetorelaximetry, antibacterial agents, and lab-on-a-chip.[5,7–16]

The abundance of review studies and research works on MNPs proclaims their impact over the last few decades; nevertheless, there are still some uncharted areas to address further improvement. For example, there is a huge concern over the adverse consequences of MNPs on the living cells and their toxicity on physiological systems. Moreover, since the size of MNPS is influential for their prolonged circulation in the human body and letting them flow through capillary organs and tissues to avoid embolism,[6,8] all these issues open manifold doors for a more in-depth look into their synthesis and development processes. Therefore, a comprehensive review focusing on the missing yet potential aspects of MNPs will be a significant addition. This review study focuses on aspects discussing the synthesis and applications of MNPs while focusing on the challenges and possible improvements.

In this review, established methodologies of MNP synthesis along with their applicability and conveniences they provide concerning biomedical applications are explored. Discussion of syntheses certainly asks for clarification from the biocompatibility outlook, and therefore, associated materials, solvents, and functionalities are discussed. Moreover, the MNPs, especially their surface modification and properties relevant to biomedical applications, are depicted. Dedicated sections are also prepared to highlight specific biomedical applications of MNPs from different imaging techniques and lab-on-a-chip application perspectives, along with possible challenges. To be comprehensive and objective from a review point of view, we have mainly presented the associated parameters with the potential research topics such as toxicity. This review presents specific syntheses discussion and biomedical applications incompletely explored by the existent literature in a nutshell.

HIGHLIGHTS

- Studied recent development of synthesis and functionalization of magnetic nanoparticles (MNPs)
- Studied toxicity of MNPs in biomedical applications
- Reviewed current state of FDA approved MNPs in the biomedical field
- Challenges and research scope of MNPs in the biomedical field is highlighted
- Reviewed recent progress with drug delivery and gene delivery using MNPs
- Explored recent development of MNPs assisted CRISPR-Cas9 mediated gene editing
- Reviewed current state of imaging modalities such as MRI, MPI, CT, and PET

2 | SYNTHESIS OF MNPs

The synthesis of nanoparticles needs much attention during its multistep procedure. The process needs to be optimized at the early design stage of synthesis because even a small variation in the whole process can bring radical change in the desired outcome.[17] Therefore, the synthesized nanoparticle's chemical and physical properties need to be controlled strictly to ensure successful use in biomedical applications. There are different ways to synthesize magnetic nanoparticles. The particles can be made either in "top-down" or "bottom-up" approach. "top-down" method involves with high energy ball milling process of a magnetic sample until the desired nanoscale size is achieved.[18] The advantage of "top-down" method is, high number of particles can be achieved in a single batch while the disadvantage is the control over particle shape and size is compromised which is important in biomedical application.[18] "Bottom-up" method depends on starting with a salt of ferrous (Fe^{2+}) or Ferric (Fe^{3+}) ion and undergoing a different chemical process to nucleate and induce seeded growth to grow particles to the desired hydrodynamic diameter.[19] There are different "bottom-up" approaches reported in the literature.[20–22] Of them, most reported methods are co-precipitation,[23–27] hydrothermal method,[28–31] thermal decomposition method,[32–39] and polyol method.[40–43] Other methods include flow injection technique, microwave-assisted, solvothermal, sol–gel, sonochemical, chemical vapor deposition, physical vapor deposition, electrodeposition, combustion, laser pyrolysis, preparation within micelles, carbon ARC, microemulsion.[44] However, different methods have been followed to produce nanoparticle having various sizes and shapes, for example, spherical, pallet, hierarchical superstructures, nanorods, nanotubes, and so many.[17]

2.1 | Co-precipitation

The word "co-precipitation" means the process where precipitation of one or more material occurs—generally

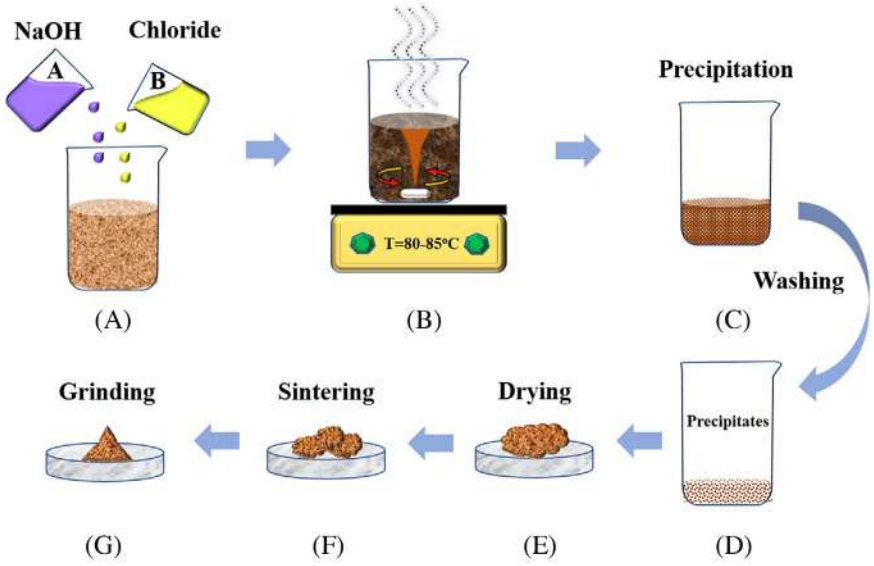

FIGURE 1 Steps to synthesize ferrite nanoparticles using co-precipitation method: (A) solution of NaOH and chloride precursors, (B) stirring at 80–85°C for 1 hour, (C) precipitation, (D) precipitates after washing, (E) drying at 80°C, (F) sintering at 1100°C, and (G) grinded final product

soluble in those particular conditions—via nucleation as well as grain growth.[45] Co-precipitated nanomaterials are widely used for various biological applications because of the easy preparation method, less harmful precursors needed, and easy application.[17] Co-precipitation is generally carried out with salt solutions and base, typically in a water medium, with or without a precipitating agent's assistance to produce insoluble solid particles.[17] Following this method, magnetic nanoparticles can be synthesized at room temperature or high temperature, resulting in high yield, various shape, and size.[46] The size and shape of synthesized nanoparticle depend on various factors such as the type of salts used, pH value of the solution, the ratio of ions, ionic strength of the media, reaction temperature, and other reaction conditions, including the addition rate of the basic solution, and rate of stirring.[47] For successful precipitation, the pH should be between 8 and 14 range.[46] However, the size of MNPs decreases with an increase of both ionic strength and pH value in the medium.[17] Both the factors alter the chemical structure surface and the electrostatic surface charge of the nanoparticles.[48]

Generally, co-precipitation method starts with a 2:1 ratio of ferrous and ferric salt and a basic condition at room temperature or at elevated temperature (80-85°C).[49] The basic condition is achieved by adding different bases such as NaOH or NH_4Cl.[50] Precipitation forms in the bottom the reactor when the reaction is complete and subsequent washing, drying, sintering and grinding results in produced MNPs.[51] Figure 1 represents the co-precipitation method of nanoparticle synthesis. During the co-precipitation method, the reaction can be presented as Equations (1)-(3):

$$Fe^{2+} + 2OH^- \rightarrow Fe(OH)_2 \quad (1)$$

$$Fe^{3+} + 3OH^- \rightarrow Fe(OH)_3 \quad (2)$$

$$Fe(OH)_2 + 2Fe(OH)_3 \rightarrow Fe_3O_4 + 4H_2O \quad (3)$$

Other scientists have used ferrous and ferric salts with 1,6-hexanediamine as base to prepare Fe_3O_4 NPs.[17] According to this study, the ratio of ferrous and ferric salts played an important role formation of large hydroxide particles (precursor of Fe_3O_4 NPs); thus, affecting the final size of these MNPs.[17] The experimental saturation magnetization values for both the ferrous and ferric salts in these experiments also matched the literature value.[17]

At higher pH, nucleation of Fe_3O_4 is facilitated, which results in the co-precipitation of spherical superparamagnetic iron oxide nanoparticles (SPION) of less than 25 nm.[17] Increasing pH value and ionic strength in the medium has an inverse effect on the particle size of the MNP.[17] Temperature also plays a role in MNP formation. Co-precipitation below 60°C facilitates Fe_2O_3 growth whereas higher temperature (>80°C) favors Fe_3O_4 formation.

The nanoparticle's agglomeration is very common during this preparation method as the nanoparticles pose a greater specific surface and high surface energy due to its tiny particle size. Also, close attention should be given to the influence of alkali, reaction temperature, and emulsifier as they dominate produced nanoparticles.[17] Besides, in both the synthesis and purification steps, maintaining a uniform and monodisperse shape of particles is very challenging.[47]

2.2 | Hydrothermal

The hydrothermal method (also called solvothermal method) is considered the most popular wet chemical

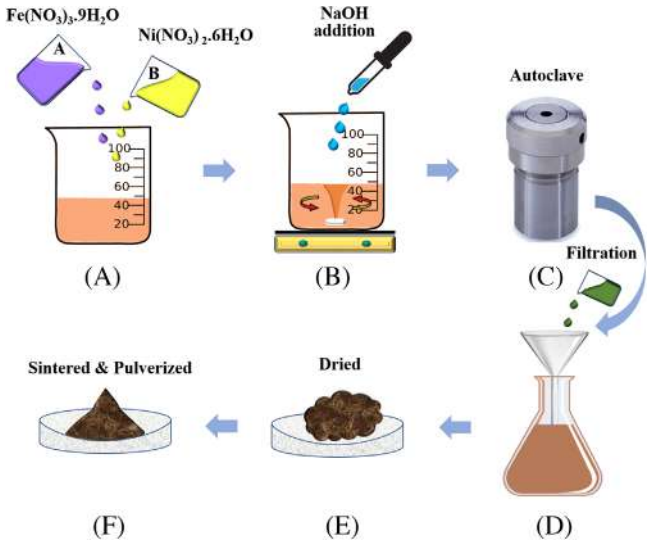

FIGURE 2 Illustration of ($NiFe_2O_4/Fe_2O_3$) nanocomposite synthesis via hydrothermal method: (A) addition of $Fe(NO_3)_3{\cdot}9H_2O$ and $Ni(NO_3)_2{\cdot}6H_2O$ precursors, (B) magnetic stirring during the addition of NaOH(1 M) until to pH 12, (C) autoclave the mixture for 20 hours at 180°C, (D) filtration, (E) drying at 100°C, and (F) annealed in the air for 2 hours at 400-800°C and pulverized to get the final product

approach to produce inorganic nanoparticles, particularly metal and oxides.[17] Figure 2 represents the hydrothermal method of nanoparticle synthesis. A wide range of magnetic nanoparticle scans can be synthesized via the hydrothermal method. Hydrothermal method usually contains wet-chemical techniques for crystallization in a sealed container.[17] The aqueous solution in the container is kept at high temperature (130–250°C) and high pressure (0.3–4 MPa).[17] Hydrothermal method usually produces NPs of larger diameter.[17] In presence of surfactant like sodium bis sulfosuccinate, Fe_3O_4 NPs of 27 nm diameter was produced.[17] Alternatively, Fe_3O_4 powder with a diameter of 40 nm was prepared using this method at 140°C for 6 hours.[17] Using hydrothermal method, nanomaterial's tuning is possible from a few nanometers to hundred nanometers.[52–54] Generally, the size of the synthesized nanoparticle and its distribution becomes dominant by the concentration of the precursors, the total time of the reaction, and the reaction temperature.

The hydrothermal process offers many advantages. For example, the first-rate reaction of the reagents, easy morphology control of the product, and excellent crystallization. Besides, under a pressure condition, forming a metastable phase and unique condensed phase is also possible. Many researchers have been demonstrated that magnetic nanoparticles in various shapes such as nanowires, nanorods, nanosheets, nanoplates, nanorings nanospheres, nanotubes, nanoparticles, etc. can be synthesized via hydrothermal synthesis process.[55] Most significantly, there is no use of organic solvents and no treatment of nanoparticles is needed after synthesis; therefore, the hydrothermal synthesis process is considered a versatile and eco-friendly method.[45] The most prominent drawback of this method is it fails obtain NPs smaller than 10 nm.[17] The other problem of this method is the slow reaction kinetics at high temperature.[17]

2.3 | Thermal decomposition

Thermal decomposition is a well-known method for the successive synthesis of various nanoparticles.[17] It also avails fine-tuning of the mean diameter of the produced particles.[56] The two most basic ways of achieving thermal decomposition are "heating-up" and "hot-injection." In the heating-up process, nanoparticles start clustering and growing by continuous heating of pre-mixed precursor materials, solvent, and surfactant up to a specific temperature range.[33,57] On the other hand, in the hot-injection method, rapid and consistent nucleation occurs when the reagent is injected into hot surfactant through a controlled growth phase.[17] However, both processes commonly involve the decomposition of precursors in the presence of organic surfactants to produce the desired nanoparticles.[58] The most used non-magnetic precursors are acetylacetonates and iron carbonyls as well as surfactants such as fatty acids, hexadecylamine, oleic acid, etc. The optimum temperature choice falls between 100°C and 350°C to produce nanoparticles with size 4 to 30 nm and a high degree of uniformity.[56,59] Alternatively, monodisperse magnetite NPs with sizes from 3–20 nm were prepared in high temperature (265°C) in presence of iron (III) acetylacetonate in phenyl ether and alcohol, oleic acid and oleylamine.[17] If organometallic precursors (such as $Fe(CO)_5$) are thermally decomposed, initially it leads to metal NPs. However, further oxidation leads to monodisperse NPs.[17] In contrast, cationic metal precursor (such as $Fe(acac)_3$) decomposition leads to direct MNP formation.[17] This process offers excellent yield quantity, particle size control, fine size distribution, crystallinity, and dispersibility to synthesized nanoparticles.[17] The nanoparticles' size is a crucial parameter when used for MRI; thus, nanoparticles produced following thermal decomposition synthesis is one of the best choices for this application.[48] The ratio of the precursors, such as organometallic compounds, surfactant, and solvent as well as reaction time and temperature, aging period plays the most vital role for precise control of the size and morphology of the synthesized particles.[53] Figure 3 represents the thermal decomposition method of nanoparticle synthesis.[60]

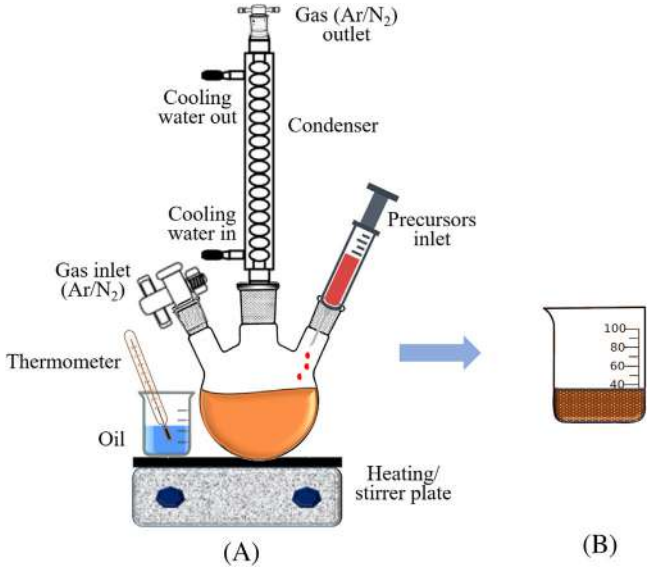

FIGURE 3 A) Experimental setup for nanoparticle synthesis following the thermal decomposition method. B) In this method, iron pentacarbonyl $Fe(CO)_5$ was added to octyl ether, and oleic acid mixture at 100°C then refluxed for 1 hour. Dehydrated $(CH_3)_3NO$ was added to the solution at room temperature and then again heated to 130°C under an argon atmosphere for 2 hours. After the formation of a brown-colored solution, the temperature was increased slowly and refluxed for more than 1 hour. Ethanol was added to the mixture at room temperature to produce a black precipitate of γ-Fe_2O_3 nanoparticles and then separated by centrifuging[60]

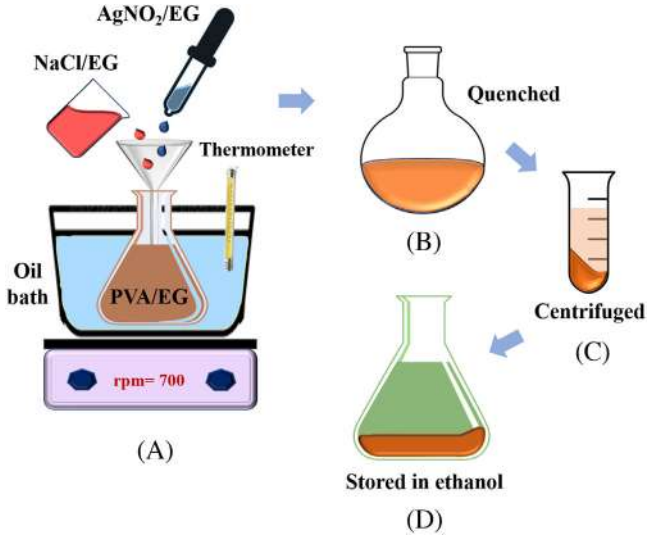

FIGURE 4 Steps to the synthesis of silver nanorods following polyol method: (A) NaCl/EG and $AgNo_3$/EG are added to PVA/EG solution and stirred at 700 rmp using magnetic starrier, (B) quince at room temperature, (C) centrifuged at 6000 rpm, and (D) stored in ethanol

However, nanoparticles produced through this method demand laborious purification steps before using biomedical applications.[61] Besides, nanoparticles' organic-soluble properties limit its use in many biological applications; thus, surface treatment becomes essential for those particles.[46] Most significantly, resulting in nanoparticles dissolves well, mostly in nonpolar solvents only.[47]

2.4 | Polyol method

The polyol method is another commonly used route for nanoparticle synthesis due to water-comparable and the chelating features of polyols.[17]. Figure 4 represents the polyol method of nanoparticle synthesis. In this method, liquid polyol acts as a solvent for metallic precursor, a redcing agent and in some cases as complexing agent for cations.[17] This solution is stirred and heated at a certain temperature (boiling point of the polyol) for less reducible metals.[17] The size of these NPs can be controlled by heterogenous nucleation (seeding the medium with foreign particles).[17] Precursor compounds such as oxides, acetates are dissolved or suspended in diol (ethylene glycol or diethylene glycol).[17] The mixture is then heated to 180-199°C.[17] Precise control of the NP size is possible by controlling the reaction temperature or nucleation process.[17] Magnetic nanomaterials, including metal, oxides of metal, metal chalcogenides, can be produced following this method. Also, bio-metallic clusters and nanocrystalline alloys can be produced via this process. Following this method, nanoparticles can be produced with regular size, minimum possibilities of agglomeration, and high production rate. Easy dissolving and suspending properties of oxides, acetates, and nitrates in diols makes it possible to synthesize nanoparticles at a relatively low temperature, which is the main reason for this method's becoming very popular. This bottom-up process is feasible for producing large batches of magnetic nanoparticles with ultra-small particle diameter, starting from 1 nm and up to several microns with very less or no agglomeration.[62] The particle size depends on the organometallic precursors, type of polyol solvent, the concentration of water, reaction time, reaction temperature, heating method, etc. Generally, nanoparticles size increases with the increase of precursor concentration and water quantity. Hot injection of starting materials and/or water helps to produce nanoparticles with a tiny size.[45] As the polyols are low cost, green solvents, this has been used extensively in industries.[17]

However, the synthesis of less-noble metals is limited due to re-oxidation because of the protic polyol.[17] Quick thermal decomposition near the boiling point limits the temperature range for nanoparticle synthesis. Sometimes the production of nanoparticles with minimum size becomes challenging for the solubility of the produced particles in polyol medium.[45]

2.5 | Other methods

Other methods to synthesize MNPs include microemulsion, sol–gel method, sonochemical, electrochemical and biological methods like microbial incubation, etc..[17] The microemulsion is a two-phase method. The microemulsion method utilizes two liquids' immiscibility properties (one precursor of MNP), and through a series of emulsion steps, MNP is produced.[45] The sizes of MNPs in this method are relatively bigger (10′s of nm), and the reaction kinetics is on the slower side even though it requires high temperature.[45,63] In the sol–gel method, the precursor is dissolved in water (preparing "sol" or colloidal solution).[45] After a series of stirring and heating, the MNP is dried, preparing "gel" for the process.[64] The final step is solvent removal until the desired MNP is obtained.[64] The sol–gel process produces MNPs of high purity and homogeneity even though it leads to the formation of hard-to-remove impurities (resulting from the sol–gel matrix).[65–68] Thermal methods like sputter deposition, vapor deposition (physical deposition, PVD, and chemical vapor deposition, CVD) is found in the literature.[45,69] However, complicated clean-room instrumentation limits their application. The more recent methods of MNP synthesis incorporate the so-called "green" synthesis process. The sonochemical process is one of those methods. In this method, ultrasonic irradiation causes cavitation in the solution, which can be used to tune nucleation, formation and growth of the MNPs.[65] The electrochemical method also presents an eco-friendly, low-cost procedure.[70] This method is capable of fine-tuning even the maghemite and magnetic component of MNPs.[71] However, a few confounding factors like current density, pH, electrolyte concentration, electrode type, and surface coating materials may reduce the reproducibility of this method.[70] The microwave-assisted method can also produce MNPs of uniform shapes and sizes for biomedical imaging applications; however, the process requires a microwave reactor and the process can be time consuming.[65] In a biological process like biomineralization MNPs are synthesized from living organisms like plants or living cells. This process produces non-toxic and biocompatible MNPs that are especially useful biomedical applications. Table 1 summarizes the MNP synthesis process with its advantages and disadvantages.

3 | FUNCTIONALIZATION OF MNPs

Surface modification or functionalization is an essential aspect of magnetic nanoparticle (MNP) synthesis and application. Functionalized MNPs have been the focus of the biomedical application. The primary purposes of surface modification of MNPs are (1) to prevent agglomeration, (2) to improve surface catalytic activity, (3) to improve physiochemical and mechanical properties, and 4. to increase solubility and biocompatibility.[94] The functionalization process that gives MNPs their typical morphology can be one of the four types of core-shell structure, matrix dispersed structure, Janus structure, or shell-core-shell structure.[94,95] Surface functionalization can be done both in-situ (simultaneous synthesis and functionalization) and post-synthesis methods (functionalization after synthesis).[96] Surface functionalization of these MNPs is done using three mechanisms (1) ligand addition, (2) ligand exchange, (3) encapsulation.[96] The prevalence of functionalization groups facilitates the covalent bonds to the affinity ligands, and the balance between intermolecular forces drive the interaction between functional groups and nearby MNPs.[97] Between the mechanisms mentioned, encapsulation is the most widely used. It is the best method in terms of the materials available for coating-since both organic material (polymers, surfactants) and inorganic material (silica, carbon, metal, metal oxides) can be used for encapsulation.[94] Functionalization with polymers is the most comprehensive used method for biomedical applications, especially in nanomedicine.[94] Dextran, chitosan, alginate, polyethylene glycol (PEG), polyvinyl alcohol (PVA), polydopamine (PDA), polysaccharide, polyethylenimine, polyvinylpyrrolidone (PVP), polyacid polyetherimide, and polyamidoamine (PAMAM) are the most commonly used polymers for the surface modification of MNPs.[94] PEG is a water-soluble polymer widely used for biomedical applications like magnetic resonance imaging (MRI) contrast agents for cancer visualization and biosensors.[94,98] Dextran is also a material with excellent biocompatibility, water solubility, and low cytotoxicity.[94,99] This dextran coated MNPs have been used for a biomedical application like in-vivo cancer drug carriers and MRI contrast agents.[94,100] Some polymers like PEI can be used to enhance the biocompatibility of MNPs and are used in cancer cell separation and hypothermia.[94,101] Other polymers like PVP are used to kill breast cancer agents, whereas PVA, polyacrilic acids are used in anticancer drug delivery applications.[94] Polydopamine formed from dopamine at a low pH has been used as a biosensor and catalyst for biological reactions.[94] Chitosan (a hydrophilic polymer) has low toxicity, good compatibility, and it can also be used with other polymers like PEG and PAA.[94] Chitosan functionalized MNPs have been used in MRI imaging, microwave therapy, hyperthermia, and tissue engineering applications.[94,102] Other naturally available polymers have been used for the encapsulation of MNPs. Such molecules include starch (contrasting and imaging), alginate (controlled

TABLE 1 MNP synthesis methods with their advantages and disadvantages

Method	Advantages	Disadvantages	Ref.
Co-precipitation	- Rapid reaction - Mild reaction conditions - Can be produced in large batches	- Poor size distribution - Low reproducibility - Surface oxidation	[72,73]
Hydrothermal	- Superior control in size, shape, dispersion - Magnetic controllability - Excellent crystallinity - Eco friendly	- High temperature and pressure - Longer synthesis time - Adsorption of capping agents	[72,74–76]
Thermal decomposition	- High yield - Superior size distribution - High reproducibility	- Safety issues for high temperature and pressure - Solubility in organic solvents - Toxicity	[72,74,76,77]
Polyol	- Chelating effect - Bio(water)compatibility - Low cost industrial application	- Difficult to synthesize small size-particles - Instable oxidation	[45,76,78–80]
Microemulsion	- Controllable particle growth, nucleation, and agglomeration - High magnetization values	- Residual surfactants - Difficult to scale up production	[65,76,81]
Sol–gel	- Low cost - Homogeneity - High purity	- Formation of secondary phase - Hard to remove the residual organics from porous gel	[65–68]
Flow-injection	- Reproducibility - Homogeneity - Controllable flow for drug targeting	- Requires continuous mixing - Closed system (in a capillary reactor)	[65,82,83]
Sonochemical	- Simple, “green” process - Diverse application, for example, sensors/biomedicine, MRI - Narrow size distribution	- The working mechanism is not well understood - “Cavitation” can cause adverse reaction conditions	[65,84–87]
Gas/aerosol	- High-quality output - High purity - Relatively straightforward process	- Low quantity, difficult to scale up - Large aggregates - High cost	[65,88]
Microwave irradiation	- Fast, low-cost, low energy consumption - Uniform shape and size distribution - Especially useful for biomedical imaging	- Slow reaction kinetics - Complicated setup (microwave reactor) required	[65,89,90]
Electrochemical	- Eco-friendly “green” method - Selective and low-cost - Diverse application in biomedical and/or electronics	- Poor reproducibility - High number of confounding factors	[65,70]
Sputter deposition	- Tunable properties - Fast, low solvent contamination - No toxic precursors	- Low yield - Poor quality - Very high temperature	[45,91,92]
Vapor deposition	- Flexibility - Tunable distribution - Scalable process	- Complicated setup - Cost associated with clean-room	[17,69]
Biological methods	- Reproducibility and scalability - High yield, low cost - Biocompatibility and low toxicity	- Slow and laborious - Sometimes produces irregular shapes	[65,93]

TABLE 2 Different functionalization material and biomedical application associated with MNPs

Material	Biomedical Applications	Ref.
Ployethylene glycol (PEG)	MRI contrast agent, biosensor, biocompatible drug delivery	[65,94,106]
Silica	Drug delivery, biosensor, toxicity studies	[45,55,94,104,107]
Polyvinylvinyl pyrrolidone (PVP)	MRI contrast agent, drug delivery for breast cancer	[94]
Dextran	MRI imaging, drug delivery, diagnostic agent	[45,94,100]
Chitosan	Magnetic hypothermia, tissue engineering, imaging, drug delivery	[45,94,108]
Polyvinyl alcohol (PVA)	Imaging, drug delivery, biosensor, toxicity studies	[45,94,109]
Gelatin	MRI imaging, gelling agent, emulsifier	[45,110]
Amino acids	Radio-labeling for PET/CT imaging, cancer detection	[94]
Aminosilane	Drug delivery, viability studies	[45,111,112]
Lipids	Gene therapy, multi-modal imaging	[94]
Polyethylenimine (PEI)	Cell separation, hyperthermia, drug delivery	[94,113]
3-aminopropyltriethyloxysilane (APTES)	MRI imaging, heavy molecule adsorption	[94,103,114]
Carbon	Drug delivery, cancer treatment	[45,115]

drug release), polyphenol (magnetic hypothermia), flavonoids (cell imaging, nano-drug carrier), amino acids (radio-labeling, cancer detection), and lipids (gene therapy, multi-modal imaging).[94] Small molecules like silane agents can be used on bare MNP surface for improved biocompatibility in biomedical applications.[94] 3-aminopropyltriethyloxysilane (APTES), mercaptopropyltriethoxysilane (MPTES), and triethoxyvinylsilane (VTES) are the common silane coupling agents used in the functionalization of MNPs.[94] These functionalized MNPs have been used for magneto-rheological fluids and in vivo MRI applications.[94,103] In the case of inorganic encapsulation, silica coating is the most available method. Stober mechanism, microemulsion, aerosol pyrolysis, and sodium silicate based methods are the widely used silica encapsulation method.[94] These functionalized MNPs have acceptable biocompatibility, hydrophilic properties and have found numerous biomedical applications like drug delivery.[94,104] Other inorganic coating materials like carbon, metals, and metal oxide functionalization have seen little or no application in biomedical applications.[94] However, carbon-based functionalization is used in electronic applications like supercapacitors and lithium-battery materials.[94,105] Table 2 summarizes the surface coating materials and their associated biomedical applications.

4 | BIOMEDICAL APPLICATIONS OF MNPs

Magnetic nanoparticles are an excellent choice as drug delivery module due to their high surface area to volume ratio, low toxicity, and high targeting efficacy.[116] Moreover, magnetic nanoparticles are being used in magnetic hyperthermia to reduce tumor volume and eradicate cancer cells from a targeted region.[117] Magnetic bioseparation is useful in case of separating a specific molecule from a library of different molecules.[118] For instance, magnetic bioseparation is being used to isolate viral RNA to further analyze using polymerase chain reaction (PCR) method.[119] Furthermore, magnetic particles have imaging properties that make these particles excellent choice as multimodal theranostics platform, which enables us to perform diagnostics and therapy simultaneously.[117] Magnetic resonance imaging (MRI), magnetic particle imaging (MPI), computed tomography (CT), and positron emission tomography (PET) are major imaging techniques that utilize the magnetic properties of the particles. In this section, we will briefly discuss different usage of magnetic particles in the biomedical field.

4.1 | Drug or gene delivery

The recent progress in the field of nanoscaled drugs/gene carriers such as micelles,[120,121] liposomes,[122,123] hydrogels,[124] dendrimers,[125] and mesoporous silica nanoparticles [126] is phenomenal. Still, these nanocarrier suffers from some challenges such as off-targeting accumulation of carriers,[127] low penetration through blood brain barrier (BBB),[125] low circulating time in blood,[122] low physical and chemical stability,[123] premature release of cargo molecules [128] and low drug loading efficacy.[123] These challenges can be addressed by incorporating magnetic nanoparticles with these nanocarriers to create unique magnetic nanocomposites (MNCs). Figure 5 illustrates commonly used magnetic nanocomposites for drug and gene delivery. Drug/gene molecules can be attached to the surface ligand of magnetic nanoparticles

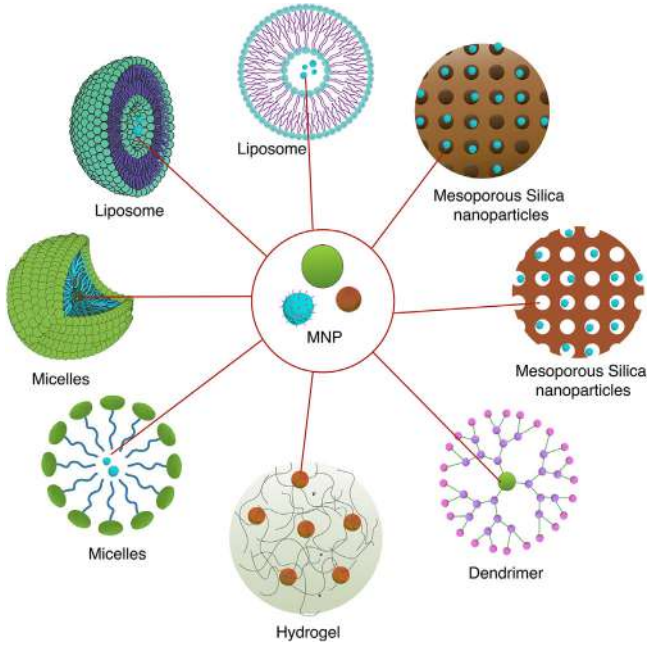

FIGURE 5 Different nanocomposite containing magnetic nanoparticles. The high surface area of the nanoparticles loaded inside the nanocarriers makes them excellent choices for drug and gene delivery module

either by physicochemical interaction or electrostatic interaction.[129] Later, these MNCs can be used to deliver cargo to the targeted sites under the influence of an external magnetic field.[130] Furthermore, magnetic particles can be utilized as on demand and controlled therapeutic agent release platform into desired sites.[131] External stimuli such as alternating magnetic field can be used to release attached therapeutic molecules into targeted localized region.[130] In this section, different types of nanocarriers incorporated with magnetic particles to increase the overall efficacy of drug/gene delivery will be discussed.

4.1.1 | Hydrogel

Magnetic hydrogel nanocomposites are being evaluated for various biomedical applications such as wound healing,[132] nerve repair [133] and controlled drug delivery.[134–136] As mentioned earlier, magnetic particle exhibits low biotoxicity and have a high surface area to volume ratio, which makes them preeminent candidate to be used in hydrogel matrix as a carrier for therapeutic molecules. Recently, Chitosan (CS) and polyacrylic acid (PAA) coated 94 nm iron oxide magnetic nanoparticles showed promising potentiality as a drug carrier module to deliver anticancer drug 5- fluorouracil.[137] The drug loading capacity of CS/PAA/Fe_3O_4 was reported as 100%; however, these nanocarrier suffers from initial burst release of 40% of the loaded drugs which can introduce challenges in certain applications where sustained release is paramount.[138] To surmount initial burst release challenge, Hyati et al. [139] reported a temperature, pH and magnetic triple sensitive nanogel hydrogel composite for controlled drug release to the targeted site. Briefly, Hyati et al. incorporated magnetic nanoparticles into poly(*N*-isopropylacrylamide)-co-((2-dimethylaminoethyl) methacrylate) (PNIPAM-co-PDMA) which was then grafted onto sodium alginate as a biocompatible polymer. The drug release profile of these 9-11 nm nanoparticles were studied at varying pH, varying temperatures and in the presence and absence of an alternating magnetic field (AMF). The release profile exhibits no initial burst release of the loaded doxorubicin (DOX) drug which overcomes the inherent challenges with many other drug carriers. Although we have mentioned one of the prominent characteristics of magnetic particles being inherently low-toxic, they still can induce toxicity in certain applications, especially in sensitive areas; such as the eyes.[140] To address this challenge, Kim et al. [140] reported a bilayer hydrogel nanocomposite, composed of an MNP layer and a therapeutic layer to treat retinoblastoma Y79 cancer cells. Upon reaching the targeted site under the influence of a stagnant magnetic field, the hydrogel nanocomposite was exposed to an AMF to assist the release of PLGA-DOX drug molecules. The MNP layer of the nanocomposite bilayer consists of PEGDA 700 and Iron oxide particles, whereas the attached therapeutic layer contains gelatin, PVA and PLGA-DOX drug particles. Once the PLGA-DOX particles are released, the magnetic layer of the carrier can be retrieved by using a stagnant magnetic field (Figure 6). Kim et al. [141] reported similar working principle monolayer hydrogel nanocomposite with retrievable MNPs synthesized with gelation and PVA. The Hydrogel matrix was loaded with MNP and PLGA-DOX nanoparticles. The nanocomposite was driven to the desired site under the influence of a stagnant magnetic field, and upon arrival to the desired site, the hydrogel matrix decomposed upon irradiation with 808 nm NIR laser (1.65 W cm^{-2}). The decomposition of nanocomposite facilitated the release of the drug molecules in the target site. Once the drug molecules are released, the magnetic particles can be retrieved by using a stagnant magnetic field to reduce magnetic particle-induced toxicity to the targeted site.

In-addition, magneto-hydrogel are being utilized for dual therapy of controlled therapeutic agent delivery combined with magnetic hyperthermia.[142,143] Wang et al. [142] reported a hydrogel nanocomposite by copolymerization of *N*-isopropylacrylamide (NIPAm) and acrylamide (Am) which was then incorporated with vinyl-Fe_3O_4@SiO_2 for magnetic hyperthermia and controlled drug delivery.

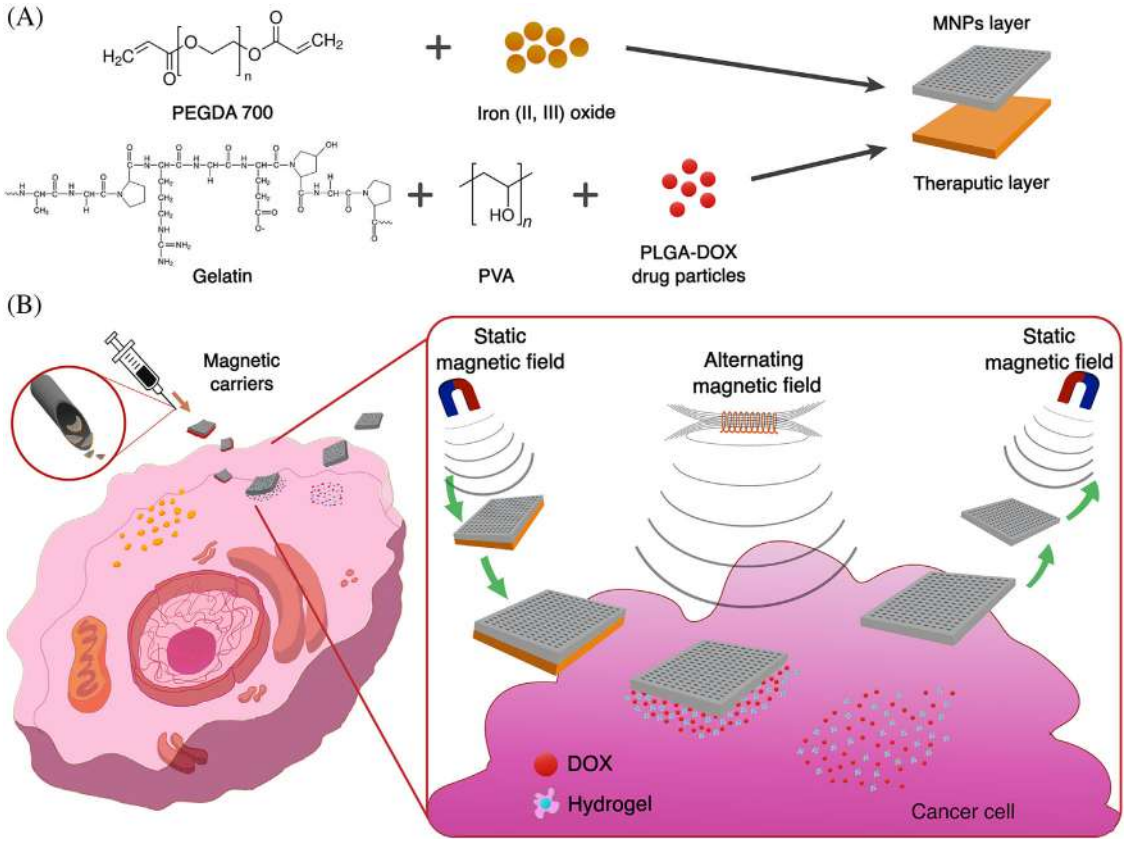

FIGURE 6 A, Structure of bilayer magnetic drug delivery vehicle. The delivery vehicle is composed of two layers with MNP layer and a therapeutic layer that contains DOX. B, The bilayer magnetic vehicles can be locally injected to the tumor site, which will then be delivered to the desired cancerous cell by a static magnetic field. Upon reaching the desired site the bilayer delivery vehicle will be exposed to an alternating magnetic field (AMF) which will facilitate an increase in temperature in the cellular microenvironment and the release of the therapeutic layer. The remaining magnetic layer will be retrieved using a static magnetic field. Recreated with permission from ref [140]

Anticancer drug chelerythrine was loaded in the hydrogel composite by immersion method. The lower critical solution temperature (LCST) of the composite hydrogel was reported to be 41°C. Applied AMF can increase the surrounding temperature to 45°C, which induced drug release and hyperthermia therapy leading to decomposition of the hydrogel matrix.[142]

Co-delivery of hydrophobic and hydrophilic drug is challenging due to low solubility and poor bioavailability of hydrophobic drugs in an aqueous medium.[144] Yongliang et al. [145] reported magnetic chitosan hydrogel embedded with two different types of drugs. Briefly, hydrophilic drug adriamycin (ADM) and hydrophobic drug rifampicin (RFP) were loaded inside the hydrogel-magnetic particle nanocomposite and was observed for drug release pattern. Without any external stimuli, the release pattern was purely diffusive.[145] When a low frequency AMF was applied to the nanocomposite, the cumulative release of hydrophilic drug ADM increased by 67.2% in a 15 minutes ON-15 minutes OFF cycle over 1 hour time frame compared to no applied external stimulus environment.[145] Apart from the co-delivery of lipophilic and hydrophilic drugs, magnetic nanoparticles embedded hydrogen has been proven to be successful in wound healing applications.[146] A groove pattern scaffold was fabricated by alginate/poly-L-ornithine/gelatin (alginate-PLO-gelatin) hydrogel sheet for cell delivery to the wound site. This grove pattern helps with cell proliferation, alignment, and elongation.[146] Additionally, the investigators embedded magnetic nanoparticles in the groove pattern to facilitate magnetic field induced transfer of cell seeded hydrogel sheet to the wounded site. Table 3 summarizes the recent development of magnetic-hydrogel nanocomposite and their usage as drug delivery module.

4.1.2 | Liposome

Liposome (a spherical vessel with lipid bilayer) can contain MNPs into their structure and have been extensively used in drug delivery to organs and tissues through a controlled magnetic field.[154] Even though they were

TABLE 3 Different magnetic nanoparticle-hydrogel nanocomposites for drug delivery

Hydrogel monomer	Crosslinker	Magnetic particles with size	Hydrodynamic diameter of nanocarrier	Drug	Cell line	Refs.
Acryl-PEG-NHS	RGDS peptide	SPION (7.3 ± 0.7 nm)	28.5 ± 4.8 nm	Doxorubicin (DOX)	HeLa cells	[147]
Hyaluronic acid	Divinyl sulfone (DVS)	SPION (6–15 nm)	–	Trimethoprim (TMP)	–	[148]
Polyvinylpyrrolidone (PVP)	PVA	Iron oxide	35.20 ± 15.29 nm	Bleomycin	L929 cells	[149]
O-acetyl-galactoglucomannan (AcGGM)	A high concentration of NaOH was used to induce deacetylation of AcGGM	Fe_3O_4(5.8 nm)	–	Bovine serum albumin (BSA) as a model drug	–	[150]
κ-carrageenan	Sodium alginate	Fe_3O_4 (less than 20 nm)	–	Riboflavin	–	[151]
2-hydroxyethyl methacrylate (PHEMA) and polyethylene glycol acrylate (PEGDA)	2-Hydroxyethyl methacrylate (HEMA) and ethylene glycol dimethacrylate (EDGMA)	Fe_3O_4 (>50 nm but <100 nm)	–	Docetaxel	Mammary carcinoma (4T1)	[152]
PVP	Irradiation with γ-ray followed by an oil-water-oil emulsion	Fe_3O_4(50 nm)	–	Bleomycin A5 hydrochloride (BLM)	VX2 squamous cell	[149]
N-isopropylacrylamide	Polyethylene glycol 400 dimethacrylate	Fe_3O_4 (20–30 nm)	–	Pyrocatechol violet dye as model drug	–	[153]
N-isopropylacrylamide (NIPAM)	(2-dimethylaminoethyl) methacrylate (DMA)	Fe_3O_4(9 nm)	94 nm	Doxorubicin (DOX)	–	[139]
Acrylic acid (AA)	*N,N′*-methylenebisacrylamide (MBA)	Fe_3O_4	98 nm	5-flurouracil	–	[137]

proposed as early as the 1980s, recent years have seen some dramatic applications biomedical field, particularly in the drug delivery category.[154] The liposomal drug delivery strategy is hindered by their poor encapsulation efficiency and thermal disruption.[154] The method to overcome this limitation is to embed the MNPs in the membrane and encapsulate the drug in the liposomal core.[154,155] Toro-Cordova explored the use of liposomes loaded with cisplatin and MNP.[154] In the physiochemical characterization of these cisplatin magnetic liposomes (Cis-MLs) were not significantly different than cisplatin liposome (Cis-Ls).[154] However, pharmacokinetic characterization in Wistar rats revealed the superior performance of Cis-MLs as was evident from bioavailability characteristics, etc.[154] They also assessed the apoptosis and cytotoxic effect of these Cis-MLs in HeLa cells and found acceptable toxicity.[154] In other works, researchers synthesized magnetic liposomes for heat-responsive localized drug delivery.[156] They designed magnetic ammonium bicarbonate (MagABC) liposomes about 210 nm in size and they showed acceptable encapsulation efficiencies and desired heat-responsive release.[156] These MagABC liposomes could successfully target the tumor cell culture model in the presence of a permanent magnet and yielded a substantial increase in intracellular particle accumulation.[156] However, their work also displayed increased cytotoxicity.[156] Other studies have used a solvent-guided method for incorporating larger MNPs (mean diameter ~10 nm) into phospholipid bilayers.[157] They solved the low insertion efficiency of the hydration method with chloroform as a supporting agent guide.[157] These magnetic liposomes (MLs) were modified with the human epidermal receptor 2 (HER2) antibody and tested for cell isolation for drug delivery.[157] A 75% isolation efficiency was observed in specific cell lines.[157] These MLs were further modified with folate and the capacity of isolation was also tested.[157] These results suggest that these large MNPs can be used to detect and analyze freely circulation tumor cells.[157] Lu et al., proposed thermosensitive liposome with MNPs and Camptosar.[158]

These materials control drug-release by magnetic fields and magneto-thermal effects.[158] These materials were validated in the xenograft brain tumor model and they also showed enhanced toxicity towards U87 glioma cells.[158] One more example of thermosensitive magnetic liposomes was demonstrated by Shen et.al..[159] The developed Fe_3O_4 encapsulated in doxorubicin in ammonium sulfate and release was triggered by near-infrared laser.[159] These materials showed significant potential for combined photothermal-chemo therapy with minimal damage to the tissue.[159] Other groups also published a method of light triggered MNP liposome preparation.[160] They prepared hyaluronic acid-MNP liposomes which can act as a vehicle for the release of an anticancer drug.[160] With the combination of photothermal radiation and chemotherapy these magnetic liposomes enhanced the therapeutic efficiency of the drug.[160] Iron oxide MNP and gold nanoclusters were conjugated with amide bonds and enclosed in liposome nanocarriers in another study.[161] Through extensive characterization techniques the authors demonstrated that these MNP liposomes can act as multifunctional liposomal drug carriers and dual imaging probes.[161] Recombinant tissue plasminogen activator (rtPA) was encapsulated in MNP liposomes to make a temperature-sensitive drug delivery method.[162] These magnetic liposomes were validated by the delivery of rtPA in the thrombus site, followed by a temperature triggered controlled release.[162] In one more innovative liposomal drug delivery application, researchers encapsulated vanadium-curcumin complex in magnetic liposomes which improved the solubility and bioavailability.[163] These materials showed increased concentration at the DNA site, and they can also act as nanocarriers for anticancer metal ion complexes.[163] More research is required to overcome the current challenges of low encapsulation efficiency and biocompatibility.

4.1.3 | CRISPR-Cas9

CRISPR is short for clustered regularly interspaced short palindromic repeats, primarily found in eukaryotic bacterial genes.[164,165] The bacterial CRISPR system works as a defence mechanism against viral attack by introducing dual RNA guided Cas-9 protein towards the invading viral DNA by introducing site-specific cleavage with molecular precision.[166,167] Target recognition is strictly dependent on Cas9-DNA interaction and the presence of a short protospacer adjacent motif (PAM) which helps the Cas9 protein to attach to the target DNA. This natural defence mechanism system is being utilized as RNA programmable DNA targeting and editing tool for gene therapy.[168] CRISPR-Cas9 system is a promising tool to treat and cure genetic disorders such as sickle cell anemia, cystic fibrosis, Alzheimer, and cardiovascular diseases.[164–167,169] Despite the various usage of this promising tool, the CRISPR-Cas9 system suffers from various obstacles such as off-targeting mutations and low transfection efficacy.[168,170] The recent development of the usage of magnetic nanoparticles to increase transfection and targeting efficiency is promising. Zhu et al. [170] reported magnetic baculoviral (BV) vehicle to induce transgene expression in vitro. Baculoviral containing luciferase (BV-LUC) and baculoviral containing enhanced green fluorescent protein (BV-eGFP) was mixed with 15 nm magnetic nanoparticle and TAT peptide (GRKKRRQRRRPQ) (MNP-TAT) for targated gene therapy. Figure 7 illustrates MNP-BV-eGFP assisted gene editing; once the MNP-BV-eGFP complex is administered into the tumor rat model, the results indicated effective transduction is triggered by an applied magnetic field which acts as an activator of genome editing and transgene expression (Figure 8).

Rohiwal et al. [171] reported polyethylamine (PEI) based MNP mediated non-viral CRISPR-Cas9 system for gene editing. Briefly, magnetic particles were prepared by co-precipitation method, the 20 nm magnetic particles were coated with positively charged PEI and CRISPR-Cas9 plasmid and were transferred into the HEK 293-TLE-3 cell line by magnetofection. The reported magnetofection efficiency was not significant compared to the non-magnetic transfection. However, the investigators reported the magnetic field-induced the movement of the magnetoplexes on the cell.[171] Branched PEI coated MNP were reported to be effective for gene transfection of vascular endothelial cells.[171] The complex branched PEI-MNP showed enhanced transfection with a 15 minutes incubation under the influence of a magnetic field with the endothelial cells,[172] which can be explained by the rapid and forced movement of the magnetic complexes towards the cells.[173,174] Kaushik et al. [175] reported magnetically guided CRISPR-Cas9 delivery across blood-brain barrier (BBB) to cure latent HIV-1 infection in microglial (hμglia)/HIV (HC69) cells. With magnetic transfection, the author reported on-demand release of Cas9/gRNA.[175] Moreover, nanospear can be used for high precision gene delivery to the targeted sites.[176] The magnetic nanospear having a tip diameter less than 50 nm exhibited cell viability more than 90% with a transfection rate of more than 80%.[176] This nanospear can be exploited for plasmid delivery into desired cells to induce CRISPR-Cas9 mediated gene editing.

4.1.4 | Micelles

Micelles are self-oriented structures of amphiphilic molecules or surfactants having a polar head group and

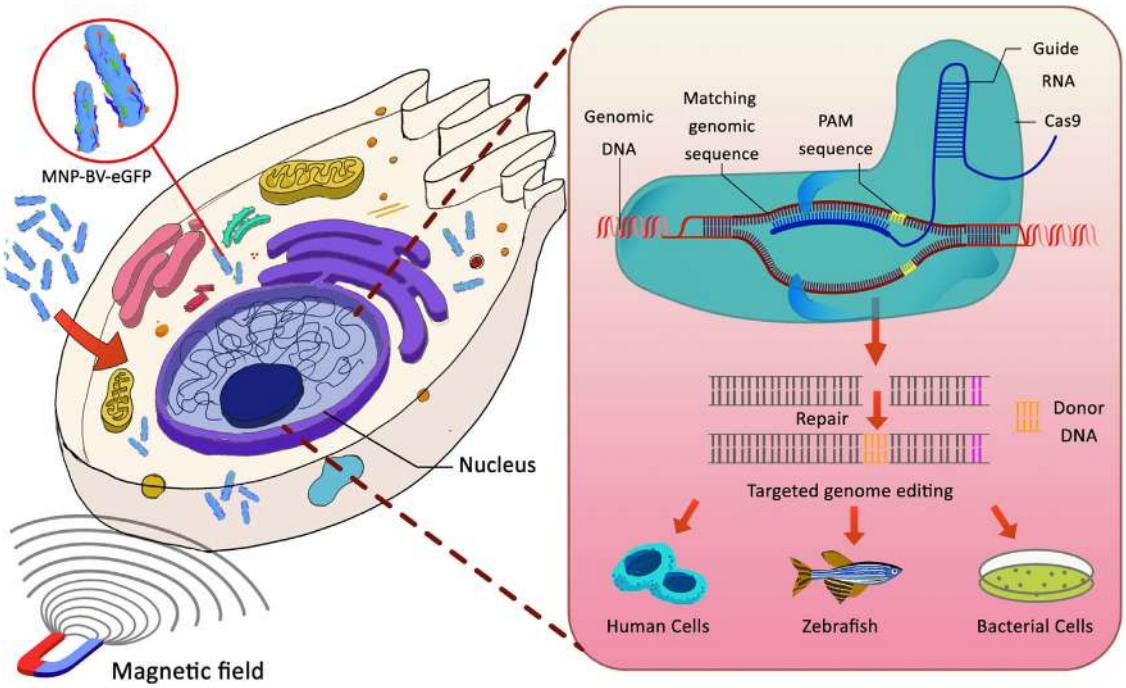

FIGURE 7 Magnetofection assisted CRISPR-Cas9 gene editing. Magnetic particles and enhanced green fluorescent protein-loaded baculoviral vector (MNP-BV-eGFP) used for high magnetofection efficacy under the influence of a static magnetic field. Protospacer adjacent motif (PAM) sequence assisted DNA cleavage, followed by donor DNA docking to repair cleaved DNA which essentially leads to successful DNA editing

a lipophilic tail group in their structure.[177] The unique structure of having lipophilic tail and hydrophilic head groups makes them thermodynamically favorable to self-assemble into micelles structures.[178] The surfactant molecules assemble themselves in the air-water interface to reduce the free energy of the system.[179] Once the air-water interface is saturated, further addition of surfactant will lead to the formation of micelles in the bulk solution. The concentration of surfactant at which the first micelle is formed is called critical micelles concentration (CMC) at a specific temperature.[179] The temperature below which the surfactant remain as monomers is called critical micellization temperature (CMT).[180] The core of the self-orienting micelles structure is lipophilic; hence, hydrophobic drugs and therapeutic agent can be loaded inside of the structure. In addition, hydrophobic surface ligand stabilized magnetic particles and hydrophobic drug-loaded magnetic particles can also potentially be loaded inside the micelle structure for targeted therapeutic applications. Outside stimuli such as increased temperature and alternating magnetic field (AMF) can be applied to the magnetic particles loaded micelles to induce on demand drug release. Ashjari et al. [181] reported a PLGA-mPEG block copolymer star-shaped micelles loaded with iron oxide for hydrophobic drug delivery to treat cancer. The 70 nm magnetic particles loaded with quercetin (hydrophobic drug) have less magnetization saturation (26 emu g^{-1}) compared to the magnetic nanoparticles alone in solution (57 emu g^{-1}).[181] The magnetic nanocarriers can be guided to the target site under the influence of a magnetic field. Moreover, magnetic particle and dasatinib (hydrophobic drug) loaded protein micelles exhibited sustained drug release over 120 hours with less than 5% initial burst release to treat human triple-negative breast cancer cells.[182] Magnetic micelles have been used to overcome challenges with delivering drug across the blood brain barrier (BBB).[183] Methoxy poly (ethylene glycol)-poly (caprolactone) (mPEG-PCL) was utilized with magnetic nanoparticles to cross BBB under the influence of mild external static magnetic field to deliver naproxen as a model drug. Furthermore, Pourjavadi et al. [184] reported self-assembled triblock co-polymer (PNIPAM-PCL-PNIPAM) micelles to deliver paclitaxel (hydrophobic drug). Briefly, oleic acid-coated 15-25 nm magnetic particles were incorporated inside of the hydrophobic core of the micelles structure. The release profile showed sustained drug release for 80 hours with less than 20% initial burst release at 37°C.[184] The release pattern was found to be temperature-dependent, which can be potentially utilized in coupled with hyperthermia treatment to treat cancer.

Wu et al. [185] reported a spherical Fe_3O_4 nanoparticle of 8 nm diameter and Doxorubicin loaded nanomicelles for NIR triggered drug release. The authors used a polymer

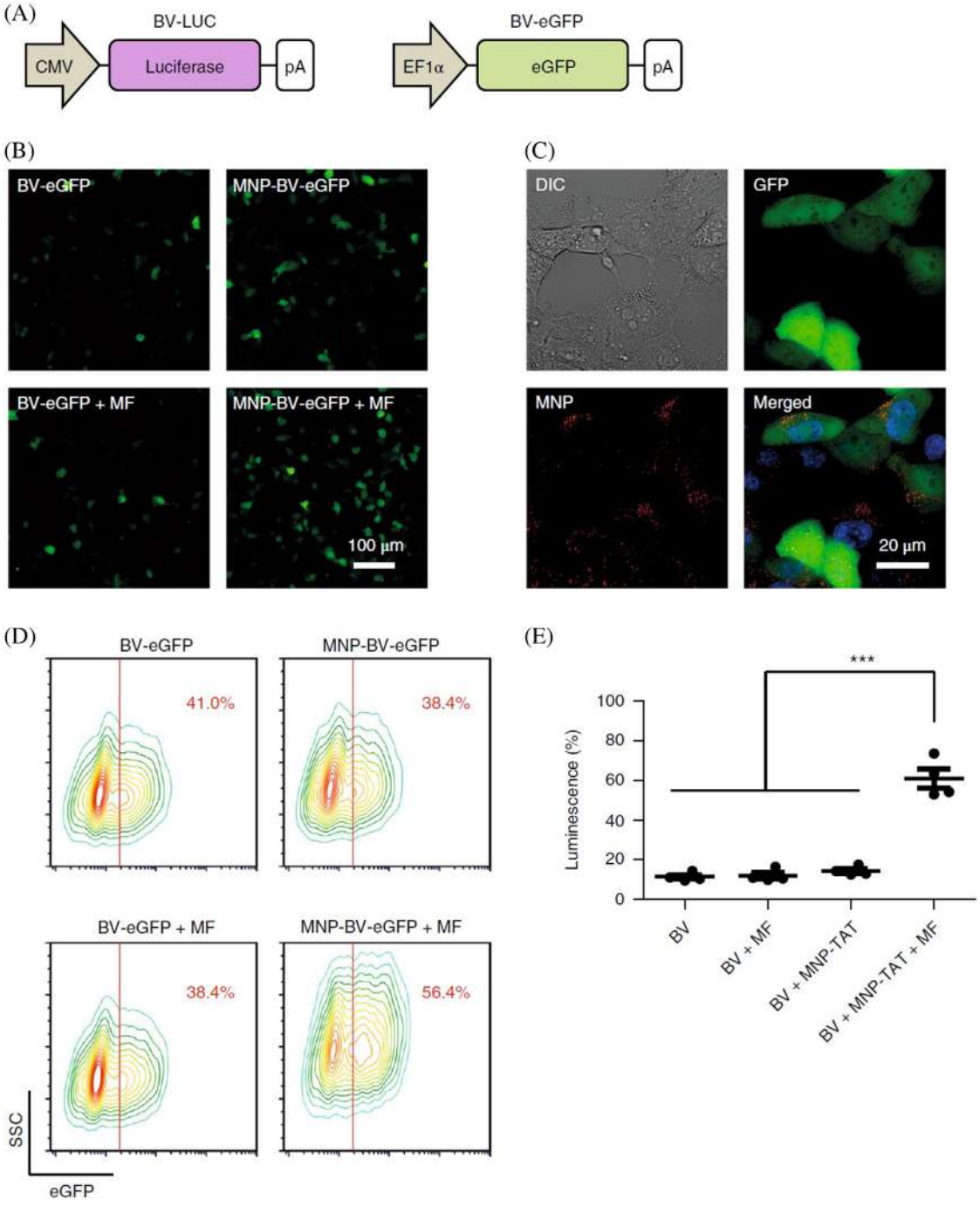

FIGURE 8 A, Baculoviral vector carrying luciferase (BV-LUC) and enhanced green protein fluorescence protein (BV-eGFP). Here cytomegalovirus is denoted as CMV; Elongation factor is denoted as EF1α and polyadenylation signal is denoted as pA. B) Fluorescence images of baculoviral vector assisted eGFP expression. BV-eGFP and MNP-BV-eGFP were incubated with Hepa 1–6 cells, respectively, for 0.5 hours in the presence and the absence of a magnetic field (MF) directing towards the cell surface. C, Localization of MNPs (red) and eGFP (green) in the cells incubated with MNP-BV-eGFP. Cell nuclei are stained with blue. Differential interference contrast is denoted as DIC. D, Quantification of baculoviral vector-mediated eGFP expression. Side scatter is denoted as SSC. Colored lines represent contour lines of cell density and the red line represents the gating. E, Baculoviral vector-assisted luciferase expression. The BV transgene expression was enhanced by combining attached MNPs and an applied magnetic field, whereas the effect of magnetic particles and magnetic field only was negligible. Reprinted with permission from ref [170]

with an upper critical temperature (UCST); these polymers undergo a phase transition from a hydrophobic state to a hydrophilic state upon being exposed to heating.[185] The synthesized polymer (poly (AAm-co-AN)-g-PEG) (PAAP) were used to encapsulate the magnetic nanoparticles and the anticancer drug in the micelles structure. These hydrophobic thermoresponsive micelle structures provide a protective layer against pre-mature leakage of the cargo being sent before reaching the desired site.[185] The cargo release can be controlled using an external stimulus. Wu et al. [185] also investigated the effect of incident NIR light at different pH. The release of DOX was over 59% at pH 6.5 with NIR light radiation and was only 16% without any incident NIR light on the micelles, indicating NIR triggered drug release due to temperature-induced phase transition of PAAP. The micelles disassemble at the temperature of 43°C which can be used to facilitate the controlled release of the encapsulated drug. The cell cytotoxicity study indicates the effect of NIR-induced DOX release inside the cell cytoplasm. The in vivo study also confirmed the efficiency of the combined photothermal therapy and thermoresponsive release of DOX using an 808 nm and 2 W cm^{-2} laser for 5 minutes.[185]

4.1.5 | Dendrimers

Dendrimers are three-dimensional branched macromolecules.[186] They have been introduced in literature in the mid-1980s.[186] In general, dendrimers consist of three parts: a central core, tree-like branching with the core and functional groups at the terminal.[186] These parts are arranged in a layer-by-layer manner, and dendrimers have a well-defined shape, size, and specific molecular weight.[186] The versatility of the terminal functional groups' dendrimers can be used in several biomedical applications, like drug delivery and contrast agent for imaging. Over the year's dendrimers have been synthesized using innovative methods and used for drug delivery. These dendrimers include polyamidoamine (PAMAM) dendrimers, chiral dendrimers, multilingual dendrimers, tecto dendrimers, hybrid dendrimers, amphiphilic dendrimers, peptide dendrimers, etc..[186] Combined with MNPs these dendrimers become powerful drug delivery agents by the use of magnetic fields. The implication of dendrimers is being studied for their potential as drug delivery systems.[187] These dendrimers have abundant functional groups on their surface, have internal cavities, and small size ideal for drug delivery applications.[188] Researchers synthesized triazine modified dendrimer-MNPs.[189] The characterization of these materials also showed good biocompatibility and degradability.[189] These MNP dendrimers were loaded with methotrexate (MTX), a chemotherapy agent and showed high encapsulation capacity.[189] Further proof of effectiveness was demonstrated by doing cytotoxicity studies of these MNP dendrimers in MCF-7, HeLa and Caov-4 cell lines.[189] These results suggested that these MNP dendrimers can be an effective anti-cancer drug carrier.[189] Nigam et al. synthesized MNP with the co-precipitation method and added surfactant (glutamic acid).[190] They then functionalized with polyethylene glycol (PEG) and PAMAM to make the dendrimers.[190] These dendrimers showed useful conjugation (loading efficiency = 55%) with anti-cancer drug EGCG and this magnetically controlled nano-drug delivery system had no adverse effect on cellular proliferation.[190] Additionally, the calorimetric characterization of these MNP-dendrimers also suggests the possible potential for hyperthermia treatments.[190] One more example of PAMAM MNP dendrimer is demonstrated in the literature.[191] These MNP dendrimers were used for combined chemo and phototherapy.[191] The combined therapeutic effect led to higher mortality of cancer cells and in-vitro results suggests that these nanostructures trigger apoptosis.[191] Moreover, the light sensitivity of these MNP dendrimers suggests that they can be used in imaging applications like MRI.[191] Adamantane – β-cyclodextrin – dendrimer-iron oxide-based multifunctional drug delivery system was also introduced in the literature.[192] These complex nanostructures were in two drug carrier models (ibuprofane and MTX).[192] They showed that at physiological pH levels (pH = 7.4) these drugs were released from dendrimers in known kinetic-diffusion models.[192] However, these MNP dendrimer's performance is pH-dependent, so pH based studies were done and characterized systematically.[192] Gadolinium-based PAMAM dendrimer with MNPs were synthesized for better MRI contrast agents.[193] Even though their primary application was for imaging applications, they had acceptable drug loading efficiency and has the potential for non-invasive cancer drug delivery system.[193] PAMAM dendrimer coated MNP have also been synthesized for breast cancer cell apoptosis and pH-sensitive biocompatible carriers.[194,195] However, there are still unsolved problems in this field, including but not limited to: large-scale manufacturing with low-cost, size control, and biocompatibility, etc..[188] Also, further research is needed for in -vivo tumor therapy.[188]

4.1.6 | Meso-porous silica nanoparticles (MSNs)

The pore of meso-porous silica nanoparticles (MSNs) can be used to load various drug or gene molecules in their structures.[196] MSNs with a magnetic core are

being utilized for a targeted therapeutic delivery module for cancer treatment [197,198] and distraction osteogenesis (DO).[199] Jia et al. [199] synthesized magnetic core MSN shell nanoparticles to treat bone defects. The magnetic nanocomposite (MNC) was also evaluated in a rat DO model. The model showed good biocompatibility and excellent ability to promote osteogenesis differentiation of mechencymal stem cells (MSCs).[199] The results from x-ray, mechanical testing, and an immunochemical assay of the rat model suggest successful bone regeneration in the defective bone areas by enhancing osteogenesis differentiation.[199] Moreover, Asgari et al. [197] reported a robust method to synthesize monodispersed core-shell magnetic-MSNs particles for effective delivery of anticancer drug 5-flurouracil. The 16.5 nm magnetic core can be adjusted with varying thickness of 3, 17, and 26 nm of SiO_2 coating. The MNCs have a reported drug loading of about 49 mg g^{-1} of core-shell particles and showed a sustained release profile of particle over 60 hours, with the exception of initial burst release at the first 4 hours of the experiment.[197] To address the challenges associated with initial burst release, Keshavarz et al. [200] reported a novel method to synthesize the nanocarriers by embedding the magnetic core MSNs shell particles into a polymeric material. Polycarboxybetaine methacrylate (PCBMA) prevents the initial burst release of the drug molecules inside the pores of the MSNs. The drug release profile was tested for 125 hours and the drug release profile suggested less than 20% of the loaded drug release in the first 24 hours, indicating reduction of the burst release effect of the nanocarriers.[200] Moreover, the magnetic nanocomposite can also be used to induce magnetic hyperthermia in the tumors. The specific absorption rate (SAR) value of the OA-Fe_3O_4@mSiO_2@PCBMA was found to be 34.79 w g^{-1}.[200]

Peralta et al. [201] reported a hybrid thermoresponsive polymer grafted iron particles MSNs based nanocarriers. The synthesis method of this carrier involves copolymer PNIPAM-co-MPS grafting on the MSNs particles. The 91 nm hybrid nanoparticle is loaded with ferroparamagnetic particles, which facilitates guided targeting and cargo release using an external magnetic field. The nanocarriers showed excellent temperature controlled 'ON-OFF' release of ibuprofen.[201] The release percentage is comeratively lower at low temperature (25°C) because of lower critical solution temperature (LSCT) properties of the grafted polymer chains allows them to be in the extended form by covering the pores of the MSNs. 20% drug release was observed at a 16 hours time period, whereas 80% of the drug was released at an elevated temperature (40°C) where the polymer undergoes a globule transition, facilitating the release of drugs by opening pores of the MSNs.[201] To facilitate temperature control via Brownian and Néel relaxation, Fe_3O_4 nanoparticles can be grafted on graphene oxide (GO) to provide an evenly distributed nanoparticle composite.[202] The hydrophobic Fe_3O_4@GO as well as DOX was loaded to MSNs which facilitated higher surface area for DOX loading, hydrophobicity, and dispersity to the nanocomposite.[202]

4.2 | Magnetic hyperthermia

Magnetic hyperthermia is a non-invasive method for cancer treatment. The working principle of magnetic hyperthermia relies on increasing the temperature of the tumor microenvironment to 41-47°C to either induce apoptosis or to 50°C to induce necrosis via a series of metabolic events which will eventually lead to cell death.[203] Figure 9 illustrates the basic principle of magnetic hyperthermia therapy using a mouse model. An increase in temperature via magnetic hyperthermia can be explained by the Brownian and Néel relaxation of the particles which are exposed to an external alternating magnetic field (AMF).[204,205] AMF can penetrate through tissue which allows us to treat tumors in different positions within patients. Néel relaxation is explained by re-orientation of magnetic particle domains within particles under the influence of an external magnetic field against an energy barrier.[206] The small magnetic domains align themselves parallel to the applied external magnetic field. The rapid alignment is opposed by particle crystalline structure, which generates heat.[203,207] Brownian relaxation is the realignment of particles by physical rotation under the influence of an external magnetic field, which creates frictional heat with the surrounding media of the suspended particles.[208] The heating efficiency depends on the particle size, particle response to an external magnetic field, amplitude (H) and frequency (F) of the applied magnetic field.[209] The inherent resistance of the particle against the applied magnetic field causes heat generation within the particles.[210] The particles magnetic to thermal energy transfer can be quantified as a specific absorption rate (SAR) given by Equation (4):[211]

$$\mathrm{SAR} = \mathrm{C}\left(\frac{\mathrm{dT}}{\mathrm{dt}}\right)\left(\frac{\mathrm{m_s}}{\mathrm{m_m}}\right) \tag{4}$$

where

C = specific heat capacity of the solvent
$\frac{\mathrm{dT}}{\mathrm{dt}}$ = initial slope of the time-dependent heating curve
m_s = mass of the solvent
m_m = mass of magnetic nanoparticles

SAR value depends on the size and shape of the particles, magnetic properties of the particles and amplitude

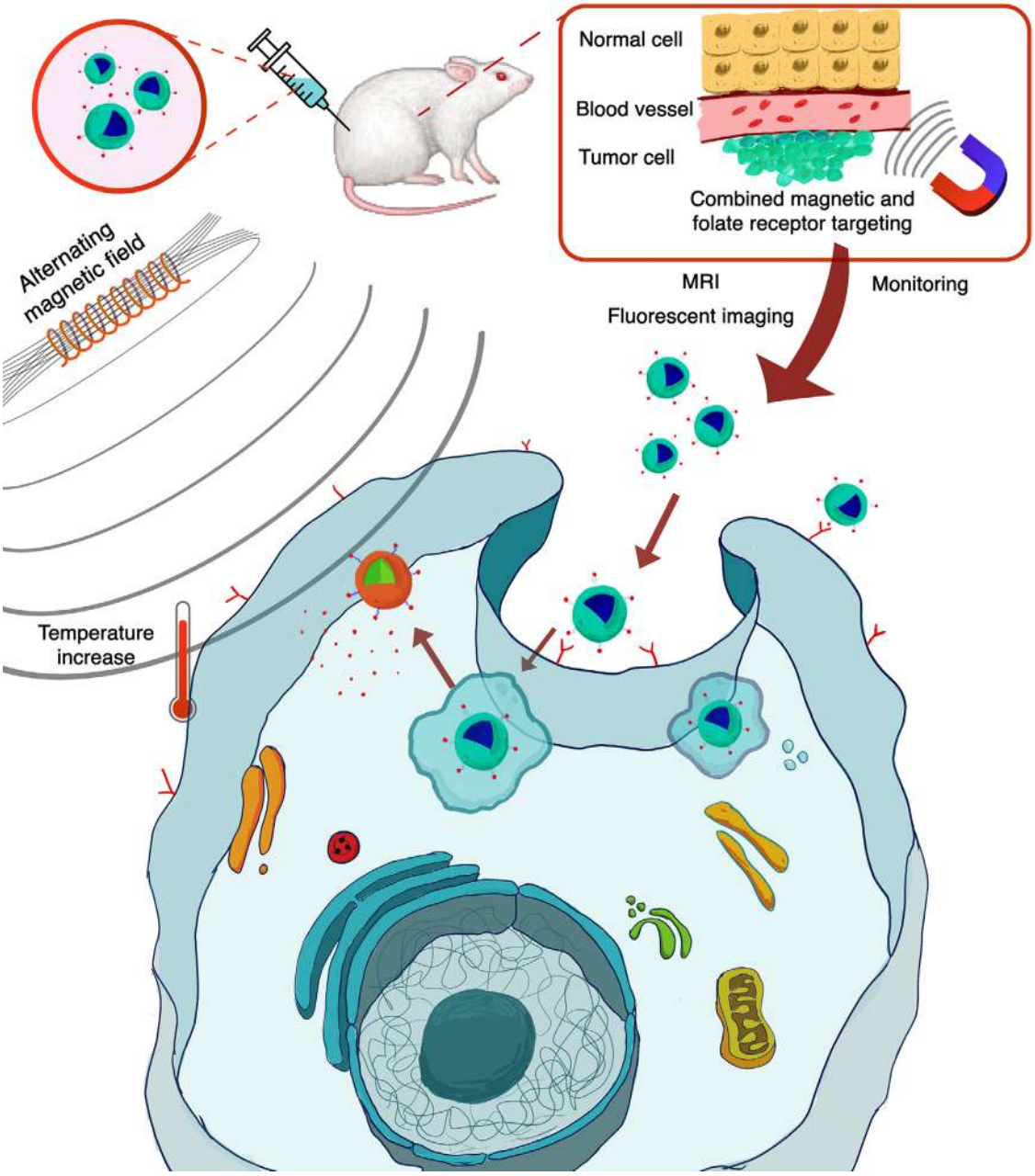

FIGURE 9 Schematic of magnetic synergistic drug delivery and magnetic hyperthermia. The magnetic nanoparticles are accumulated in the tumor site from circulating blood under the influence of a static magnetic field. Upon accumulation to the desired site, alternating magnetic field (AMF) is applied to the magnetic particle accumulated tumor site. The AMF induce Brownian and Néel relaxation which in turn increases the temperature of the tumor microenvironment. The increase in temperature facilitates either apoptosis or necrosis. Temperature responsive ligand release anticancer drugs loaded on the surface of the magnetic particles leading to a synergistic dual treatment

(H) and frequency (F) of the applied alternating magnetic field.[211] Yang et al. [212] reported graphene oxide coated tunable magnetic nanorods for effective hyperthermia in mice models. Among the three different nanorods used, 460, 350, and 250 nm, the 350 nm nanorods have the highest SAR value of 1045 W g^{-1} at 0.2 mg mL^{-1} of Fe concentration. The 350 nm nanorods exhibited sufficient tumor volume reduction in the mice model and exhibited good biocompatibility in the MTT assay.[212]

Lu et al. [158] reported thermosensitive magnetic liposome loaded with Irinotecan (CPT-11) and Cetuximab (CET) (TML-CPT-11-CET) intravenously to tumor-bearing mice, under the influence of magnetic field for 0.5 hours to investigate the effect of an alternating magnetic field (AMF) assisted temperature increase (Figures 10 and 11). Moreover, Manganese doped iron oxide nanoclusters showed promising results in applying magneto-photothermal therapy of glioblastoma.[213] The

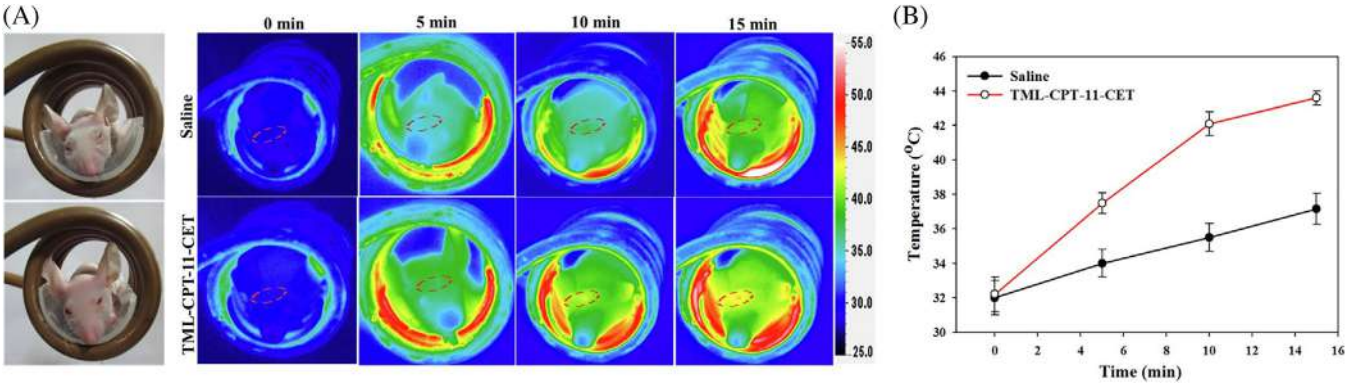

FIGURE 10 Effect of magneto thermal in-vivo after injection of 200 μL of saline or thermosensitive magnetic liposome loaded with CPT-11 and Cetuximab (CET) (TML-CPT-11-CET) intravenously to tumor-bearing mice, under the influence of magnetic field for 0.5 hour. a, Images and heat map (infrared images) of mice in the alternating magnetic field coil. The red circles are assigned the tumor areas which were analyzed. b, Temperature profiles of tumor incubated with saline or (TML-CPT-11-CET) for different AMF exposure time. Data are presented as mean ± SD (n = 5). Reprinted with permission from ref [158]

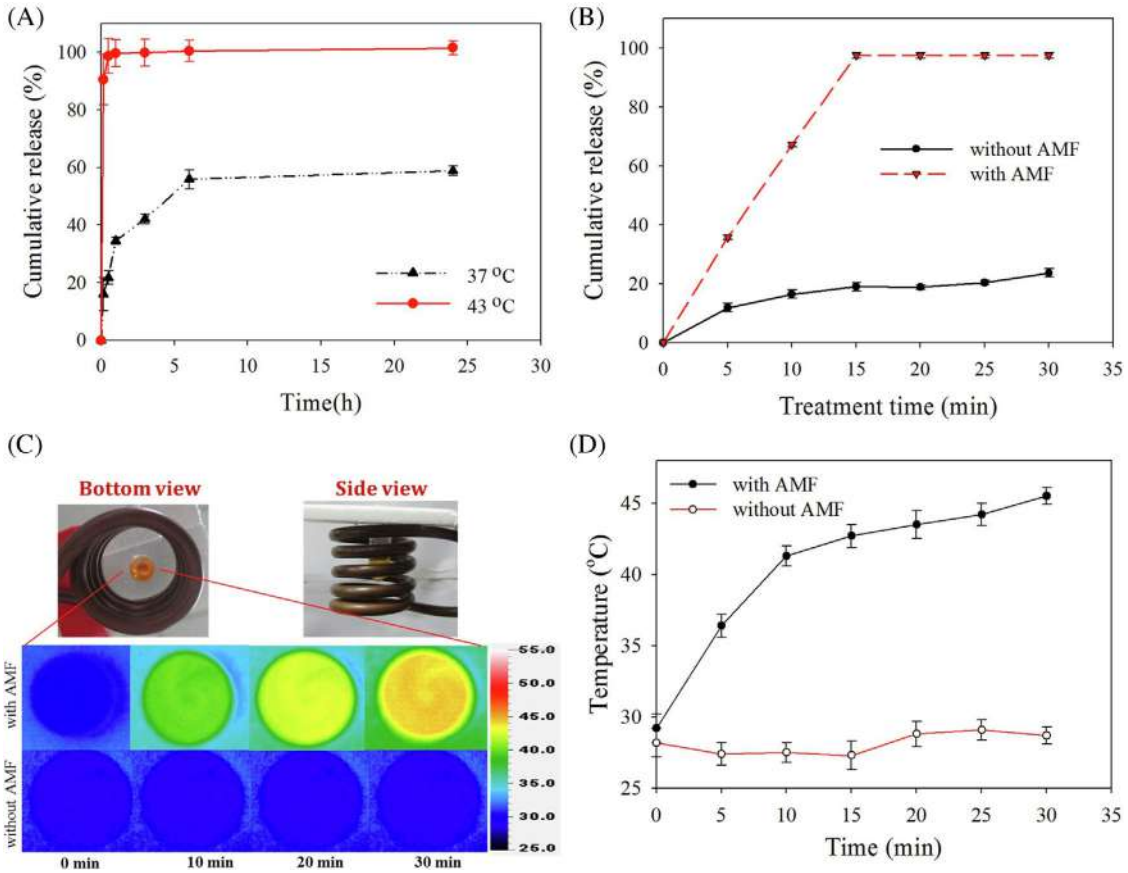

FIGURE 11 Cumulative release profiles of anticancer drug Irinotecan (CPT-11) from thermosensitive magnetic liposome loaded with CPT-11 and Cetuximab (CET) which selectively binds to anti-epidermal growth factor receptor (EGFR) monoclonal antibody expressed by most brain tumors, (TML-CPT-11-CET) in 37°C and 43°C water bath (A) in the presence and (B) absence alternating magnetic field (AMF) treatment. C, Experimental setup and heat map at a different time point in the presence and absence of AMF (D) peak temperature profiles with and without the influence of AMF. Reprinted with permission from ref [158]

high SAR value of the particles (~600 W g^{-1}) facilitates efficient hyperthermia therapy. Hyperthermia therapy along with photothermal therapy demonstrated remarkable efficiency in glioma cell death which increase the reactive oxygen species (ROS) level in the cancer cells, eventually leading to ROS mediated apoptosis through mitochondrial pathway.[213] Anticancer drug DOX loaded thermoresponsive drugs showed dual modality of controlled release of drug combined with magnetic hyperthermia treatment of human ovarian cancer cell line (SKOV-3).[214] These unique particles were synthesized by using 10 nm citrate capped Fe_3O_4 nanoparticles with a thermoresponsive polymer having a lower critical solution temperature of 38°C. The SAR values of the reported particles with a different chain length of polymer varied from ~12.6 to ~45.7 W g^{-1} in culture media.[214] Aminocellulose grafted, niclosamide loaded and PEGylated branched 107 nm magnetic nanoparticles are 7 times more effective in killing colon cancer cells using hyperthermia.[215] FDA-approved niclosamide works as an anticancer agent by inhibiting intercellular pathways which work along with hyperthermia to facilitating combined therapy against colorectal cancer cells and eventually can be used in the treatment of different cancer cells.[215]

Kaushik et al.[216] reported a biosynthesis mechanism to synthesize nanoparticles inside tumor cells to induce magnetic hyperthermia. Briefly, the investigators exposed the cancer cells to $FeCl_2$ and zinc gluconate. After sufficient uptake of the precursor, the reactive oxygen species (ROS) inside the cancer cells engaged in the glycolytic pathway to biosynthesize iron oxide and ZnO. Figure 12 illustrates the selective biosynthesis of SPIONs and ZnO to selectively induce hyperthermia in cancer cells, leaving the healthy cells unaffected. The cellular environment experienced 4°C–5°C elevation in temperature as a result of 30 minutes exposure to an alternating magnetic field.[216] As cancer cells have a higher ROS level than normal healthy cells, particle synthesis was not carried out in regular healthy cells due to lower H_2O_2 levels. Hence the mechanism is inherently targeting only cancerous cells and once the biosynthesis of the particles is done, the particles can be utilized to induce cell death using magnetic hyperthermia.[216]

Increased levels of ROS can be utilized to induce cell death via increasing cellular ROS levels and blocking the cell's natural antioxidants.[217] For example, cells were exposed to sodium nitroprusside (SNP), which acted as an exogenous reactive oxygen species generator and diethyldithiocarbamate (DDC) was selected as a superoxide dismutase 1 inhibitor.[217] DDC was loaded with a magnetic core nanoparticle ($ZnFe_2O_4$), to induce magnetic hyperthermia to breast cancer cells. The particles were incorporated with iRGD peptide moieties to effectively target integrin enriched malignant tumor cells (MDA-MB-231).[217] Wu et al. [218] reported magnetic hydrogel nanoenzyme to induce the synergistic effect of hyperthermia and the generation of ROS. The Fe_3O_4 nanoenzyme complex exerts peroxidase in the complex, which is eventually catalyzed to generate hydroxyl radical by Fenton reaction. Hydroxyl free radical further damage heat shock protein 70 (HSP 70), increasing the hyperthermia effect on the tumor.[218] An AMF was applied to the samples to induce magnetic hyperthermia, resulting in an increase of temperature in the tumor microenvironment to 42°C.[218] The hydrogel helps the particles diffuse through the tumor due to the shear thinning of the hydrogel matrix. Moreover, animal studies in nude mice model suggests that, magnetic hydrogel can be successfully used to prevent breast cancer recurrence.[219] New generation ferromagnetic vortex domain iron oxide nanorings (FIOVs) were used to obtain a higher heat induction efficiency, with significantly high specific absorption rate (SAR) value (higher than 3000 W g^{-1}) compared to the same concentration of conventional superparamagnetic iron oxide nanoparticles (SPIONs).[219] This magnetic hydrogel nanocomposite, once administered into the animal tumor model, is exposed to the AMF to induce hyperthermia in the region of interest for postoperative recurrence prevention. Although magnetic hydrogels are being reported for effective magnetic hyperthermia, recent studies suggest that the heating efficiency of magnetic nanoparticles decreases with gradual immobilization in the hydrogel matrix.[220] The SAR value in the hydrogel matrix can experience a maximum drop of 35% compared to that of magnetic particles suspended in water for a particle mesh size between 25 and 12.8 nm.[220] The decrease in the SAR value is due to impeded rotation of the magnetic particles. As mentioned earlier, the magnetic particles reorient themselves parallel to the applied magnetic field. In the presence of a more viscous matrix such as a hydrogel, the particles Brownian relaxation is strongly inhibited. In order to maximize the heating efficiency of the particles for cancer treatment, researchers need to address the gap between calculated SAR values and actual SAR values in the tissue matrix.

4.3 | Magnetic bioseparation

Magnetic bioseparation utilizes the unique magnetic properties of magnetic particles to separate various biological molecules under the influence of an external static magnetic field. DNA, proteins, antigens, and antibodies need to be purified from their library before their usage in any biomedical application.[221] For instance, DNA detection [222] and separation [223] is a vital step before the polymerase chain reaction (PCR) step to evaluate specific

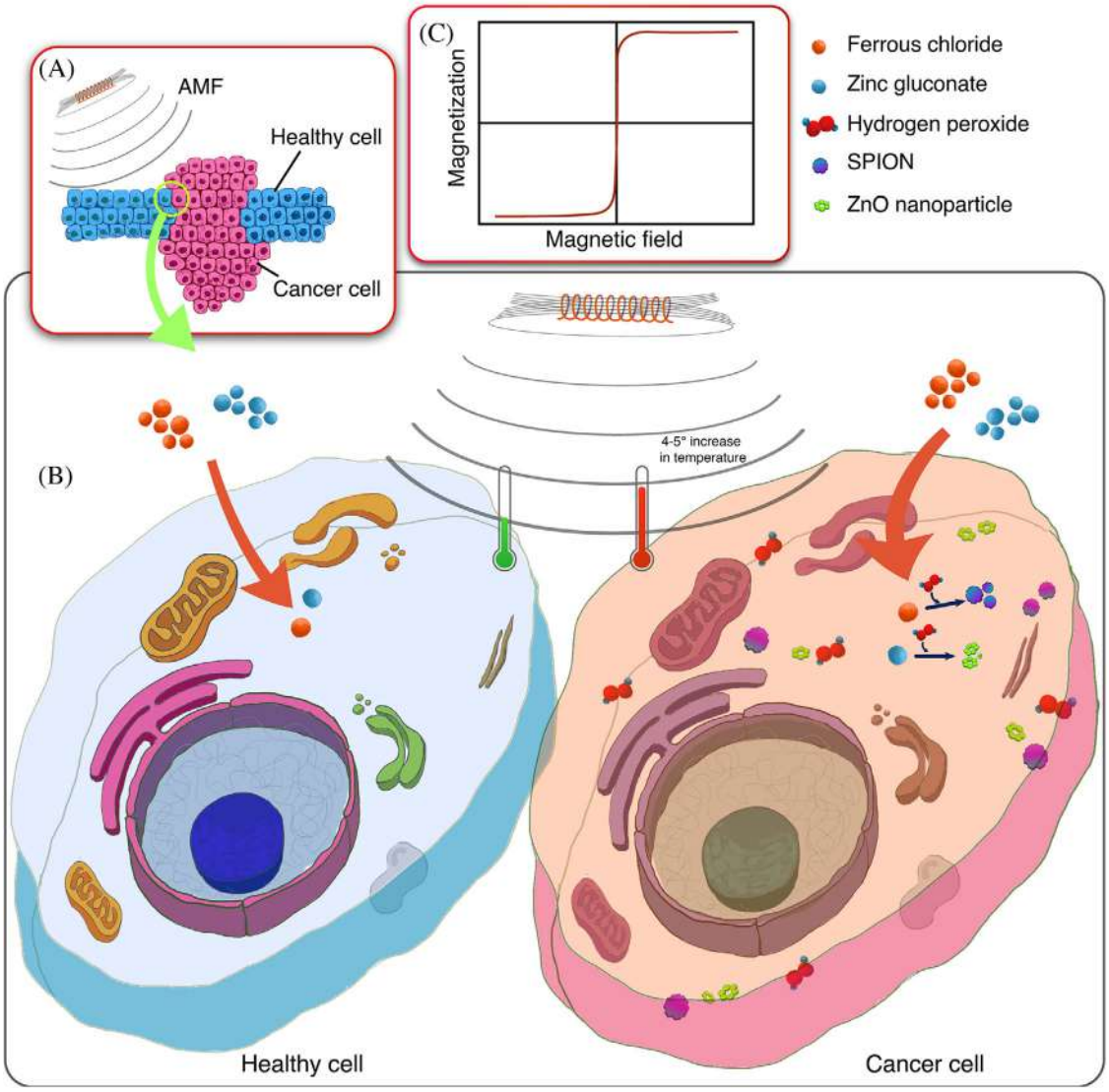

FIGURE 12 Biosynthesis of SPIONs. A, Co-existing of normal healthy cells and cancerous cells. B, Ferrous chloride and Zinc gluconate are introduced to healthy cells and cancerous cells as a precursor of SPIONs and ZnO nanoparticle. The healthy cells do not contain H_2O_2, an essential element for the reaction to form SPIONs and ZnO; hence upon exposure to an alternating magnetic field (AMF), there is no change in the cellular temperature. However, cancerous cells contain a high concentration of H_2O_2, which catalyzes the nanoparticle precursors to SPIONs and ZnO, resulting an increase of 4–5°C in the cellular microenvironment upon exposure to AMF. This selective increase in temperature induces hyperthermia in cancer cells without disturbing the regular functionality of adjacent healthy cells. C, Magnetization curve of SPIONs

gene expression. Hei and Cai [119] reported a method to purify and concentrate RNA of novel coronavirus (SERS-CoV), which is then amplified PCR to detect the genome sequence of the viral nucleic acid. Schwaminger et al. [224] reported a bare iron oxide nanoparticles (BIONs) to separate a short peptide ($Glutathione_6$) tagged proteins (Green fluorescent protein) (Figure 13). Using the tag peptide, the Green fluorescent protein (GFP) can be recognized and separated from a crude cell lysate (Figure 14). 0.2 g proteins bind to per grams of bare magnetic nanoparticles, which was recovered by using a citrate buffered system.[224] Later, Schwaminger et al. [118] again reported hexahistidine (His_6) tagged GFP protein separation using BIONs (12 nm), the purity of the recovered proteins are reported as 91% from *Escherichia coli* cell lysate. In addition, Bovine hemoglobin (Bhb) can be purified and removed by using 3-methacryloxypropyltrimethoxysilane (MPS) coated Fe_3O_4-SiO_2 nanoparticles.[225] Once the bovine hemoglobins attach to the particles, a static magnetic field separates the bovine hemoglobin from the cell lysate and the elution process is performed to recover the Bhbs. The equilibrium adsorption capacity was reported as 87.7 mg g^{-1} of particles.[225]

Tang et al. [226] reported a Fe_3O_4@SiO_2 core-shell magnetic particle surface-modified with monoamine oxidase-A (MAO-A) monoclonal antibody to isolate

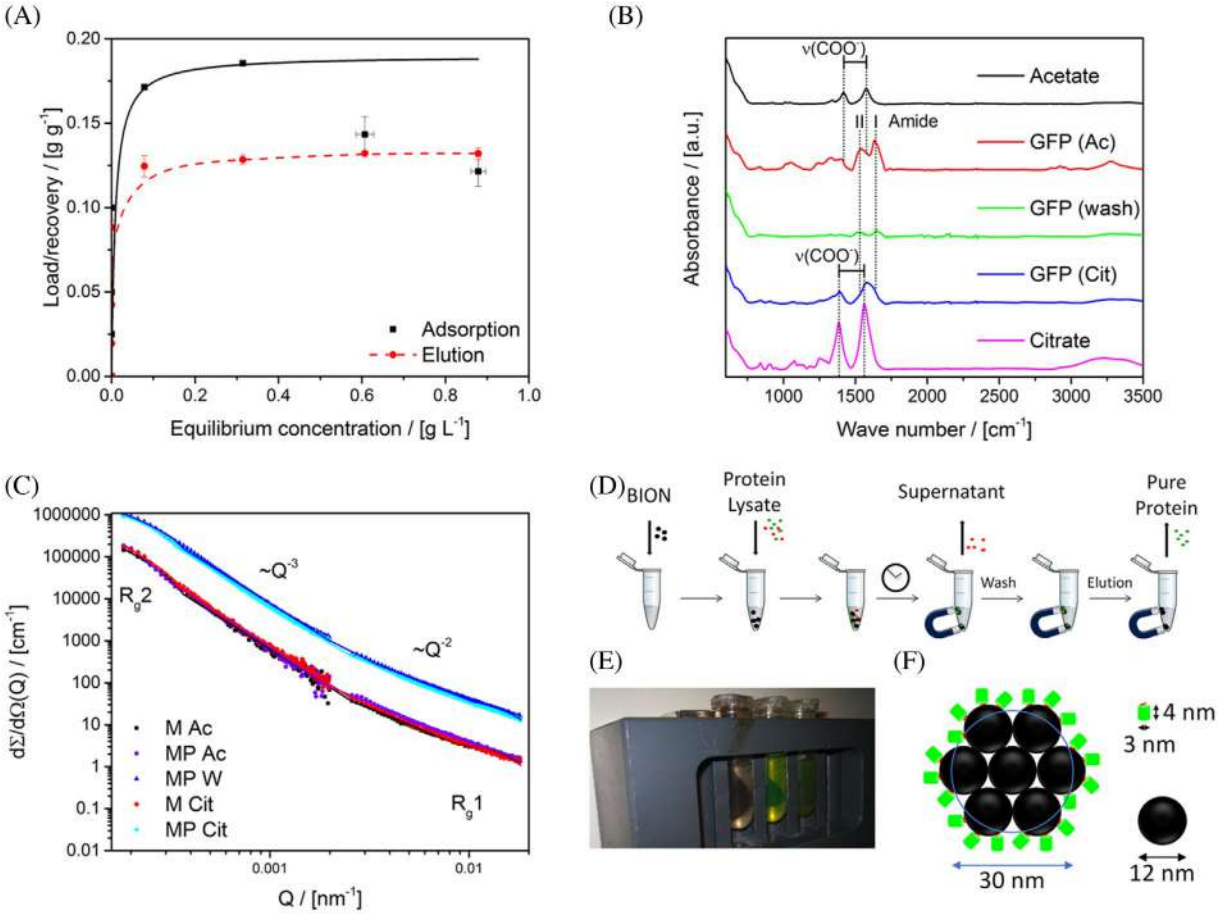

FIGURE 13 Adsorption and recovery isotherm of purified Glu6-GFP on bare iron oxide nanoparticles (BIONs). A, Adsorption isotherms of Glu6-GFP on nanoparticles (1 g L^{-1}) in acetate buffer. B, Attenuated total reflection infrared (ATR-IR) spectra of Glu6-GFP incubated with magnetic nanoparticles in acetate, washing, elution in citrate and references. C, Small-angle neutron scattering (SANS) spectra of purified Glu6-GFP (P) incubated with nanoparticles (M) in acetate (Ac), washing (W), elution in citrate (Cit). D, Schematic of experimental procedure (E) image of separation process (F) schematic of the binding capacity of BIONs. Reprinted with permission from ref [224]

mitochondria from biological samples. The purity of the isolated mitochondria was reported as 90% from an equal number of HepG2 and HeLa cell lines. Magnetic separation has been utilized for different cell separation from a biological sample.[227,228]

Recently, Ivanova et al. [227] reported a magnetic separation based technique to separate cancer stem cells (CSCs) from normal healthy cells. CSCs have tumorigenic potential and can be resistive to chemotherapy. Ivanova et al. developed a lentivirus-based reported SORE6, which can identify gene expression from embryonic stem cell factor SOX_2 and OCT_4.[227] The lentiviral reporter molecules can be potentially attached to magnetic particles, which will scavenge for the cells expressing gene factor SOX_2 and OCT_4, which can be utilized by establishing a constant magnetic field to separate the CSCs from normal healthy cells (Figure 15).

In addition, magnetic particles can be used to remove heavy metals from the blood stream.[229] Figure 16 illustrates the schematic process of heavy metal removal from blood. Succimer (meso-2,3-dimercaptosuccinic acid, DMSA) coated iron oxide nanoparticles (MNP@DMSA) can be used to remove toxic heavy metals such as Pb and Cd from the blood stream., The adsorption capacity of the MNP@DMSA in blood samples, are found to be 0.35 mg g^{-1} for Pb and 0.29 mg g^{-1} for Cd (Figure 17).

Dantsis et al. [230] reported the use of 20 nm superparamagnetic particles conjugated with anti-signal-regulatory protein alpha (SIRPA) cell surface monoclonal antibody to direct human stem cell-derived cardiomyocytes within 3D collagen hydrogel to develop customized cardiac tissues with the help of an external magnetic field.[230] The applied magnetic field orients the cells along the magnetic field direction without the help of mechanical support. The use of magnetic derived controllable orientation and condensation of cells is unique and robust compared to the conventional mechanical trap of the cells in a casted mold with additional stretching of the mold set

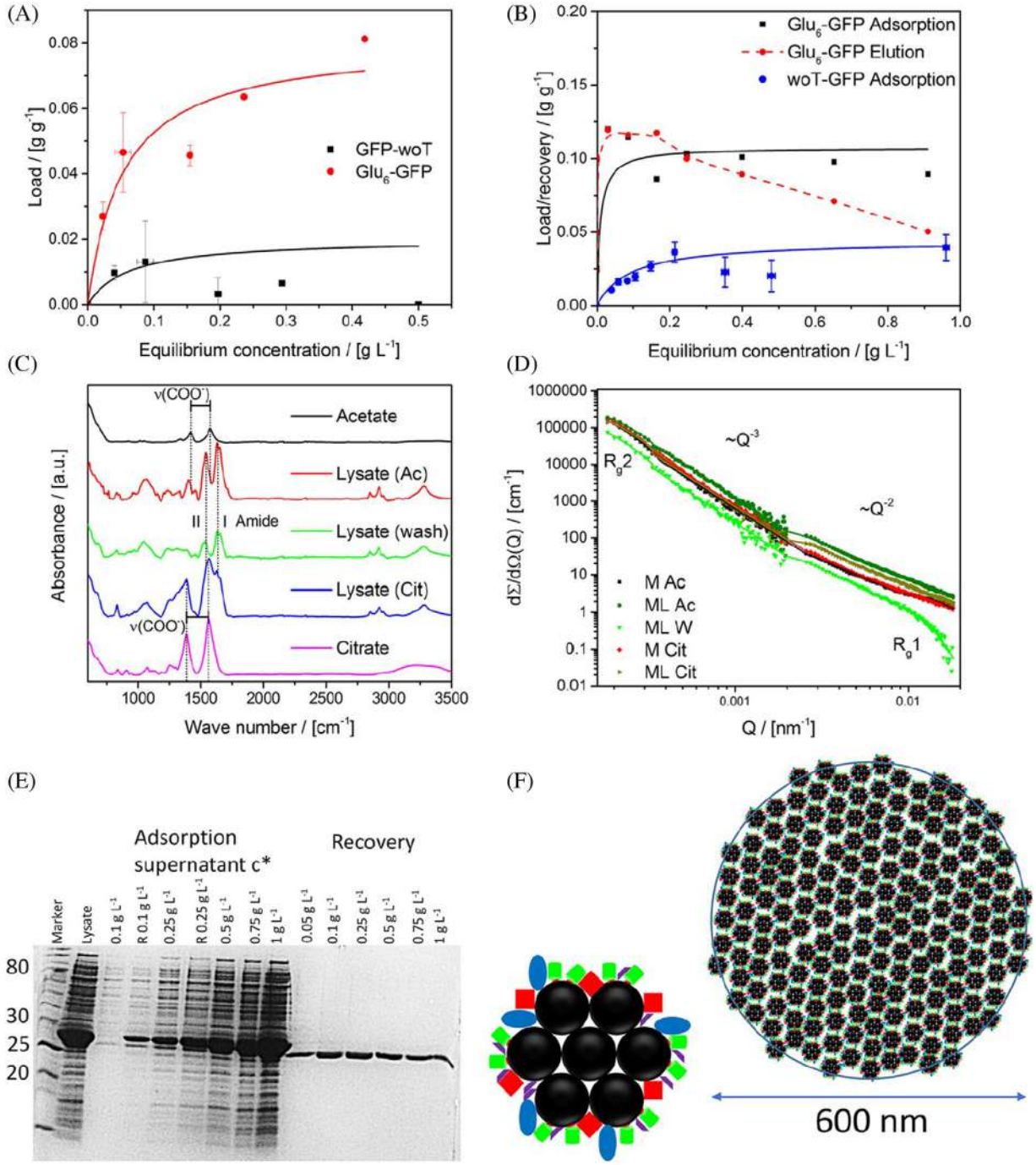

FIGURE 14 Purification of Glu6-GFP with bare iron oxide nanoparticles (BIONs) from cleared cell lysate. A, Adsorption behavior of 1:1 mixture of Glu6-GFP and woT-GFP on nanoparticles. B, Adsorption isotherms under similar conditions of Glu6-GFP and woT-GFP on BIONs, respectively. C, Attenuated total reflection infrared (ATR-IR) spectra of Glu6-GFP containing cleared cell lysate incubated with magnetic nanoparticles in acetate, washing, elution in citrate and references. D, Small-angle neutron scattering (SANS) intensities of lysate containing Glu6-GFP (L) incubated with nanoparticles (M) in acetate (Ac), washing (W), elution in citrate (Cit). E, A gel image of cell lysate and the supernatant of different lysates incubated with magnetite nanoparticles (1 g L^{-1}) for 1 hours. Sample denoted with R letters were not incubated with nanoparticles. F, Schematic illustration of the agglomeration behavior and binding of the protein-BIONs system. Reprinted with permission from ref [224]

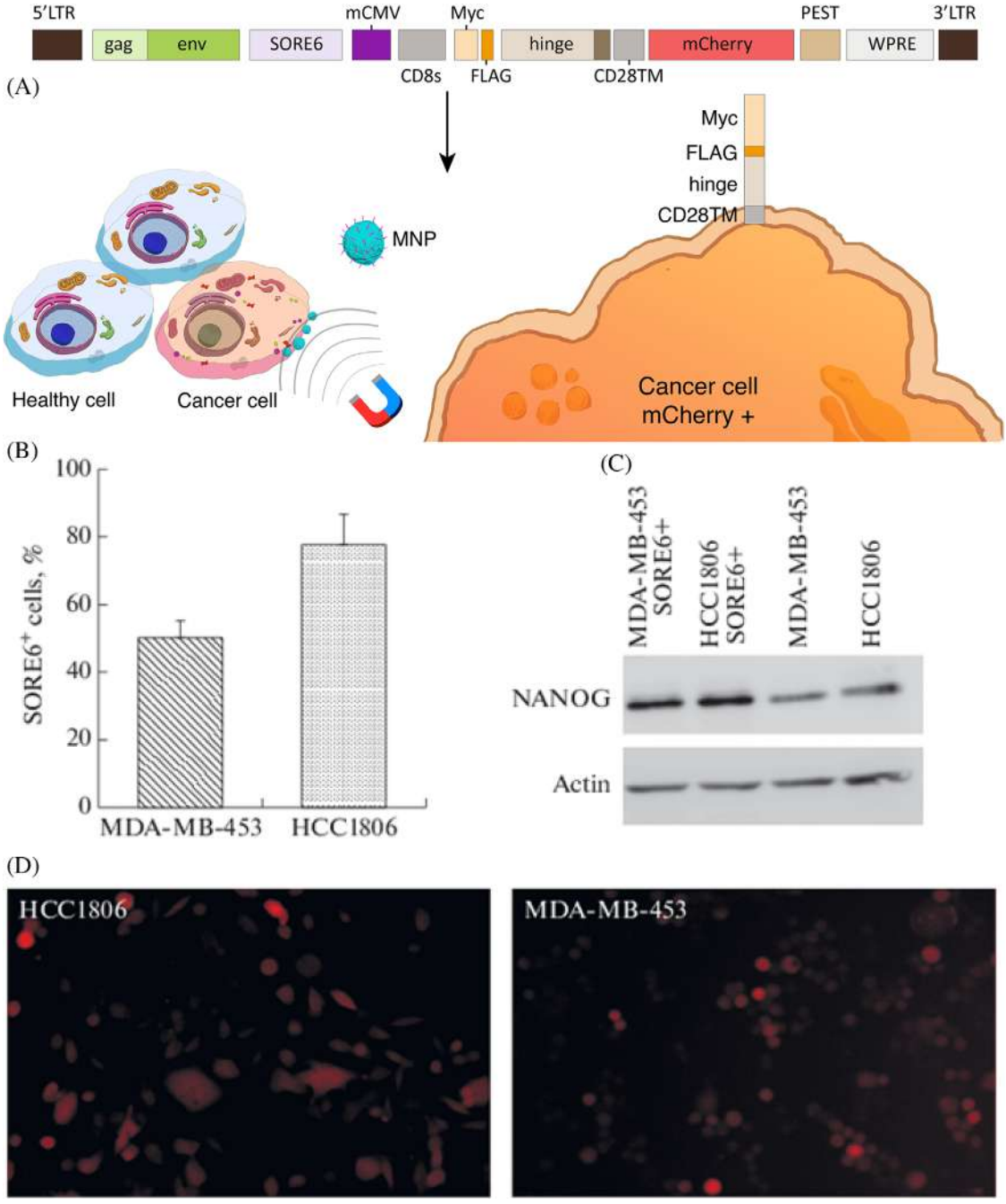

FIGURE 15 A, Scheme of the modified lentivirus-based construct obtained via cloning. B, Localization relative to the cell membrane is shown for the protein products resulting from transcription and translation of the lentivirus-based reporter construct, which is active in cancer stem cells. Accumulation and degradation of mCherry make it possible to visualize the cells that express the SOX_2/OCT_4 stem cell factors in the total cell population. The Myc-FLAG-hinge peptide sequence is anchored in the cell membrane via the CD28 transmembrane domain, and cells that express the construct are possible to select by magnetic separation; long terminal repeat is denoted as LTR; group antigens are presented as a gag; envelope protein is denoted as env; woodchuck hepatitis virus posttranscriptional regulatory element is denoted as WPRE. B, Contents of cells expressing SOX_2/OCT_4 in the MDA-MB-453 and HCC1806 cells transduced with the modified SORE6 reporter. C, The NANOG level in SORE6+ cells selected using the reporter is higher than in the total population. D, Microphotographs of HCC1806 and MDA-MB-453 cells transduced with the SORE6 reporter were obtained with a ZOE fluorescence microscope (BioRad). Reprinted with permission from ref. [227]

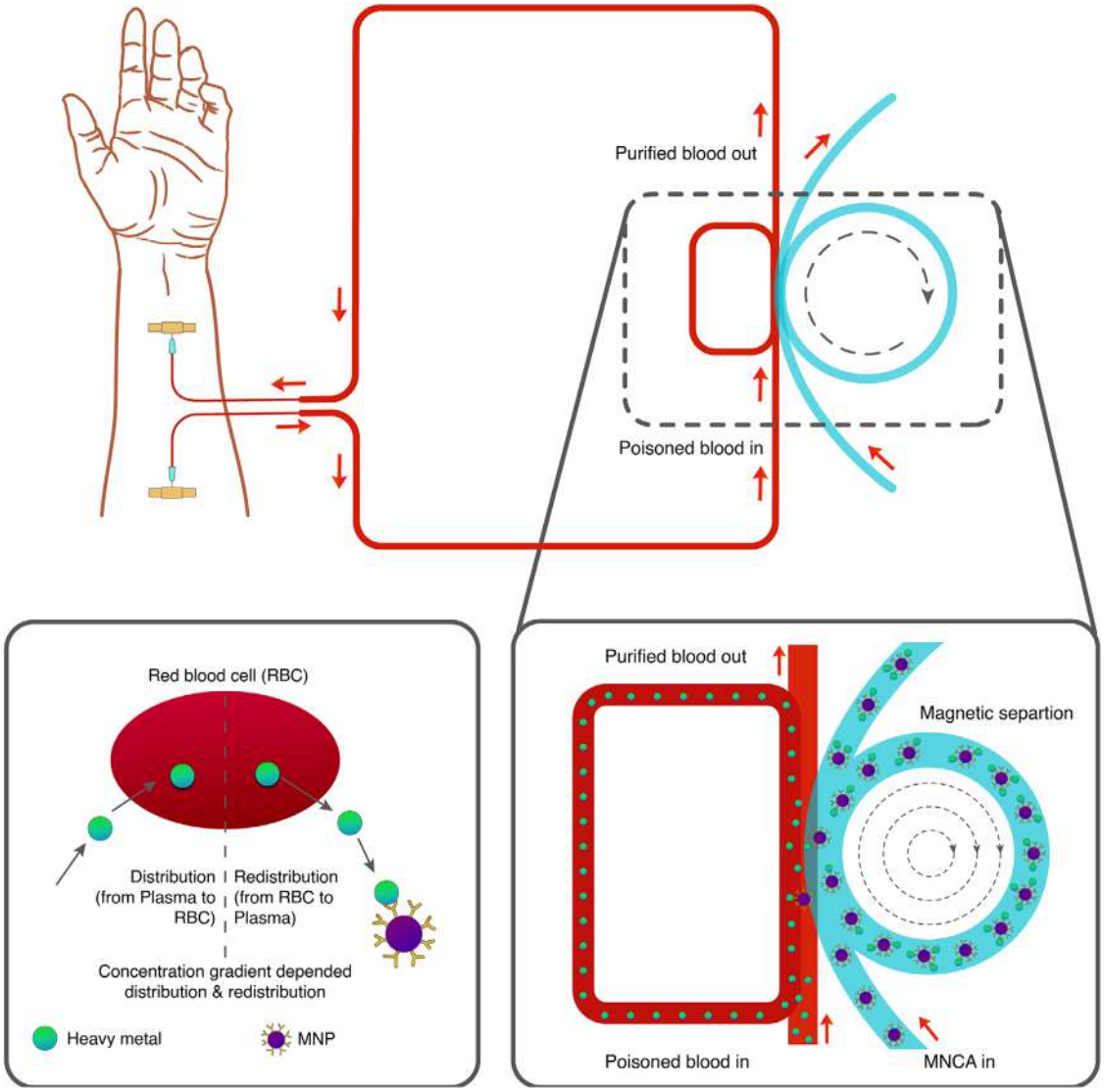

FIGURE 16 Schematic of heavy metal removal from blood by using a magnetic separation technique

up to direct the 3D structure into different shapes.[230] The geometry of the microstructure cardiomyocytes is controllable by altering the applied magnetic field and flux density. Dantsis et al. reported that with relatively low external applied magnetic fields (0.1-0.2T), the cardiac cells within collagen hydrogels assemble and direct them along the field lines to construct custom 3D geometries. Internalized magnetic nanoparticles in the cardiomyocytes cells facilitated magnetic resonance imaging (MRI) imaging of the 3D microstructures confirmed different geometrical shapes.

Additionally, Guo et al. reported superparamagnetic nanoparticles conjugated in polyacrylamide (PAA) hydrogels to detect adenosine triphosphate (ATP).[231] Briefly, modified the amino coated hydrophilic MNPs with a modified carboxyl group was used, which acted as a primer for acrylamide modified hairpins. The acrylamide hairpin on the surface of the MNPs facilitates the formation of PAA through hybridization. This hydrogel conjugated nanoparticles strips in the presence of ATP because of specific and selective conjugation of ATP and PAA.[232] As a result, part of PAA coated MNP is exposed and is detected by Low Field- Nuclear Magnetic Resonance (LF-MNR) via T_2 relaxation signal. These unique particles can be used to detect cancerous cells, as cancer cells use an excessive amount of ATP and NADH as energy sources.[232] Tumors require a high level of ATP for cell proliferation and metastasis.[233,234] A high level of ATP is indicative of cancerous cells and can be detected and quantified using the PAA coated MNPs. Recent studies reported that ATP and NADPH coated iron oxide particles have exhibited specific cancer targeting.[234] This non-invasive and robust method can be used to define tumor boundaries and outline in pre and post-surgical procedures.

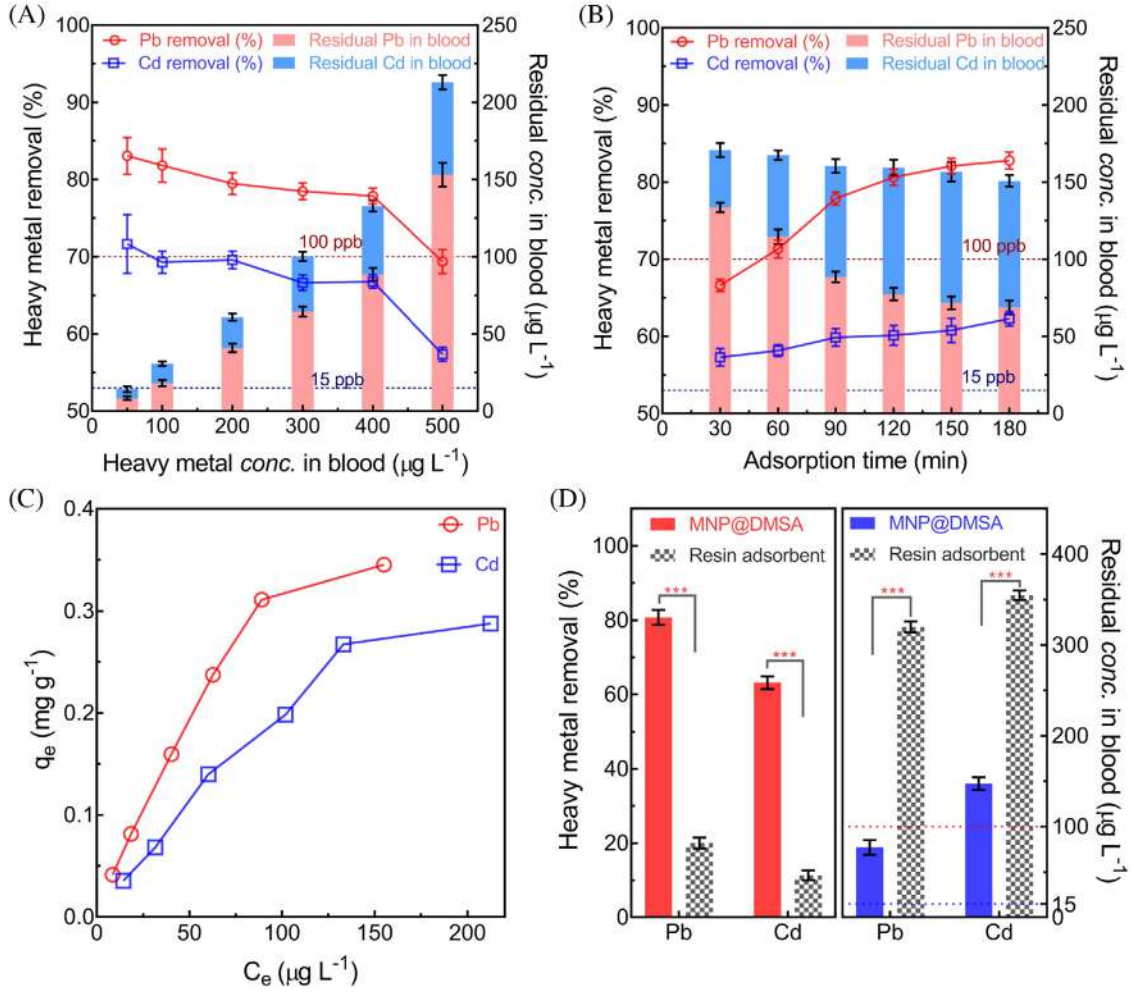

FIGURE 17 Removal metric of poisonous heavy metal from the blood sample. A, The removal efficiency of heavy metal with respect to different heavy metal concentrations in blood (B) Time-dependent adsorption of Pb and Cd. C, Adsorption isotherms of heavy metal removal from blood. D, Comparison of removal performance between MNP@DMSA and classical resin adsorbent. Concentrations of meso-2,3-dimercaptosuccinic acid (DMSA) coated MNPs, and classical resin adsorbent were 1.0 mg mL^{-1}, initial heavy metal concentration was 400 μg L^{-1}, and the temperature was 37.5°C. (n = 5, *** means $P < 0.001$). Reprinted with permission from ref [229]

4.4 | Imaging modality

The unique properties of magnetic particles can be utilized as an imaging modality to image biological sample of interest. To date, several imaging techniques, including but not limited to magnetic resonance imaging (MRI), magnetic particle imaging (MPI), computed tomography (CT), and positron emission tomography (PET) are being utilized in the biomedical field to diagnose and detect diseases in tissues. In this section, usage of these imaging modalities and their recent progress in the biomedical field is discussed.

4.4.1 | MRI

Magnetic nanoparticle facilitated MR imaging is useful in early diagnosis of atherosclerosis,[235] MRI guided photodynamic therapy,[236] stem cell labelling,[237] and cancer diagnostics.[238] Recently, Bai et al. [239] developed a dual-modal T_1-T_2 MRI contrast agent to image rabbit hepatic tumors. Briefly, 5 nm Fe_3O_4 particles were loaded into Bovine serum albumin (BSA) protein to prevent particle aggregation and prolong the circulating time in blood vessels. Smaller nanoparticles have increased T_1 enhancement ability, whereas the T_2 enhancement ability is dominant in the aggregation state of the same particles because of higher r_2 value leads to facilitating T_2 contrast image and weakening of T_1 weighted contrast.[239,240] Nanoparticles are uptaken differently in hepatic parenchyma and tumors.[239] Thus, once uptaken, the aggregated nanoparticles show a T_2 weighted signal compared to the particles in the tumor site with a slow uptake rate due to the EPR effect.[239,240] This difference in uptake rate in different tissue leads to facilitating different mode of contrast; thus,

comparing the T_1 and T_2 mode of the images, it is possible to differentiate hepatic parenchyma and tumor and accurately diagnose cancer.[239] It is reported that, higher cluster and aggregation state of the particles is beneficial for a higher T_2 signal.[241]

Furthermore, Salunkhe et al. [242] used 10 nm magnetic nanoparticle with negatively charged pluronic acid grafted to load DOX electrostatically using EDC-NHS chemistry. The nanocomposites were able to be successfully uptaken in MCF7 cells. The dipolar interaction of magnetic moment and protons presented in the cytoplasm of water enhanced T_2 weighted MR image.[242] The intensity of the darker image is directly proportional to the concentration of DOX@PM@SPIONs nanocomposite.[242] In addition, Magnetic particles are being used in cell tracking and cell proliferation to track dendrite cell migration using RNA loaded magnetic liposome.[243] The intensity of T_2 weighted image directly correlates to the dendrite cells in the lymph node, which indicates an early prediction of anticancer response to cancer treatment.[243] Similarly, Iron doped calcium phosphate nanoparticles (nCP:Fe) can be used to track stem cells in the brain using MRI.[244] The in vitro study showed that 100 μg mL^{-1} of nCP: Fe labeled mesenchymal stem cells can provide detectable T_2 contrast without inhibiting its proliferation, viability and ability to differentiate. Although another study found that while magnetic field exposure does not inhibit stem cell differentiation and proliferation, magnetic field exposure can change the development of stem cells.[245] Short term exposure (2 days) with 7 Hz and 0.5 mT intensity increase adipogenesis, whereas long term (7 days) continuous or intermittent exposure facilitates osteogenesis.[245] In-vivo study in rat brain cells confirmed the presence of cells even after 1 month of administration of nCP: Fe labeled mesenchymal stem cells using T_2 weighted dark contrast.[245] The lower r_2 value of the nanocomposite did not impair the detectable range of the nanocomposite; thus, nCP: Fe can potentially be used in stem cell tracking using an MRI contrast agent in vivo.

4.4.2 | MPI

Magnetic particle imaging has gained much attention in recent years due to its high signal to background noise ratio, zero background signal from tissues,[246] high temporal resolution (milli seconds), high spatial resolution (less than 1 millimeter) and high sensitivity (μg).[247] Magnetic particle imaging consists of two strong magnets placed at a distance where the orientation of strong magnetic dipole direct the magnetic force field in a specific way to create a field free point (FFP), where no magnetic force field is present.[248] The FFP point is not fixed and can be changed by varying relative position of the sample of interest to the position of applied magnetic field. In the presence of an external alternating magnetic field, any tracer particle present in the FFP undergoes magnetization process which induces current in a secondary receiver coil.[249] The sharp zero points at the center of magnetic setup is surrounded by a consistent and strong magnetic field gradient. Hence, all other particles outside the FFP point exhibits different magnetization signal compared to the particles present in the FFP. Magnetic particle imaging exploits the magnetization property of magnetic nanoparticle-based tracer particles.[250] The magnetic properties of the tracer particles are equally important as of the hardware setup for this imaging modality. SPIONs are excellent choices as tracer particles as they exhibits non linear magnetization and superparamagnetic properties.[247] The characterization of the SPIONs are done by Langevin magnetization, where magnetization (M) is represented as a function of magnetic field $H(t)$, and represented by the following Equations (5) and (6).

$$M(H(t)) = m_s \left[\coth(\alpha H(t)) - \left(\frac{1}{\alpha H(t)}\right)\right] \quad (5)$$

$$\alpha = \frac{\mu_0 m_s}{k_B T} \quad (6)$$

Here,

μ_0 = permeability of free space,
m_s = saturation magnetic moment,
k_B = Boltzmann constant, and
T = temperature.

The m_s is given by the following Equation (7),

$$m_s = \frac{\pi d_c^3 M_s}{6} \quad (7)$$

Here,

d_c = magnetic core diameter,
M_s = saturation magnetization of the tracer SPIONs.

Two techniques are followed to obtain MPI signals, harmonic space, and x-space.[251] In both methods, the generated signal is based on the magnetization and selective saturation of the tracer particles.[251] All the particles except the FFP points are in magnetization saturation under the influence of the permanent magnets. This allows only the particle at FFP point to respond to a time-varying magnetization field superimposed in the existing magnetic force field. As all other particles are in saturation, this time-varying magnetization in the FFP point induces

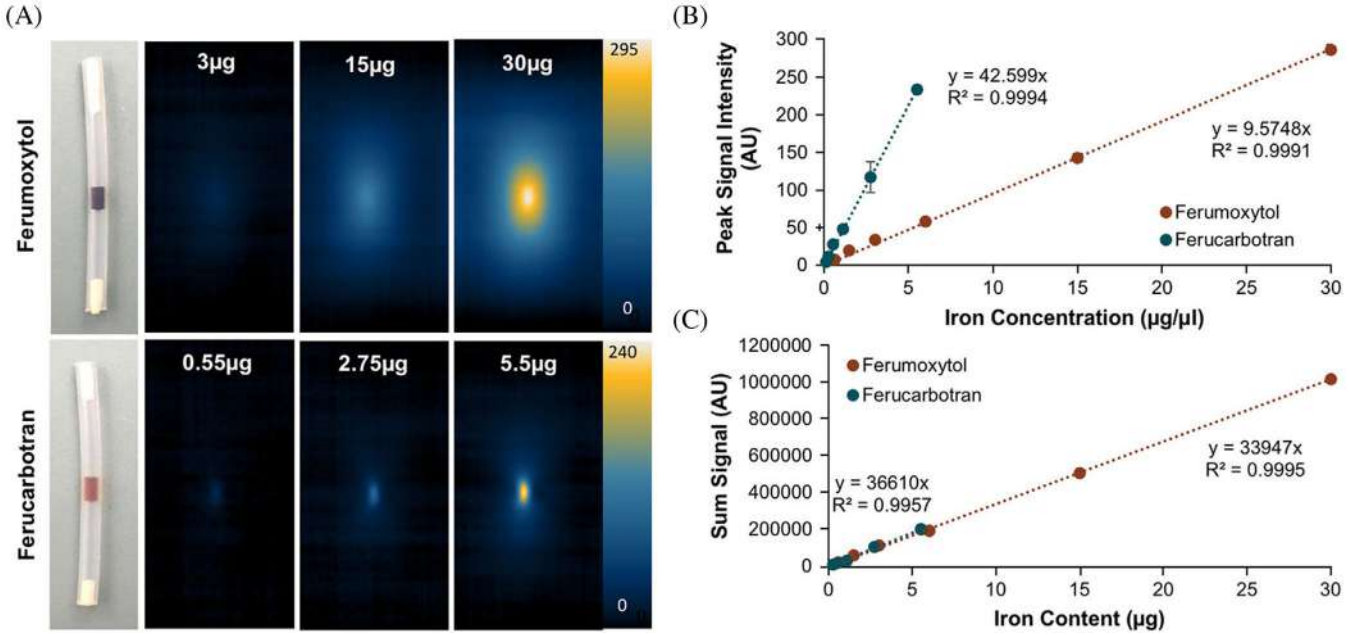

FIGURE 18 MPI properties of FDA approved ferumoxytol and ferucarbotran. A, MPI images with varying concentrations of ferumoxytol and ferucarbotran in 1 μL of PBS (=1 μm^3). Ferumoxytol exhibited a radiant effect with an MPI signal that swelled beyond the test tube boundary threshold, over an area of 5 mm^3. Whereas ferucarbotran showed less radiant effect with a signal spread over an area of 1 mm^3. B, Linear correlation with R_2 value of 0.9994 between peak MPI signal and Fe concentration for both nanotracers. A higher slope for ferucarbotran over ferumoxytol indicates better sensitivity of the MPI technique to detect ferucarbotran compared to ferumoxytol. C, Calibration data with a linear correlation ($R_2 = 0.995$) for total iron content to MPI sum signal for both tracers. Reprinted with permission from ref [254]

a voltage that is received by a detector coil.[249,251,252] As mentioned earlier, the FFP point is not fixed and is relative to the position of outside magnetic poles and sample position; by varying their relative distance, the FFP is rastered over the sample to obtain the signals for each point in the samples which is later reconstructed to generate a heat map of tracer position.[253] Figure 18 exhibits the image constructed with FDA approved nanoparticles ferumoxytol and ferucarbotran at different concentrations. Linear correlation with the iron content and peak signal intensity was observed for both nanotracers.[254]

Nejadnik et al. [254] Reported quantitative magnetic particle imaging of transplanted stem cells in a mouse model. The MPI images reported quantitative information about the transplanted stem cells, which was not attainable using MRI. The MPI data reported the iron content of tracer correlated to the transplanted Mesenchymal stem cell number in the calvarial defects in the mouse model (Figure 19). Yu et al. [255] studied the potential use of 90 nm magnetic particles for MPI to detect cancer in the thymus gland removed nude rats. The rats are xenografted with breast tumors with a subcutaneous implant of MDA-MB-231-luc cells. MPI tailored SPIONs were injected intravenously to two different groups at different concentrations. Group A with implanted tumors in lower mammary fat pad received 15 mg kg^{-1}, whereas group B with implanted tumor at right lower flank received 5 mg kg^{-1} of tracer SPIONs. MPI imaging of these two groups showed clear accumulation of the particles in the xenografted tumor region,[255] which is explained by enhanced permeation and retention (EPR) theory.[256] According to EPR, vasculatures near tumor region are defective and leaky, allowing increased concentration of the circulating particles in the tumor sites.[257] The advantage of MPI method utilizes high signal to background ratio, which can be as high as 50 at 6 hours post injection in case of A group (high SPIONs conc.).[255] The limitation of this passive targeting is embedded in the fact that EPR effect depends on vasculature pore size; thus, EPR effect is not observed in all tumors.[258] Another challenge associated with MPI is the off targeting accumulation of the SPIONs in the spleen and liver compared to the tumor site.[117] This challenge can be possibly addressed by using active targeting of tumor region by surface ligand modification of the tracer particles. This novel method of magnetic particle imaging can also be fused together with therapeutic effect of magnetic hyperthermia.[117] The platform of simultaneous use of MPI and hyperthermia can be harnessed for cancer diagnostics and therapy.[117,259]

Magnetic particle imaging provides a better understanding of stem cell proliferation, migration, metabolism, and differentiation.[260–262] Lemeaster et al. [260] reported a trimodal contrast platform, magnetic particle nanobubbles

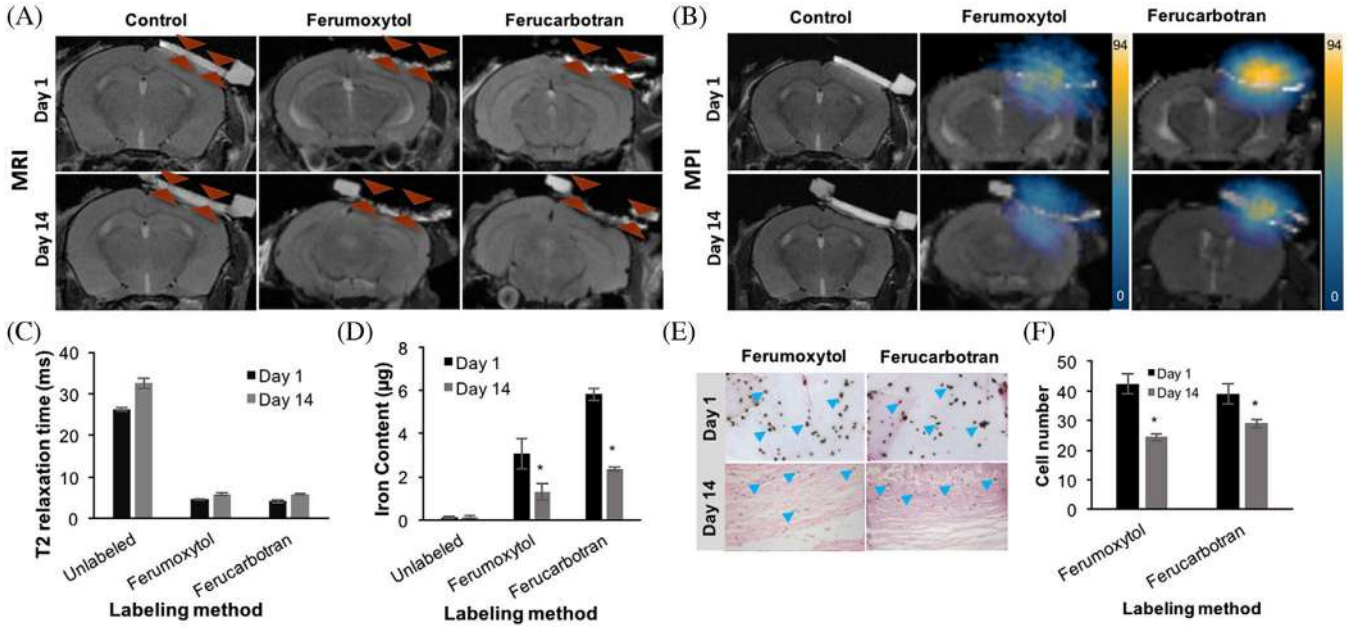

FIGURE 19 In vivo MRI, MPI, and corresponding quantifications of implanted labeled Mesenchymal stem cells (MSCs) into calvarial defects. A, Coronal fast spin-echo (FSE; TE/TR = 42 ms/3000 ms) MR images at day 1 and 14 after implantation of unlabeled, nanotracer labeled MSC in calvarial defects of experimental mice. B, Corresponding MPI images of the calvarial defects at different time points after implantation of therapeutic cells. C, Corresponding T2 relaxation times of the calvarial defects at different time points after implantation of unlabeled, ferumoxytol or ferucarbotran labeled MSCs, as measured using multi-echo spin echo (MESE) sequence (TR = 2000 ms, TE = 6, 13, 20, 27, 34, and 41 ms) Data are displayed as means and standard deviations of three animals per experimental group. D, The corresponding Fe content of the calvarial defects at different time points after implantation of unlabeled, ferumoxytol, or ferucarbotran labeled MSC, as measured using MPI signals. E-F, Corresponding DAB-Prussian blue stain and quantification of transplanted MSCs seeded in the scaffold at day 1 and day 14. *indicates significant differences between data obtained on day 1 and day 14 ($P < 0.05$). Reprinted with permission from ref [254]

facilitated ultrasound imaging, photoacuostic imaging and MPI. The PLGA based nanobubbles had a spherical size of about 185 nm containing magnetic nanoparticles with 4.2 nm core diameter and 62 nm mean hydrodynamic diameter.[260] The MPI signal of this multimodal platform was reported as 20 times higher than negative control.[260] Moreover, Wang et al. [261] reported real-time monitoring of migration and distribution patterns of stem cells using cubic iron oxide nanoparticles. The advantage of MPI over MRI and CT is the ability of its real-time data acquisition within a shorter time domain and no radiation exposure compared to CT.[263] Using MPI tracer particles, it is possible to acquire crucial information on vascular anatomy, blockage of the carotid artery, differentiation of venous and arterial vessels, and the real-time monitoring of heart rate with single beat precision.[264] Additionally, gastrointestinal bleeding of the murine model mouse can be successfully detected using MPI imaging.[265] MPI, along with CT hybrid system, would be an excellent choice that can utilize high sensitivity of MPI and high anatomical resolution image of CT.[266] Non ionizing SPIONs tracer for MPI could be beneficiary for chronic kidney disease (CKD) patients with weak kidney as they struggle to clear out iodine from their system, which leads to the increased complexity of performing CT angiogram.[246] Furthermore, the MPI signal can be utilized to monitor in-vivo real-time drug release.[267] PLGA coated SPIONs with DOX loaded nanocomposite degrade at pH 6.5, resulting in the release of the DOX and change in MPI signal with the change in SPIONs nanocluster, which exhibits linear co-relation with the release rate of DOX. MPI can also be utilized for image guided localized hyperthermia therapy in cancer treatment. Tay et al. [117] reported MPI guided localized magnetic hyperthermia therapy in rodent model demonstrating arbitrary control of hyperthermic heating spot by not affecting off targeting organs such as liver and spleen.

4.4.3 | CT

Computed tomography (CT) is a powerful tool in biomedical imaging applications. It is done by scattering X-rays from different angles to produce an image of a particular cross-section. Though CT is an excellent tool for anatomical imaging, it is relatively weak in functional imaging.[268] However, combined with MRI, it can be used as a multimodal imaging technique.[268] For example, in

tumor imaging and contour selection, MRI provides high-resolution soft tissue information while CT offers real-time 3-dimensional hard tissue information.[269] Various MNPs were used as multimodal contrast agents for MRI-CT imaging modes. These offered a more precise diagnostic tool for the clinical settings. Gold is often times mixed with iron oxide nanoparticles to get dual-contrast agent.[268] Wang and colleagues developed ultra-small Fe_3O_4 NP in Au nanocages with folic acid functionalization.[270] These folic acid functionalizations enabled them to distinguish between malignant and non-malignant tumors.[270] These MNPs were biocompatible and displayed low aggregation (desirable for biomedical applications).[270] Additionally, they validated their results in vivo to show that these MNPs have long term circulation, renal clearance properties and superior accumulation capability in tumor tissues.[270] Li and colleagues prepared Au- Fe_3O_4 NP by hydrothermal process and used it for a dual model contrast agent for MRI-CT.[271] In the first step of this process, Au NPs were modified with a complex polymer mPEG-PEI.NH_2 conjugate via the reduction of $HAuCl_4$.[271] These were mixed with Fe^{2+} and the positive charge was reduced by the acetylation process.[271] The researchers validated these MNPs as MRI-CT dual agents after intravenous injection and subsequent imaging.[271] Zhu and coworkers proposed an Au- Fe_3O_4 MNP by decomposition method and further functionalization with tetramethylammonium hydroxide.[272] They validated these probes in vivo to test their capability as contrast agents.[272] Zhao and collaborators also presented an Au- Fe_3O_4 MNP by coprecipitation method and functionalization with mercaptosuccinic acid (DMSA).[273] This resulted in strawberry-like MNP nanocluster of around 1 nm.[273] These MNPs were validated as MRI-CT contrast agents in liver disease model.[273] One more type of MNPs was developed by Cai and colleagues.[101] In this method, they used the coprecipitation method to obtain Fe_3O_4 MNP and then assembling them with multiple polymer layers.[101] After that, they are assembled with gold NPs and amine groups on the surface is acetylated to get rid of the surface charges.[101] These MNPs demonstrated their potential as MRI-CT contrast agents.[101] One other group reported MNP synthesis by thermal decomposition of Au and Fe precursors and subsequent coating with amphiphilic nano-emulsion.[274] This MNPs showed 1.6 times more contrast enhancement in murine hepatoma model, and the relaxivity coefficient was greater than commercially available agent.[274] Recently MNP without gold coating has also been proposed in the literature.[275] Li et al., proposed Fe@Bi_2S_3 nanocomposites modified with polymer molecules.[275] Although the primary goal of their research was to use these MNPs for thermoradiotherapy, the MNPs showed strong potential for imaging applications.[275] The magnetic core of Fe and the Bi_2S_3 shell components have the capability to serve as a contrasting agent for MRI-CT imaging modes.[275]

4.4.4 | PET

Positron emission tomography (PET) is an imaging technique that uses radioactive tracers to visualize physiological changes in the body. PET is often used with other techniques like CT and MRI. In the case of PET-CT modality, they are used sequentially whereas in the case of PET-MRI, they used simultaneously.[276] In the case of PET-CT, PET monitors metabolic activity and CT reconstructs hard tissue images.[276] It gives better localization, higher accuracy, low-noise and shorter scan time.[276] It has been used for cancer diagnosis and dementia monitoring.[276] However, in the case of PET-MRI, MRI confirms soft tissue presence. MRI-PET provides high spatial and temporal resolution, high sensitivity and no ionizing radiation.[276,277] This modality has been used to detect brain tumors, stroke, neurodegenerative disorder and epilepsy.[276] As a result, various research groups worldwide have sought to improve upon PET-MRI or PET-CT modalities. MNP plays a vital role in developing these techniques with better contrasting agents. For example, Thorek and colleagues prepared ^{89}Zr radiolabeled MNPs to image axillary lymph nodes in healthy wild mice.[278] In this study, MNP core was coated with polyglucose sorbitol and desferrioxamine.[278] After administering these MNPs in Hi-Myc mice with prostatic adenocarcinoma, PET-MRI image gave clearly defined draining nodes in the abdomen and inguinal region.[278] Moreover, Lu et al. [158] reported thermoresponsive magnetic liposome containing Cetuximab (TML-CET) in the control group, whereas the treatment group was administered with Irinotecan (CPT-11) loaded TML-CPT-11-CET. PET-MRI scanning revealed magnetic localization and alternating magnetic field treatment for a different time point (Figure 20). In another work, ^{64}Cu radiolabeled with iron oxide NPs was used for PET-MRI.[279] The functionalization of these MNPs was done with bisphosphonates and dithiocarbamate allowing these MNPs to be stable in human serum for 48 hours.[279] These MNPs were used with PET-CT and PET-MRI in-vivo lymphatic system models.[268,279] PET imaging confirmed MNP uptake in popliteal and iliac lymph nodes.[279] An injection of these MNPs also resulted in an MRI signal decrease, which again confirms particle accumulation.[279] Xie et al., modified MNPs with dopamine, human serum albumin, and labeled them with Cy5.5 dye and ^{64}Cu.[280] After their injection into the U87MG xenograft mouse model PET imaging showed a higher signal-to-noise ratio compared to MRI.[280] Later MRI scans showed inhomogeneous distribution for their spatial distribution confirmed

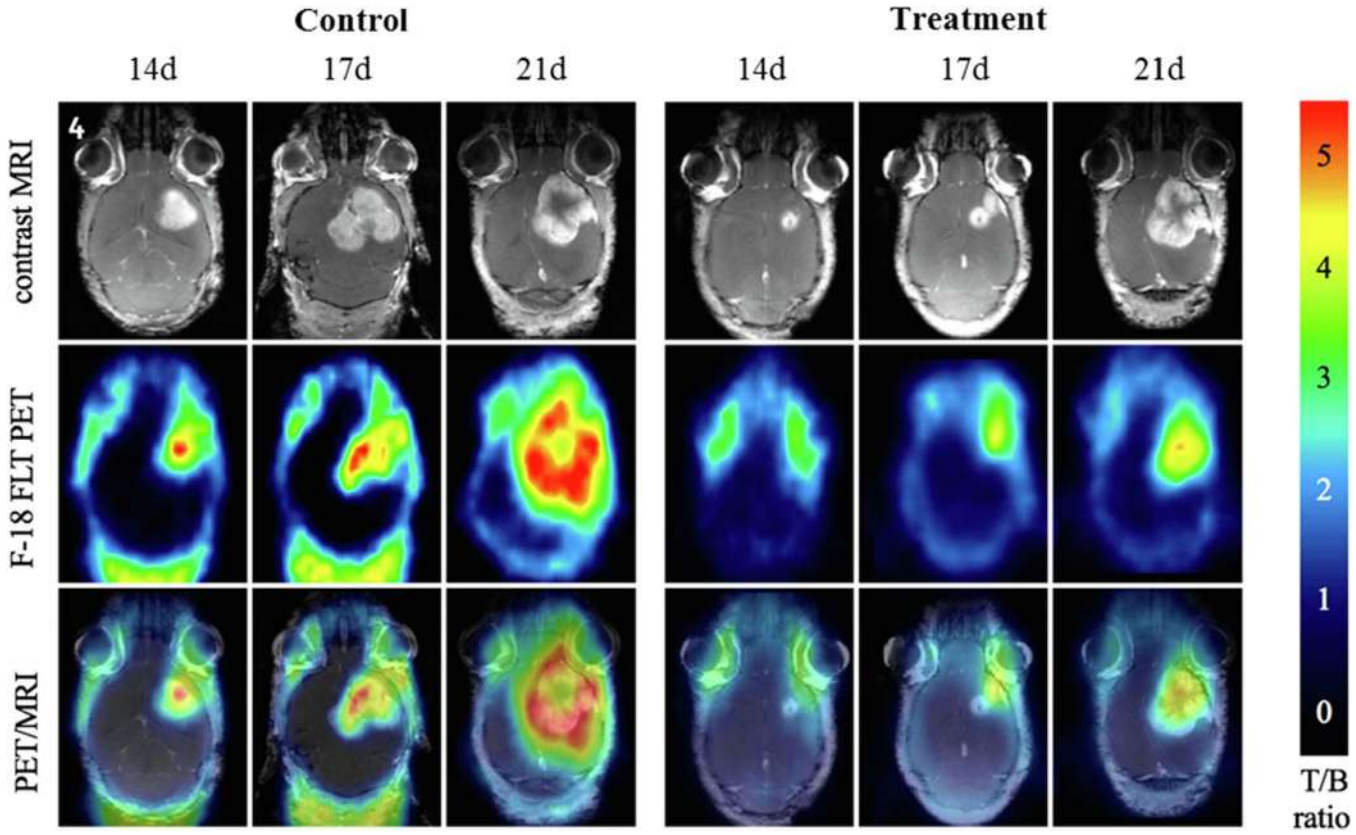

FIGURE 20 Evaluation of antitumor efficacy using PET/MRI analysis. Two tumor-bearing mice were placed in the control group with thermoresponsive magnetic liposome containing Cetuximab (TML-CET), and the treatment group TML-CET loaded with Irinotecan (CPT-11) (TML-CPT-11-CET) under magnetic localization and alternating magnetic field treatment for different time point, at day 14 (14d), day 17 (17d) and day 21 (21d) post-implantation of U87 cells. Reprinted with permission from ref [158]

by immunohistochemistry.[280] These MNPs also showed longer circulation time and less macrophage uptake, making them suitable for drug-delivery applications.[280] Lee and coworkers conjugated RGD with ^{64}Cu radiolabeled with iron oxide NPs and coated them with polyaspartic acid for better conjugation.[281] Imaging of these MNPs on the U87MG model confirmed the accumulation of particles with both PET and MRI.[281] Recently (in 2019), researchers proposed a new chelator-free iron-oxide NPs with ^{64}Cu radiolabel and polymer conjugation.[282] PET-MRI with these MNPs enabled the detection and localization of sentinel lymph nodes in C57BL/6J mice.[282] The stability, accumulation and biodistribution of these MNPs were satisfactory.[282] An innovative MNP for PET/MRI imaging applications was proposed by Thomas et al..[283] They coated MNPs with different functional groups, polymers and chelators before radiolabeling them with ^{64}Cu.[283] It proved to be a good candidate for bimodal tracers in PET-MRI applications.[283] Kim and colleagues injected ^{68}Ga labelled iron-oxide NPs in colon-cancer mice models with oleanolic acid as a targeting molecule.[284] PET-MRI imaging with these MNPs showed inhibition of colon cancer as well as the induction of apoptosis and cancer cell death.[284,285] These results were verified with binding assays and immunohistochemistry.[285] The disadvantages of these modalities include high cost, higher radiation dosage (PET-CT), heating in the scanner (PET-MRI) and damage in the narrow bore system (PET-MRI).[276] Despite these limitations, MNP based PET imaging modalities are one of the most powerful techniques in biomedical visualization models.

4.5 | Lab-on-a-chip

Lab-on-chip (LOC), often termed as total micro analysis systems, is used to fit all desired functions in a single chip with an area of few centimeters with the ability to detect toxins, disease markers and/or localized drug delivery.[5] For example, hollow Fe/Ga based MNPs were synthesized in a PDMS microfluidic reactor with a diameter as low as 150 nm.[286] These hollow MNPs along with the microfluidic system proved to a very effective tool for drug delivery.[286]. The nucleation, growth conditions and reaction parameters of MNP synthesis can be controlled in microfluidic systems.[5] A PDMS microfluidic system

was combined with an aluminum foil in the presence of UV light and it was able to control the sizes and shapes of γ-Fe_2O_3 MNPs.[287] One more interesting method was proposed by Sheng Lin et al., who proposed to control the release of diclofenac with iron-oxide NPs.[288] This allowed for rapid drug release and gliobastoma cell culture proved that this microfluidic system could be used in tissue engineering applications.[288] Recent technological advances also enable us to manipulate microfluidic MNPs even in nanoliter volumes, which allows us to isolate and detect circulating tumor cells (CTCs).[5] Scientists used a microchip with silicon nanowires and MNP nanocomposite to improve the capture efficiency and purity of CTCs.[289] This system was able to improve the capture purity of CTCs in blood samples by almost 82%.[289] It also allowed for real-time sensing and photodynamic therapy of CTCs.[289] MNPs with microfluidic arrangements were also done in a successful diagnosis of malaria.[5] Microfluidic arrangements allowed for the separation of infected red blood cells (iRBCs) from healthy red blood cells (hRBCs) through margination.[290] This system demonstrated the capability of detecting malaria parasites as low as 0.0005%.[290] $MnFe_2O_4$ based microfluidic system for detection of influenza virus is also available.[291] These MNPs had very high sensitivity, low limit of detection and long-term thermal stability.[291] This microfluidic chip has also been verified in clinical specimens.[291] Other than viruses like norovirus and HIV detection platform has also been realized in MNPs microfluidic platform.[5] Bacteria detection has also been done automated MNP based microfluidic μ-hall platform.[5] μ-hall LOC is capable of measuring a single magnetically tagged bacteria with minimal sample processing, faster assay time at a low cost.[292] The detection limit for this process is similar to other available culture tests and it can be used in resource-limited hospital environments.[292] MNP based microfluidic systems for the detection of various biological molecules is also available in the literature.[5] Glucose and creatinine were successfully detected with a microfluidic chip modified with enzyme coated MNP.[293] Another low cost glucose sensor was designed with a microfluidic system where MNPs were packed with enzyme microreactors.[291] This novel idea of LOC offers superior benefits compared to conventional counterparts.

5 | TOXICITY OF MNPs

Magnetic nanoparticles (MNPs) contain a magnetic core with biocompatible coating or polymer.[294] Safety is an ever-present issue in MNPs and toxicity studies provide information on this issue.[294] Moreover, toxicity evaluation is a significant part of drug formulation and development. Therefore, research on the toxic effects of MNPs is a key area of research, especially in the biomedical engineering field,[295] especially some studies have shown the lethal effects of MNPs.[296] Studies have specifically shown the toxic effects of MNPs on different organs and physiological systems. MNPs have poisonous effects on the circulatory system, digestive system, immune system, nervous system, urinary system and reproductive system.[295] Iron oxide MNPs have adverse effects of the heart, liver, spleen, lung, kidneys, brain, thyroid gland, gills/muscles of fish, human skin fibroblasts and reproductive system of Wister rats.[295] Various mechanisms accelerate this toxic effect. These mechanisms include (but are not limited to): oxidative stress, DNA damage, denaturation, necrosis, increase in manganese level, hemolysis.[295,297–301] Oral administration of iron oxide manifests itself in hormonal imbalance in the thyroid gland.[295] In the case of pulmonary administration of iron oxide in Waster rats manifest themselves in lung inflammation resulting in toxicity in the reproductive system.[300] Iron oxide also causes chromosomal aberrations in the gills and muscles of fish, affecting their immune system.[302] Oral/intraperitoneal administration of zinc oxide MNPs can damage the heart, reproductive system and urinary system.[303–305] The damages manifest themselves through testicular damage, decrease in cell viability and changes in metabolism patterns.[303–305] Intravenous or oral administration of nickel can damage heart, liver, spleen, lungs and reproductive system (rat model).[306,307] Cardiac arrhythmias and hormonal imbalance are common symptoms observed in this type of toxicity.[306,307] Cobalt ferrite has shown adverse effects in the zebrafish circulatory system and urinary model NRK-52E cells.[296,308] These MNPs can cause unstable heart rate, oedema and DNA damage.[296,308] In animal models or in vitro cell models, superparamagnetic nanoparticles do the most damage to the nervous system.[295] They result in limited ocular toxicity in Sprague-Dawley rat models, necrosis in EC5v cell lines and hearing displacement in albino guinea pigs.[295,309] Titanium di-oxide effect can damage multiple organs like the brain, lung, spleen, liver, kidneys and urinary system and they can also change urea/uric acid levels in the kidney.[310,311] Intraperitoneal administration of zirconia oxide can damage the liver and kidney by induction of ROS and oxidative stress.[312] Cobalt oxide affects the immune system of keratinocytes by means of necrosis.[313] Magnetite can also affect the immune system and the study showed that it induces an immunological change in white mice.[314] Other MNPs like manganese oxide or other metal oxides can cause damage in the reproductive system either by inducing hormonal imbalance [315] or lung inflammation.[316] Table 4 discusses the toxic effects on the different physiological systems for different MNPs.

TABLE 4 Observed toxicity in the essential physiological system for different types of magnetic nanoparticles

Type of magnetic nanoparticles	Affected physiological system	Refs.
Iron oxide	Circulatory, digestive, endocrine, immune, reproductive, urinary	[295,297–300,305]
Zinc oxide	Circulatory, urinary	[303–305]
Nickel	Circulatory, reproductive	[306,307]
Cobalt ferrite	Circulatory, reproductive	[296,308]
Super paramagnetic	Nervous	[295,309]
Titanium di-oxide	Immune	[310,311]
Zirconia oxide	Digestive	[312]
Cobalt oxide	Immune	[313]
Magnetite	Immune	[314]
Manganese oxide	Reproductive, digestive	[312,315]
Metal oxides	Reproductive	[316]

6 | CLINICAL TRIAL OR TRANSLATION

Nanoparticles and drugs have to undergo an extensive and rigorous trial before approval by the food and drug administrator (FDA). Developed drug/therapeutic agent, once developed in the lab has to be tested on animals prior to a clinical trial. Once passed through the animal study, the therapeutic agent has to be tested in 4 phases, wherein phase 1 utilizes 20-80 healthy volunteers to determine side effect, excretion from the body and metabolic activity while the therapeutic agent is administered. Phase 2 emphasizes effectiveness utilizing 100 patients where the therapeutic agent is tested against a placebo. One thousand patients should take part in phase 3, which will allow detailed investigation about the associated therapeutic module's effectiveness. Finally, phase 4 is the post-marketing monitoring of the therapeutic agent which will update the FDA periodically about side effects and effectiveness. The complete guideline can be found in the FDA regulation for the clinical trial. Iron nanoparticles with different surface ligand have been already clinically approved for the MR imaging technique. Dextran coated iron oxide (Ferumoxide) with a size range of 80-150 nm has been approved for cellular labeling and imaging of mononuclear phagocyte system under the trade name of Feridex (USA) and Endorem (England). Dextran coated smaller magnetic nanoparticles within the size range of 20-40 nm were approved for perfusion and lymph node imaging under the trade name of Combidex (USA) and Sinerem (European Union). Ferucarbotran, which is 60 nm carboxydextran coated iron oxide nanoparticles, have been approved for cell labelling and hepatocellular carcinoma.[317] The ferucarbotran nanoparticles are under the business trade name of Resovist (USA, European Union) and Cliavist (France). 17-30 nm iron oxide nanoparticle named Feraheme (USA) and polyglucose sorbitol carboxymethylether coated (ferumoxytol) were approved for MRI imaging of iron deficiency anemia. FDA approved ferumoxytol was on clinical trial and was waiting for two different approval for monitoring response to bevacizumab therapy in the malignant tumor of the glial tissue of the nervous system (glioma) (NCT00769093), which was terminated due to inadequate enrollment of participant.[317] Table 5 summarizes nanoparticles that are currently on clinical trials for different biomedical applications.

7 | CHALLENGES AND PROSPECTS

Developments in nano-fabrication technologies have allowed for the synthesis of large numbers of magnetic nanoparticles (MNPs). These are currently available in a wide variety of consumer products and nanomedicines.[318] Research has shown the enormous potential of Iron oxide NPs and superparamagnetic iron oxide nanoparticles (SPIONs) in biomedical research.[319] SPIONs are being used as MRI contrast agents and drug delivery systems.[320] SPION drug formulation like Feraheme, Feridex and GastroMARK is available as FDA approved medicine (however, Feridex and GastroMARK have been withdrawn).[319] Iron Oxide NPs are mainly used for contrast agents for MRI.[319] FDA-approved nanodrugs with iron-oxide formulations for iron replacement therapies are also available.[319] Iron oxide core with hydrophilic polymers like dextran sucrose is also available for chronic kidney diseases.[319] One of the most important issues of MNPs is their toxicity in biomedical applications.[318] It is hard to report accurate MNP toxicity because it depends on multiple factors.[318] Therefore, the study of the toxicity of MNPs is the most crucial research field of the hour. Since MNPs are considered for clinical application, validating cytotoxicity in vitro is not enough. They need to be put to the test in vivo conditions also. Over the years various, there have been a number of studies on the cytotoxicity of MNPs in various cells and organs.[295] For example, Fe_3O_4 MNPs showed acceptable biocompatibility and limited toxicity in the L929 cell line.[321] However, they showed maximum inhibition rate in MCF-7 cell lines.[321] They solved this challenge by controlling the doses.[321] Other toxicity investigations showed the effect of MNPs in the digestive system, endocrine system, immune system, nervous system and reproductive system.[295] Few investigators eliminated this challenge by improving the surface coating of these MNPs.[322] MNPs can also contribute to oxidative stress due to size and shape.[295] The toxicity of MNPs reveals themselves

TABLE 5 Clinical trial of magnetic nanoparticles and their potential usage in the biomedical field[317]

Drug	MNPs size	Motivation	Indication	Phase	Trial no.
Ferumoxytol	17-30 nm	Enhanced MR imaging to assess myocardial infraction	Myocardial infraction, Inflammation	Phase 2	NCT01995799
Iron nanoparticles	–	Thermoablation to treat cancer cells	Prostate cancer	Early phase 1	NCT02033447
Ferumoxytol	17-30 nm	Noninvasive imaging to monitor kidney transplant rejection	Kidney transplant	–	NCT02006108
Iron oxide nanoparticles	–	Detection of minimal residual diseases (MRD) in leukemia patients	Leukemia	Remark- (The study was withdrawn due to challenges in particle synthesis)	NCT01411904
Ferumoxytol	17-30 nm	MR imaging of papillary carcinoma of thyroid gland, metastatic medullary thyroid cancer, follicular thyroid cancer lymph node metastasis	Thyroid cancer	–	NCT01927887
Ferumoxytol	17-30 nm	Lymph node imaging	Cancer of lymph node	–	NCT01815333
Ferumoxytol	17-30 nm	To investigate the certain spreads kind of cancer by MR imaging	Head and neck cancer	Early Phase 1	NCT01895829
Gold nanoparticles with Iron oxide-silica shell	–	Alternative to stenting and bypass surgery by rejuvenating arteries using plasmonic photothermal therapy (PPTT)	Coronary artery disease, atherosclerosis	Phase 1 Remarks- (The study was terminated)	NCT01436123
Silica-gold-Iron bearing NPs	–	–	Stable angina, heart failure, atherosclerosis, multivessel coronary artery diseases	–	NCT01270139
SPION	–	Simultaneous use of neoadjuvant chemotherapy+SPIONs/spinning magnetic field (SMF)	Osteosarcoma	Phase 1	NCT04316091
Ferumoxytol	17-30 nm	To detect Lymph node metastases using MRI	Pancreatic cancer	Phase 4	NCT00920023
USPIONs	–	To validate USPION-MRI imaging to detect Lymph node in pancreatic cancer	Pancreatic cancer, periampullary cancer	–	NCT04311047
Ferumoxytol	17-30 nm	To evaluate Feraheme as an effective contrast agent at revealing inflammatory activity	Multiple sclerosis	Withdrawn (2018)	NCT01973517
Ferumoxytol	17-30 nm	Intravenous administration of MNPs to visualize damaged cardiac muscles after a heart attack	Myocardial infraction	–	NCT01323296
Ferumoxytol	17-30 nm	Investigation of cranial a meningeal arteries using Black blood imaging (BBI)	Migraine headache,	–	NCT02549898

through the upregulation of inflammatory genes such as tumor necrosis factor or interleukins.[295] DNA damage, cellular genotoxicity and apoptosis are among the toxic effects of multiple types of MNPs.[323] Some studies have found that rod-shaped MNPs are less toxic than spherical shaped MNPs.[295] The main challenge in explaining the MNPs effect on oxidative stress is the lack of explicit theories or reports.[295] This is one of the potential research need at present. Regarding the size-dependent toxicity, there is still a lack of clear consensus among scientists. Some researchers have reported toxicity increased with reduced size of MNPs,[309] whereas some reported the opposite phenomenon.[299] More research needs to be done to find the effect of MNP size on the toxicity of biological systems.

The other important challenge MNP based therapeutic application can localize them in the desired site.[318] Scientists used to do control the direction with a permanent magnet which was not ideal for particle focusing and had very low tissue penetration depth.[318] Scientists initially solved this problem by implanting small magnetic carriers that can attract the MNPs if necessary.[318] They also developed several models to predict the trajectory of MNPs for therapeutic use.[318] Few models also derived the analytical expression of MNP volume to ensure delivery in the target tumor site.[324] Shapiro et al., further developed this model by dynamic control of magnetic fields in deep tissue structure.[325] It was shown in this study that this controlled magnetic field can drive the MNPs in the target hot spot through a magnetic fluid channel.[325] Although the model was very promising, the in vivo control of these MNPs proved very complicated.[318] In the last decade, scientists have developed a better in-vivo model for more localized applications of MNPs. Giannaccini et al. reported MNP localization in the retinal pigmented epithelium layer of Xenopus and Zebrafish.[326] The injected these MNPs at 25 mg mL^{-1} concentration via the intravitreal route.[326] Although this localization is site-specific, it was dependent on the characteristic of the particles.[326] The prevalent theory is that physical characteristic does not predict the site-specificity of MNPs. More research is needed to close this research gap.

8 | CONCLUSION AND OUTLOOK

Magnetic nanoparticles are being used extensively in all aspects of the biomedical field ranging from drug delivery vehicles to therapeutic agents to imaging modality. The recent development in synthesis and functionalization of monodispersed, tunable, and controllable size and shape of magnetic particles pioneered the scientific community to address and overcome many challenges associated with clinical usage of the magnetic particles. Higher surface area to volume ratio as well as unique magnetic properties makes the magnetic nanoparticles an excellent choice for targeted drug delivery. Magnetic nanocomposites such as magnetic liposome, magnetic hydrogel, magnetic dendrimers, etc. allowed the research community to overcome challenges such as premature burst release of loaded drugs and increased targeting efficacy compared to these nanocarriers alone. Magnetic hyperthermia assisted apoptosis and necrosis bestowed the medical community a tremendous tool to fight various diseases such as cancer. The synergistic effect of localized magnetic hyperthermia and drug delivery to the targeted diseased site showed promising results in treating diseases. Moreover, magnetic nanoparticles are being used as a theranostics platform to diagnose and treat diseases simultaneously. Imaging modalities such as MRI, MPI, and PET and CT are promising aspects of simultaneous diagnosis and treatment of disease with high precision. However, low magnetization, the tendency to aggregate due to inherent magnetism, the toxicity of magnetic nanoparticles are still significant challenges that need dire attention of the research community. The future of magnetic particles in the biomedical field lies in the actual behavior study of magnetic particles in the complex biological system, which will allow us a broad perspective of particle therapeutic efficacy and toxicology.

ACKNOWLEDGMENTS

M.I. Anik and M.K Hossain contributed equally to this work.

CONFLICT OF INTEREST

The authors declare that they have no known competing financial interests or personal relationships that could have influenced the work reported in this paper.

ORCID

Muzahidul I. Anik https://orcid.org/0000-0002-5054-4175

M. Khalid Hossain https://orcid.org/0000-0003-4595-6367

REFERENCES

1. H. Shang, B. Wu, X. Liang, Y. Sun, X. Han, L. Zhang, Q. Wang, W. Cheng, *Drug Deliv*. **2019**, *26*, 944.
2. B. Wu, H. Shang, X. Liang, Y. Sun, H. Jing, X. Han, W. Cheng, *FASEB J.* **2019**, *33*, 14129.
3. A. Naskar, S. Lee, Y. Lee, S. Kim, K. Kim, *Pharmaceutics* **2020**, *12*, 841.
4. S. Hossen, M.K. Hossain, M.K. Basher, M.N.H. Mia, M.T. Rahman, M.J. Uddin, *J. Adv. Res.* **2019**, *15*, 1.
5. V. F. Cardoso, A. Francesko, C. Ribeiro, M. Bañobre-López, P. Martins, S. Lanceros-Mendez, *Adv. Healthc. Mater.* **2018**, *7*, 1700845.

6. I. Ban, J. Stergar, U. Maver, *Nanotechnol. Rev.* **2018**, *7*, 187.
7. J. Wong, J. Prout, A. Seifalian, *Curr. Pharm. Des.* **2017**, *23*, 2908.
8. J. Stergar, I. Ban, U. Maver, *Magnetochemistry* **2019**, *5*, 66.
9. C. S. S. R. Kumar, F. Mohammad, *Adv. Drug Deliv. Rev.* **2011**, *63*, 789.
10. C. Sun, J. S. H. Lee, M. Zhang, *Adv. Drug Deliv. Rev.* **2008**, *60*, 1252.
11. L. Mohammed, H. G. Gomaa, D. Ragab, J. Zhu, *Particuology* **2017**, *30*, 1.
12. A. K. Hauser, R. J. Wydra, N. A. Stocke, K. W. Anderson, J. Z. Hilt, *J. Control. Release* **2015**, *219*, 76.
13. Dobson, *Int. J. Nanomedicine* **2008**, *3*, 169.
14. F. Ludwig, E. Heim, S. Mäuselein, D. Eberbeck, M. Schilling, *J. Magn. Magn. Mater.* **2005**, *293*, 690.
15. R. A. Ismail, G. M. Sulaiman, S. A. Abdulrahman, T. R. Marzoog, *Mater. Sci. Eng. C* **2015**, *53*, 286.
16. A. Ito, M. Shinkai, H. Honda, T. Kobayashi, *J. Biosci. Bioeng.* **2005**, *100*, 1.
17. S. Majidi, F. Zeinali Sehrig, S. M. Farkhani, M. Soleymani Goloujeh, A. Akbarzadeh, Artif. Cells*Nanomed. Biotechnol.* **2016**, *44*, 722.
18. E. Öztürk Er, G. Dalgıç Bozyiğit, Ç. Büyükpınar, S. Bakırdere, *Crit. Rev. Anal. Chem.* **2020**, 1. https://doi.org/10.1080/10408347.2020.1797465.
19. J. Mosayebi, M. Kiyasatfar, S. Laurent, Adv. Healthc. *Mater.* **2017**, *6*, 1700306.
20. T. Hyeon, *Chem. Commun.* **2003**, 34, 927.
21. T. Osaka, T. Matsunaga, T. Nakanishi, A. Arakaki, D. Niwa, H. Iida, *Anal. Bioanal. Chem.* **2006**, *384*, 593.
22. K. Maaz, A. Mumtaz, S. K. Hasanain, A. Ceylan, *J. Magn. Magn. Mater.* **2007**, *308*, 289.
23. L. B. de Mello, L. C. Varanda, F. A. Sigoli, I. O. Mazali, *J. Alloys Compd.* **2019**, *779*, 698.
24. I. de la Calle, J. Páez-Cabaleiro, I. Lavilla, C. Bendicho, *Talanta* **2019**, *199*, 449.
25. H. Liu, A. Li, X. Ding, F. Yang, K. Sun, *Solid State Sci.* **2019**, *93*, 101.
26. Y. Wei, B. Han, X. Hu, Y. Lin, X. Wang, X. Deng, *Procedia Eng.* **2012**, *27*, 632.
27. S. Hosseinzadeh, M. Behboudnia, L. Jamilpanah, M. H. Sheikhi, E. Mohajerani, K. Tian, A. Tiwari, P. Elahi, S. M. Mohseni, *J. Magn. Magn. Mater.* **2019**, *476*, 355.
28. M. Sertkol, Y. Köseoğlu, A. Baykal, H. Kavas, A. C. Başaran, *J. Magn. Magn. Mater.* **2009**, *321*, 157.
29. H. Zhang, G. Zhu, *Appl. Surf. Sci.* **2012**, *258*, 4952.
30. J. Peng, M. Hojamberdiev, Y. Xu, B. Cao, J. Wang, H. Wu, *J. Magn. Magn. Mater.* **2011**, *323*, 133.
31. Y. Köseoğlu, M. Bay, M. Tan, A. Baykal, H. Sözeri, R. Topkaya, N. Akdoğan, *J. Nanoparticle Res.* **2011**, *13*, 2235.
32. Y. C. Han, H. G. Cha, C. W. Kim, Y. H. Kim, Y. S. Kang, *J. Phys. Chem. C* **2007**, *111*, 6275.
33. W. Glasgow, B. Fellows, B. Qi, T. Darroudi, C. Kitchens, L. Ye, T. M. Crawford, O. T. Mefford, *Particuology* **2016**, *26*, 47.
34. L. Gonzalez-Moragas, S.-M. Yu, N. Murillo-Cremaes, A. Laromaine, A. Roig, *Chem. Eng. J.* **2015**, *281*, 87.
35. M. Unni, A. M. Uhl, S. Savliwala, B. H. Savitzky, R. Dhavalikar, N. Garraud, D. P. Arnold, L. F. Kourkoutis, J. S. Andrew, C. Rinaldi, *ACS Nano* **2017**, *11*, 2284.
36. D. Amara, I. Felner, I. Nowik, S. Margel, *Colloids Surfaces A Physicochem. Eng. Asp.* **2009**, *339*, 106.
37. V. Popkov, V. Tolstoy, V. G. Semenov, *J. Alloys Compd.* **2020**, *813*, 152179.
38. L. Kubíčková, J. Koktan, T. Kořínková, M. Klementová, T. Kmječ, J. Kohout, A. Weidenkaff, O. Kaman, *J. Magn. Magn. Mater.* **2020**, *498*, 166083.
39. T. Shahjuee, S. M. Masoudpanah, S. M. Mirkazemi, *J. Supercond. Nov. Magn.* **2019**, *32*, 1347.
40. Y. J. Lee, K. Kim, I. S. Shin, K. S. Shin, *J. Nanoparticle Res.* **2020**, *22*, 1.
41. A. Saddique, Z. Ahmad, C. Hoskins, M. A. Mirza, A. Naz, J. Ahmad, *Mater. Chem. Phys.* **2020**, *249*, 122950.
42. A. H. Oh, H. Y. Park, Y. G. Jung, S. C. Choi, G. S. An, *Ceram. Int.* **2020**, *46*, 10723.
43. Z. Lalegani, S. A. S. Ebrahimi, B. Hamawandi, L. La Spada, M. S. Toprak, *Opt. Mater.* **2020**, *108*, 110381.
44. A. Akbarzadeh, M. Samiei, S. Davaran, *Nanoscale Res. Lett.* **2012**, *7*, 144.
45. S. Ansari, E. Ficiarà, F. Ruffinatti, I. Stura, M. Argenziano, O. Abollino, R. Cavalli, C. Guiot, F. D'Agata, *Materials.* **2019**, *12*, 465.
46. M. Faraji, Y. Yamini, M. Rezaee, J. Iran. *Chem. Soc.* **2010**, *7*, 1.
47. W. Wu, Q. He, C. Jiang, *Nanoscale Res. Lett.* **2008**, *3*, 397.
48. P. Tartaj, M. a del P. Morales, S. Veintemillas-Verdaguer, T. Gonz lez-Carre o, C. J. Serna, *J. Phys. D. Appl. Phys.* **2003**, *36*, R182.
49. K. Ananjana, S. Swetha, P. Prakash, K. V. Nishad, M. Komath, B. N. Nair, G. S. Sailaja, *New J. Chem.* **2020**, *44*, 1962.
50. R. Rahmani, M. Gharanfoli, M. Gholamin, M. Darroudi, J. Chamani, K. Sadri, A. Hashemzadeh, *Ceram. Int.* **2020**, *46*, 3051.
51. V. Dubey, V. Kain, *Mater. Manuf. Process.* **2018**, *33*, 835.
52. A. Lassoued, M. S. Lassoued, B. Dkhil, S. Ammar, A. Gadri, *Phys. E Low-dimensional Syst. Nanostructures* **2018**, *101*, 212.
53. A.-H. Lu, E. L. Salabas, F. Schüth, *Angew. Chemie Int. Ed.* **2007**, *46*, 1222.
54. K. Nejati, R. Zabihi, *Chem. Cent. J.* **2012**, *6*, 23.
55. S.-N. Sun, C. Wei, Z.-Z. Zhu, Y.-L. Hou, S. S. Venkatraman, Z.-C. Xu, *Chinese Phys. B* **2014**, *23*, 037503.
56. S. Belaïd, D. Stanicki, L. Vander Elst, R. N. Muller, S. Laurent, *Nanotechnology* **2018**, *29*, 165603.
57. N. A. Frey, S. Peng, K. Cheng, S. Sun, *Chem. Soc. Rev.* **2009**, *38*, 2532.
58. F. B. Effenberger, R. A. Couto, P. K. Kiyohara, G. Machado, S. H. Masunaga, R. F. Jardim, L. M. Rossi, *Nanotechnology* **2017**, *28*, 115603.
59. N. Jović Orsini, B. Babić-Stojić, V. Spasojević, M. P. Calatayud, N. Cvjetićanin, G. F. Goya, *J. Magn. Magn. Mater.* **2018**, *449*, 286.
60. T. Hyeon, S. S. Lee, J. Park, Y. Chung, H. Bin Na, *J. Am. Chem. Soc.* **2001**, *123*, 12798.
61. A. Eatemadi, H. Daraee, N. Zarghami, H. Melat Yar, A. Akbarzadeh, Artif. Ce*lls Nanomedicine Biotechnol.* **2016**, *44*, 111.
62. H. Dong, Y.-C. Chen, C. Feldmann, *Green Chem.* **2015**, *17*, 4107.
63. R. López, M. Pineda, G. Hurtado, R. León, S. Fernández, H. Saade, D. Bueno, *Int. J. Mol. Sci.* **2013**, *14*, 19636.
64. S. F. Hasany, I. Ahmed, R. J, A. Rehman, *Nanosci. Nanotechnol.* **2013**, *2*, 148.
65. A. Ali, H. Zafar, M. Zia, I. ul Haq, A. R. Phull, J. S. Ali, A. Hussain, *Nanotechnol. Sci. Appl.* **2016**, *9*, 49.

66. A. H. Choi, R. C. Conway, S. Cazalbou, B. Ben-Nissan, In Fundamental Biomaterials: Ceramics, Elsevier, **2018**, pp. 63–93.
67. Y. Lu, W. Dong, J. Ding, W. Wang, A. Wang, In Nanomaterials from Clay Minerals, Elsevier, **2019**, pp. 485–536.
68. A. L. Andrade, D. M. Souza, M. C. Pereira, J. D. Fabris, R. Z. Domingues, *Cerâmica* **2009**, *55*, 420.
69. D. Farhanian, G. De Crescenzo, J. R. Tavares, *Sci. Rep.* **2018**, *8*, 12223.
70. D. Ramimoghadam, S. Bagheri, S. B. A. Hamid, *J. Magn. Magn. Mater.* **2014**, *368*, 207.
71. M. Starowicz, P. Starowicz, J. Żukrowski, J. Przewoźnik, A. Lemański, C. Kapusta, J. Banaś, *J. Nanoparticle Res.* **2011**, *13*, 7167.
72. K. Yan, P. Li, H. Zhu, Y. Zhou, J. Ding, J. Shen, Z. Li, Z. Xu, P. K. Chu, *RSC Adv.* **2013**, *3*, 10598.
73. R. K. Gautam, M. C. Chattopadhyaya, In *Nanomaterials for Wastewater Remediation*, Elsevier, Netherlands **2016**, pp. 139–159.
74. S. Laurent, D. Forge, M. Port, A. Roch, C. Robic, L. Vander Elst, R. N. Muller, *Chem. Rev.* **2008**, *108*, 2064.
75. M. D'Arienzo, R. Scotti, B. Di Credico, M. Redaelli, In *Studies in Surface Science Catalysis*, Elsevier Inc., **2017**, pp. 477–540.
76. S. Gul, S. B. Khan, I. U. Rehman, M. A. Khan, M. I. Khan, *Front. Mater.* **2019**, *6*, 1.
77. T. D. Clemons, R. H. Kerr, A. Joos, In Comprehensive Nanoscience and Nanotechnology, Elsevier, **2019**, pp. 193–210.
78. S. Arulmani, S. Anandan, M. Ashokkumar, In *Nanomaterials for Green Energy*, Elsevier, **2018**, pp. 1–53.
79. F. Fiévet, S. Ammar-Merah, R. Brayner, F. Chau, M. Giraud, F. Mammeri, J. Peron, J.-Y. Piquemal, L. Sicard, G. Viau, *Chem. Soc. Rev.* **2018**, *47*, 5187.
80. K. Eid, H. Wang, L. Wang, In *Supra-Materials Nanoarchitectonics*, Elsevier, **2017**, pp. 135–171.
81. M. J. Williams, E. Sánchez, E. R. Aluri, F. J. Douglas, D. A. MacLaren, O. M. Collins, E. J. Cussen, J. D. Budge, L. C. Sanders, M. Michaelis, C. M. Smales, J. Cinatl, S. Lorrio, D. Krueger, R. T. M. de Rosales, S. A. Corr, *RSC Adv.* **2016**, *6*, 83520.
82. G. Salazar-Alvarez, M. Muhammed, A. A. Zagorodni, *Chem. Eng. Sci.* **2006**, *61*, 4625.
83. S. Kayal, D. Bandyopadhyay, T. K. Mandal, R. V. Ramanujan, *RSC Adv.* **2011**, *1*, 238.
84. A. B. Patil, B. M. Bhanage, In *Handbook of Nanoparticles*, Cham, Springer International Publishing, **2016**, pp. 143–166.
85. Y. Wang, I. Nkurikiyimfura, Z. Pan, *Chem. Eng. Commun.* **2015**, *202*, 616.
86. G. Unsoy, S. Yalcin, R. Khodadust, G. Gunduz, U. Gunduz, *J. Nanoparticle Res.* **2012**, *14*, 964.
87. X. Wang, G. Chen, W. Guo, *Molecules* **2003**, *8*, 40.
88. B. Buesser, S. E. Pratsinis, *Annu. Rev. Chem. Biomol. Eng.* **2012**, *3*, 103.
89. I. Fernández-Barahona, M. Muñoz-Hernando, F. Herranz, *Molecules* **2019**, *24*, 1224.
90. S. Riaz, R. Ashraf, A. Akbar, S. Naseem, *IEEE Trans. Magn.* **2014**, *50*, 1.
91. C. Ganesh Kumar, Y. Poornachandra, S. Pombala, in *Nanostructures Drug Deliv*ery, Elsevier, **2017**, pp. 1–61.
92. E. A. Dawi, A. H. Ismail, A. AbdelKader, A. A. Karar, *Appl. Phys. A* **2020**, *126*, 316.
93. K. B. Narayanan, N. Sakthivel, *Adv. Colloid Interface Sci.* **2010**, *156*, 1.
94. N. Zhu, H. Ji, P. Yu, J. Niu, M. Farooq, M. Akram, I. Udego, H. Li, X. Niu, *Nanomaterials* **2018**, *8*, 810.
95. W. Wu, Z. Wu, T. Yu, C. Jiang, W.-S. Kim, *Sci. Technol. Adv. Mater.* **2015**, *16*, 023501.
96. R. A. Bohara, N. D. Thorat, S. H. Pawar, *RSC Adv.* **2016**, *6*, 43989.
97. R. A. Frimpong, J. Z. Hilt, *Nanomedicine* **2010**, *5*, 1401.
98. B. Thapa, D. Diaz-Diestra, J. Beltran-Huarac, B. R. Weiner, G. Morell, *Nanoscale Res. Lett.* **2017**, *12*, 312.
99. Z. Shaterabadi, G. Nabiyouni, M. Soleymani, *Mater. Sci. Eng. C* **2017**, *75*, 947.
100. H. Unterweger, L. Dézsi, J. Matuszak, C. Janko, M. Poettler, J. Jordan, T. Bäuerle, J. Szebeni, T. Fey, A. Boccaccini, C. Alexiou, I. Cicha, *Int. J. Nanomedicine* **2018**, *13*, 1899.
101. H. Cai, K. Li, M. Shen, S. Wen, Y. Luo, C. Peng, G. Zhang, X. Shi, *J. Mater. Chem.* **2012**, *22*, 15110.
102. S. Tang, Q. Du, T. Liu, L. Tan, M. Niu, L. Gao, Z. Huang, C. Fu, T. Ma, X. Meng, H. Shao, *Nanoscale Res. Lett.* **2016**, *11*, 334.
103. K. Li, M. Shen, L. Zheng, J. Zhao, Q. Quan, X. Shi, G. Zhang, *Nanoscale Res. Lett.* **2014**, *9*, 304.
104. S. I. Uribe Madrid, U. Pal, Y. S. Kang, J. Kim, H. Kwon, J. Kim, *Nanoscale Res. Lett.* **2015**, *10*, 217.
105. T.-T. Yang, W.-K. Zhu, W.-L. Liu, F.-G. Kong, M.-M. Ren, Q.-Z. Liu, Z.-Z. Yang, X.-Q. Wang, X.-L. Duan, *J. Mater. Sci. Mater. Electron.* **2017**, *28*, 11569.
106. A. K. Gupta, A. S. G. Curtis, *J. Mater. Sci. Mater. Med.* **2004**, *15*, 493.
107. R. Alwi, S. Telenkov, A. Mandelis, T. Leshuk, F. Gu, S. Oladepo, K. Michaelian, *Biomed. Opt. Express* **2012**, *3*, 2500.
108. L. Arias, J. Pessan, A. Vieira, T. Lima, A. Delbem, D. Monteiro, *Antibiotics* **2018**, *7*, 46.
109. D. Shi, G. Mi, S. Bhattacharya, S. Nayar, T. Webster, *Int. J. Nanomedicine* **2016**, *11*, 5371.
110. S. Margel, E. Corem-Salkmon, B. Perlstein, *Int. J. Nanomedicine* **2012**, *7*, 5517.
111. Z. Sun, M. W. Yathindranath, C. Thliveris, H. Parkinson, D. Miller, *Int. J. Nanomedicine* **2013**, *8*, 961.
112. C. J. Rivet, Y. Yuan, D.-A. Borca-Tasciuc, R. J. Gilbert, *Chem. Res. Toxicol.* **2012**, *25*, 153.
113. R. Wang, V. Degirmenci, H. Xin, Y. Li, L. Wang, J. Chen, X. Hu, D. Zhang, *Int. J. Mol. Sci.* **2018**, *19*, 2230.
114. M. E. Mahmoud, M. F. Amira, A. A. Zaghloul, G. A. A. Ibrahim, *Chem. Eng. J.* **2016**, *293*, 200.
115. X. Zhang, L. Hao, H. Wang, X. Zhu, Z. Zhang, X. Hu, W. Jiang, *J. Wuhan Univ. Technol. Sci. Ed.* **2017**, *32*, 42.
116. Z. M. Avval, L. Malekpour, F. Raeisi, A. Babapoor, S. M. Mousavi, S. A. Hashemi, M. Salari, *Drug Metab. Rev.* **2020**, *52*, 157.
117. Z. W. Tay, P. Chandrasekharan, A. Chiu-Lam, D. W. Hensley, R. Dhavalikar, X. Y. Zhou, E. Y. Yu, P. W. Goodwill, B. Zheng, C. Rinaldi, S. M. Conolly, *ACS Nano* **2018**, *12*, 3699.
118. S. P. Schwaminger, P. Fraga-García, S. A. Blank-Shim, T. Straub, M. Haslbeck, F. Muraca, K. A. Dawson, S. Berensmeier, *ACS Omega* **2019**, *4*, 3790.
119. A.-L. Hei, J.-P. Cai, *DNA Cell Biol*. **2005**, *24*, 479.
120. H. Cabral, K. Miyata, K. Osada, K. Kataoka, **2018**, *118*, 6844.
121. P. Nimtrakul, D. B. Williams, W. Tiyaboonchai, C. A. Prestidge, *Pharmaceuticals* **2020**, *13*, 121.
122. L. Sercombe, T. Veerati, F. Moheimani, S. Y. Wu, A. K. Sood, S. Hua, *Front. Pharmacol.* **2015**, *6*, 286.

123. V. Van Tran, J. Y. Moon, Y. C. Lee, *J. Control. Release* **2019**, *300*, 114.
124. B. Das, D. Chattopadhyay, D. Rana, *Biomater. Sci.* **2020**, *8*, 4665.
125. Y. Zhu, C. Liu, Z. Pang, *Biomolecules* **2019**, *9*, 790.
126. Y. Song, Y. Li, Q. Xu, Z. Liu, *Int. J. Nanomedicine* **2017**, *12*, 87.
127. Y. Yang, M. Zhang, H. Song, C. Yu, *Acc. Chem. Res.* **2020**, *53*, 1545.
128. X. Fan, Z. Li, X. J. Loh, *Polym. Chem.* **2016**, *7*, 5898.
129. L. Guo, H. Chen, N. He, Y. Deng, *Chinese Chem. Lett.* **2018**, *29*, 1829.
130. A. Ręk orajska, A. Szuplewska, A. Ręk orajska Joniec, E. Pocztańska, P. Krysiński, A. Dybko, M. Chudy, *Nanotechnology* **2019**, *30*, 315101.
131. M. E. Fortes Brollo, A. Domínguez-Bajo, A. Tabero, V. Domínguez-Arca, V. Gisbert, G. Prieto, C. Johansson, R. Garcia, A. Villanueva, M. C. Serrano, M. D. P. Morales, *ACS Appl. Mater. Interfaces* **2020**, *12*, 4295.
132. S. Nezami, M. Sadeghi, H. Mohajerani, *Polym. Degrad. Stab.* **2020**, *179*, 109255.
133. C. S. Lacko, I. Singh, M. A. Wall, A. R. Garcia, S. L. Porvasnik, C. Rinaldi, C. E. Schmidt, *J. Neural Eng.* **2020**, *17*, 016057.
134. Z. Naderi, J. Azizian, E. Moniri, N. Farhadyar, *J. Inorg. Organomet. Polym. Mater.* **2020**, *30*, 1339.
135. S. Forouzandehdel, S. Forouzandehdel, M. Rezghi Rami, *Carbohydr. Res.* **2020**, *487*, 107889.
136. A. Chyzy, M. Tomczykowa, M. E. Plonska-Brzezinska, *Materials.* **2020**, *13*, 188.
137. M. S. Amini-Fazl, R. Mohammadi, K. Kheiri, *Int. J. Biol. Macromol.* **2019**, *132*, 506.
138. A. J. Thote, J. T. Chappell, R. B. Gupta, R. Kumar, *Drug Dev. Ind. Pharm.* **2005**, *31*, 43.
139. M. Hayati, G. Rezanejade Bardajee, M. Ramezani, S. S. Hosseini, F. Mizani, *Polym. Int.* **2020**, *69*, 156.
140. D. Kim, H. Lee, S. Kwon, Y. J. Sung, W. K. Song, S. Park, *Adv. Healthc. Mater.* **2020**, *9*, 2000118.
141. D. Kim, H. Lee, S. Kwon, H. Choi, S. Park, *Sensors Actuators B Chem.* **2019**, *289*, 65.
142. Y. Wang, M. Zhong, L. Wang, Y. Liu, B. Wang, Y. Li, *J. Drug Deliv. Sci. Technol.* **2019**, *54*, 101293.
143. B. Chen, J. Xing, M. Li, Y. Liu, M. Ji, *Colloids Surfaces B Biointerfaces* **2020**, *190*, 110896.
144. A. Pourjavadi, S. Asgari, S. H. Hosseini, *J. Drug Deliv. Sci. Technol.* **2020**, *56*, 101542.
145. Y. Wang, B. Li, F. Xu, Z. Han, D. Wei, D. Jia, Y. Zhou, *Biomacromolecules* **2018**, *19*, 3351.
146. M. Noh, Y. H. Choi, Y.-H. An, D. Tahk, S. Cho, J. W. Yoon, N. L. Jeon, T. H. Park, J. Kim, N. S. Hwang, *ACS Biomater. Sci. Eng.* **2019**, *5*, 3909.
147. C. Nazli, G. S. Demirer, Y. Yar, H. Y. Acar, S. Kizilel, *Colloids Surfaces B Biointerfaces* **2014**, *122*, 674.
148. P. Ilgin, G. Avci, C. Silan, S. Ekici, N. Aktas, R. S. Ayyala, V. T. John, N. Sahiner, *Carbohydr. Polym.* **2010**, *82*, 997.
149. D. Guowei, K. Adriane, X. Chen, C. Jie, L. Yinfeng, *Int. J. Pharm.* **2007**, *328*, 78.
150. W. Zhao, K. Odelius, U. Edlund, C. Zhao, A.-C. Albertsson, *Biomacromolecules* **2015**, *16*, 2522.
151. G. R. Mahdavinia, Z. Rahmani, S. Karami, A. Pourjavadi, *J. Biomater. Sci. Polym. Ed.* **2014**, *25*, 1891.
152. H. Li, G. Go, S. Y. Ko, J.-O. Park, S. Park, *Smart Mater. Struct.* **2016**, *25*, 027001.
153. N. S. Satarkar, J. Zach Hilt, *Acta Biomater.* **2008**, *4*, 11.
154. A. Toro-Cordova, M. Flores-Cruz, J. Santoyo-Salazar, E. Carrillo-Nava, R. Jurado, P. Figueroa-Rodriguez, P. Lopez-Sanchez, L. Medina, P. Garcia-Lopez, *Molecules* **2018**, *23*, 2272.
155. A. Floris, C. Sinico, A. M. Fadda, F. Lai, F. Marongiu, A. Scano, M. Pilloni, F. Angius, C. Vázquez-Vázquez, G. Ennas, *J. Colloid Interface Sci.* **2014**, *425*, 118.
156. M. Dai, C. Wu, H.-M. Fang, L. Li, J.-B. Yan, D.-L. Zeng, T. Zou, *J. Microencapsul.* **2017**, *34*, 408.
157. W. Il Choi, A. Sahu, F. R. Wurm, S.-M. Jo, *RSC Adv.* **2019**, *9*, 15053.
158. Y.-J. Lu, E.-Y. Chuang, Y.-H. Cheng, T. S. Anilkumar, H.-A. Chen, J.-P. Chen, *Chem. Eng. J.* **2019**, *373*, 720.
159. S. Shen, D. Huang, J. Cao, Y. Chen, X. Zhang, S. Guo, W. Ma, X. Qi, Y. Ge, L. Wu, *J. Mater. Chem. B* **2019**, *7*, 1096.
160. V. Du Nguyen, S. Zheng, J. Han, V. H. Le, J.-O. Park, S. Park, *Colloids Surfaces B Biointerfaces* **2017**, *154*, 104.
161. C.-L. Huang, W.-J. Hsieh, C.-W. Lin, H.-W. Yang, C.-K. Wang, *Ceram. Int.* **2018**, *44*, 12442.
162. H.-L. Hsu, J.-P. Chen, *J. Magn. Magn. Mater.* **2017**, *427*, 188.
163. E. Halevas, B. Mavroidi, C. H. Swanson, G. C. Smith, A. Moschona, S. Hadjispyrou, A. Salifoglou, A. A. Pantazaki, M. Pelecanou, G. Litsardakis, *J. Inorg. Biochem.* **2019**, *199*, 110778.
164. M. Heidenreich, F. Zhang, *Nat. Rev. Neurosci.* **2016**, *17*, 36.
165. R. Barrangou, J. A. Doudna, *Nat. Biotechnol.* **2016**, *34*, 933.
166. M. L. Maeder, C. A. Gersbach, *Mol. Ther.* **2016**, *24*, 430.
167. A. Strong, K. Musunuru, *Nat. Rev. Cardiol.* **2017**, *14*, 11.
168. F. Jiang, J. A. Doudna, *Annu. Rev. Biophys.* **2017**, *46*, 505.
169. X. Xiong, M. Chen, W. A. Lim, D. Zhao, L. S. Qi, *Annu. Rev. Genomics Hum. Genet.* **2016**, *17*, 131.
170. H. Zhu, L. Zhang, S. Tong, C. M. Lee, H. Deshmukh, G. Bao, *Nat. Biomed. Eng.* **2019**, *3*, 126.
171. S. S. Rohiwal, N. Dvorakova, J. Klima, M. Vaskovicova, F. Senigl, M. Slouf, E. Pavlova, P. Stepanek, D. Babuka, H. Benes, Z. Ellederova, K. Stieger, *Sci. Rep.* **2020**, *10*, 4619.
172. M. Arsianti, M. Lim, C. P. Marquis, R. Amal, *Langmuir* **2010**, *26*, 7314.
173. B. F. Grześkowiak, Y. Sánchez-Antequera, E. Hammerschmid, M. Döblinger, D. Eberbeck, A. Woźniak, R. Słomski, C. Plank, O. Mykhaylyk, *Pharm. Res.* **2015**, *32*, 103.
174. M. Hryhorowicz, B. Grześkowiak, N. Mazurkiewicz, P. Śledziński, D. Lipiński, R. Słomski, *Mol. Biotechnol.* **2019**, *61*, 173.
175. A. Kaushik, A. Yndart, V. Atluri, S. Tiwari, A. Tomitaka, P. Gupta, R. D. Jayant, D. Alvarez-Carbonell, K. Khalili, M. Nair, *Sci. Rep.* **2019**, *9*, 3928.
176. X. Xu, S. Hou, N. Wattanatorn, F. Wang, Q. Yang, C. Zhao, X. Yu, H.-R. Tseng, S. J. Jonas, P. S. Weiss, *ACS Nano* **2018**, *12*, 4503.
177. B. Zehner, F. Schmidt, W. Korth, M. Cokoja, A. Jess, *Langmuir* **2019**, *35*, 16297.
178. K. Motomura, M. Yamanaka, M. Aratono, *Colloid Polym. Sci.* **1984**, *262*, 948.
179. S. Deodhar, P. Rohilla, M. Manivannan, S. P. Thampi, M. G. Basavaraj, *Langmuir* **2020**, *36*, 8100.
180. C.-F. Lee, C.-H. Yang, T.-L. Lin, P. Bahadur, L.-J. Chen, *Colloids Surfaces B Biointerfaces* **2019**, *183*, 110461.

181. M. Ashjari, F. Panahandeh, Z. Niazi, M. M. Abolhasani, *J. Drug Deliv. Sci. Technol.* **2020**, *56*, 101563.
182. S. A. Sabra, S. A. Sheweita, M. Haroun, D. Ragab, M. A. Eldemellawy, Y. Xia, D. Goodale, A. L. Allan, A. O. Elzoghby, S. Rohani, *J. Pharm. Sci.* **2019**, *108*, 1713.
183. Z. Karami, S. Sadighian, K. Rostamizadeh, S. H. Hosseini, S. Rezaee, M. Hamidi, *Mater. Sci. Eng. C* **2019**, *100*, 771.
184. A. Pourjavadi, Z. Mazaheri Tehrani, L. Dastanpour, *Int. J. Polym. Mater. Polym. Biomater.* **2019**, *68*, 741.
185. L. Wu, L. Zong, H. Ni, X. Liu, W. Wen, L. Feng, J. Cao, X. Qi, Y. Ge, S. Shen, *Biomater. Sci.* **2019**, *7*, 2134.
186. M. Rashid, Q. Zaid Ahmad Tajuddin, In Applications of Targeted Nano *Drugs Delivery System*, Elsevier, **2019**, pp. 297–325.
187. A. Taheri-Kafrani, H. Shirzadfar, E. Tavassoli-Kafrani, In *Nano-Microscale Drug Delivery System*, Elsevier, **2017**, pp. 75–94.
188. W. Sun, S. Mignani, M. Shen, X. Shi, *Drug Discov. Today* **2016**, *21*, 1873.
189. A. Landarani-Isfahani, M. Moghadam, S. Mohammadi, M. Royvaran, N. Moshtael-Arani, S. Rezaei, S. Tangestaninejad, V. Mirkhani, I. Mohammadpoor-Baltork, *Langmuir* **2017**, *33*, 8503.
190. S. Nigam, D. Bahadur, *IEEE Trans. Magn.* **2016**, *52*, 1.
191. A. Jędrzak, B. F. Grześkowiak, E. Coy, J. Wojnarowicz, K. Szutkowski, S. Jurga, T. Jesionowski, R. Mrówczyński, *Colloids Surfaces B Biointerfaces* **2019**, *173*, 698.
192. J. Kurczewska, M. Cegłowski, G. Schroeder, *Mater. Chem. Phys.* **2018**, *211*, 34.
193. T. W. Mekonnen, Y. S. Birhan, A. T. Andrgie, E. Y. Hanurry, H. F. Darge, H.-Y. Chou, J.-Y. Lai, H.-C. Tsai, J. M. Yang, Y.-H. Chang, *Colloids Surfaces B Biointerfaces* **2019**, *184*, 110531.
194. N. Taghavi Pourianazar, U. Gunduz, *Biomed. Pharmacother.* **2016**, *78*, 81.
195. H. Nosrati, M. Adibtabar, A. Sharafi, H. Danafar, M. Hamidreza Kheiri, *Drug Dev. Ind. Pharm.* **2018**, *44*, 1377.
196. M. Manzano, M. Vallet-Regí, *Adv. Funct. Mater.* **2020**, *30*, 1902634.
197. M. Asgari, M. Soleymani, T. Miri, A. Barati, *J. Mol. Liq.* **2019**, *292*, 111367.
198. Y. Wang, L. Wang, L. Guo, M. Yan, L. Feng, S. Dong, J. Hao, *New J. Chem.* **2019**, *43*, 4908.
199. Y. Jia, P. Zhang, Y. Sun, Q. Kang, J. Xu, C. Zhang, Y. Chai, *Nanomedicine Nanotechnol. Biol. Med.* **2019**, *21*, 102040.
200. H. Keshavarz, A. Khavandi, S. Alamolhoda, M. R. Naimi-Jamal, *New J. Chem.* **2020**, *44*, 8232.
201. M. E. Peralta, S. A. Jadhav, G. Magnacca, D. Scalarone, D. O. Mártire, M. E. Parolo, L. Carlos, *J. Colloid Interface Sci.* **2019**, *544*, 198.
202. A. Pourjavadi, Z. M. Tehrani, S. Jokar, *J. Ind. Eng. Chem.* **2015**, *28*, 45.
203. J. K. Kang, J. C. Kim, Y. Shin, S. M. Han, W. R. Won, J. Her, J. Y. Park, K. T. Oh, *Arch. Pharm. Res.* **2020**, *43*, 46.
204. I. Obaidat, B. Issa, Y. Haik, *Nanomaterials* **2015**, *5*, 63.
205. A. E. Deatsch, B. A. Evans, *J. Magn. Magn. Mater.* **2014**, *354*, 163.
206. R. Kötitz, W. Weitschies, L. Trahms, W. Semmler, *J. Magn. Magn. Mater.* **1999**, *201*, 102.
207. D. Chang, M. Lim, J. A. C. M. Goos, R. Qiao, Y. Y. Ng, F. M. Mansfeld, M. Jackson, T. P. Davis, M. Kavallaris, *Front. Pharmacol.* **2018**, *9*, https://doi.org/10.3389/fphar.2018.00831.
208. F. C. Lin, J. I. Zink, *J. Am. Chem. Soc.* **2020**, *142*, 5212.
209. C. Fan, W. Gao, Z. Chen, H. Fan, M. Li, F. Deng, Z. Chen, *Int. J. Pharm.* **2011**, *404*, 180.
210. P. Lemal, S. Balog, C. Geers, P. Taladriz-Blanco, A. Palumbo, A. M. Hirt, B. Rothen-Rutishauser, A. Petri-Fink, *J. Magn. Magn. Mater.* **2019**, *474*, 637.
211. G. Kandasamy, A. Sudame, P. Bhati, A. Chakrabarty, D. Maity, *J. Mol. Liq.* **2018**, *256*, 224.
212. Y. Yang, M. Huang, J. Qian, D. Gao, X. Liang, *Sci. Rep.* **2020**, *10*, 8331.
213. R. Gupta, D. Sharma, *ACS Appl. Nano Mater.* **2020**, *3*, 2026.
214. Z. Ferjaoui, E. Jamal Al Dine, A. Kulmukhamedova, L. Bezdetnaya, C. Soon Chang, R. Schneider, F. Mutelet, D. Mertz, S. Begin-Colin, F. Quilès, E. Gaffet, H. Alem, *ACS Appl. Mater. Interfaces* **2019**, *11*, 30610.
215. A. Ahmad, A. Gupta, M. M. Ansari, A. Vyawahare, G. Jayamurugan, R. Khan, *ACS Biomater. Sci. Eng.* **2020**, *6*, 1102.
216. S. Kaushik, J. Thomas, V. Panwar, H. Ali, V. Chopra, A. Sharma, R. Tomar, D. Ghosh, *ACS Appl. Bio Mater.* **2020**, *3*, 779.
217. H.-Y. Cho, A. Mavi, S.-T. D. Chueng, T. Pongkulapa, N. Pasquale, H. Rabie, J. Han, J. H. Kim, T.-H. Kim, J.-W. Choi, K.-B. Lee, *ACS Appl. Mater. Interfaces* **2019**, *11*, 23909.
218. H. Wu, L. Liu, L. Song, M. Ma, N. Gu, Y. Zhang, *ACS Nano* **2019**, *13*, 14013.
219. F. Gao, W. Xie, Y. Miao, D. Wang, Z. Guo, A. Ghosal, Y. Li, Y. Wei, S. Feng, L. Zhao, H. M. Fan, *Adv. Healthc. Mater.* **2019**, *8*, 1900203.
220. U. M. Engelmann, J. Seifert, B. Mues, S. Roitsch, C. Ménager, A. M. Schmidt, I. Slabu, *J. Magn. Magn. Mater.* **2019**, *471*, 486.
221. K. Salimi, D. D. Usta, İ. Koçer, E. Çelik, A. Tuncel, *Int. J. Biol. Macromol.* **2018**, *111*, 178.
222. A. Gómez Pérez, E. González-Martínez, C. R. Díaz Águila, D. A. González-Martínez, G. González Ruiz, A. García Artalejo, H. Yee-Madeira, *Colloids Surfaces A Physicochem. Eng. Asp.* **2020**, *591*, 124500.
223. A. Sebastianelli, T. Sen, I. J. Bruce, *Lett. Appl. Microbiol.* **2008**, *46*, 488.
224. S. P. Schwaminger, S. A. Blank-Shim, I. Scheifele, V. Pipich, P. Fraga-García, S. Berensmeier, *Biotechnol. J.* **2019**, *14*, 1800055.
225. X. Xie, Q. Hu, R. Ke, X. Zhen, Y. Bu, S. Wang, *Chem. Eng. J.* **2019**, *371*, 130.
226. L. Wang, *Mol. Med. Rep.* **2012**, *5*, 1271.
227. A. E. Ivanova, D. S. Kravchenko, S. P. Chumakov, *Mol. Biol.* **2020**, *54*, 82.
228. A. Saei, S. Asfia, H. Kouchakzadeh, M. Rahmandoust, *J. Biomed. Mater. Res. Part B Appl. Biomater.* **2020**, *108*, 2633.
229. X. Guo, W. Wang, X. Yuan, Y. Yang, Q. Tian, Y. Xiang, Y. Sun, Z. Bai, *J. Colloid Interface Sci.* **2019**, *536*, 563.
230. L. Zwi-Dantsis, B. Wang, C. Marijon, S. Zonetti, A. Ferrini, L. Massi, D. J. Stuckey, C. M. Terracciano, M. M. Stevens, *Adv. Mater.* **2020**, *32*, 1904598.
231. Q.-Y. Guo, S.-Y. Ren, J.-Y. Wang, Y. Li, Z.-Y. Yao, H. Huang, Z.-X. Gao, S.-P. Yang, *Anal. Chim. Acta* **2020**, *1094*, 151.
232. P. M. Tedeschi, E. K. Markert, M. Gounder, H. Lin, D. Dvorzhinski, S. C. Dolfi, L. L. Y. Chan, J. Qiu, R. S. DiPaola, K. M. Hirshfield, L. G. Boros, J. R. Bertino, Z. N. Oltvai, A. Vazquez, *Cell Death Dis.* **2013**, *4*, e877.
233. A. Carracedo, L. C. Cantley, P. P. Pandolfi, *Nat. Rev. Cancer* **2013**, *13*, 227.

234. D. Bonvin, J. A. M. Bastiaansen, M. Stuber, H. Hofmann, M. Mionić Ebersold, *J. Mater. Chem. B* **2017**, *5*, 8353.
235. S. Sherin, S. Balachandran, A. Abraham, *Vet. Anim. Sci.* **2020**, *10*, 100090.
236. X. Zhao, R. Shen, L. Bao, C. Wang, H. Yuan, *Carbohydr. Polym.* **2020**, *245*, 116509.
237. J. Li, Z. Feng, N. Gu, F. Yang, *J. Mater. Sci. Technol.* **2020**, https://doi.org/10.1016/j.jmst.2020.02.045.
238. A. Lazaro-Carrillo, M. Filice, M. J. Guillén, R. Amaro, M. Viñambres, A. Tabero, K. O. Paredes, A. Villanueva, P. Calvo, M. del Puerto Morales, M. Marciello, *Mater. Sci. Eng. C* **2020**, *107*, 110262.
239. C. Bai, P. Hu, N. Liu, G. Feng, D. Liu, Y. Chen, M. Ma, N. Gu, Y. Zhang, *ACS Appl. Nano Mater.* **2020**, *3*, 3585.
240. D. Ma, M. Shi, X. Li, J. Zhang, Y. Fan, K. Sun, T. Jiang, C. Peng, X. Shi, **2019**, *31*, 352.
241. E. S. Guang Choo, X. Tang, Y. Sheng, B. Shuter, J. Xue, *J. Mater. Chem.* **2011**, *21*, 2310.
242. A. Salunkhe, V. Khot, S. I. Patil, S. A. M. Tofail, J. Bauer, N. D. Thorat, *ACS Appl. Bio Mater.* **2020**, *3*, 2305.
243. A. J. Grippin, B. Wummer, T. Wildes, K. Dyson, V. Trivedi, C. Yang, M. Sebastian, H. R. Mendez-Gomez, S. Padala, M. Grubb, M. Fillingim, A. Monsalve, E. J. Sayour, J. Dobson, D. A. Mitchell, *ACS Nano* **2019**, *13*, 13884.
244. I. M. Anna, B. N. Sathy, A. Ashokan, G. S. Gowd, R. Ramachandran, A. K. Kochugovindan Unni, M. Manohar, D. Chulliyath, S. Nair, K. Bhakoo, M. Koyakutty, *ACS Appl. Bio Mater.* **2019**, *2*, 5390.
245. L. Labusca, D.-D. Herea, C.-M. Danceanu, A. E. Minuti, C. Stavila, M. Grigoras, D. Gherca, G. Stoian, G. Ababei, H. Chiriac, N. Lupu, *Mater. Sci. Eng. C* **2020**, *109*, 110652.
246. E. U. Saritas, P. W. Goodwill, L. R. Croft, J. J. Konkle, K. Lu, B. Zheng, S. M. Conolly, *J. Magn. Reson.* **2013**, *229*, 116.
247. A. Meola, J. Rao, N. Chaudhary, G. Song, X. Zheng, S. D. Chang, *World Neurosurg.* **2019**, *125*, 261.
248. J. W. M. Bulte, *Adv. Drug Deliv. Rev.* **2019**, *138*, 293.
249. N. Talebloo, M. Gudi, N. Robertson, P. Wang, *J. Magn. Reson. Imaging* **2020**, *51*, 1659.
250. K. Wu, D. Su, R. Saha, J. Liu, J. P. Wang, *J. Phys. D. Appl. Phys.* **2019**, *52*, 335002.
251. P. W. Goodwill, E. U. Saritas, L. R. Croft, T. N. Kim, K. M. Krishnan, D. V. Schaffer, S. M. Conolly, *Adv. Mater.* **2012**, *24*, 3870.
252. H. Paysen, J. Wells, O. Kosch, U. Steinhoff, J. Franke, L. Trahms, T. Schaeffter, F. Wiekhorst, *Phys. Med. Biol.* **2018**, *63*, 13NT02.
253. R. M. Ferguson, A. P. Khandhar, K. M. Krishnan, In *J. Appl. Phys.*, American Institute Of PhysicsAIP, **2012**, 07B318.
254. H. Nejadnik, P. Pandit, O. Lenkov, A. P. Lahiji, K. Yerneni, H. E. Daldrup-Link, *Mol. Imaging Biol.* **2019**, *21*, 465.
255. E. Y. Yu, M. Bishop, B. Zheng, R. M. Ferguson, A. P. Khandhar, S. J. Kemp, K. M. Krishnan, P. W. Goodwill, S. M. Conolly, *Nano Lett.* **2017**, *17*, 1648.
256. Y. Tahara, T. Yoshikawa, H. Sato, Y. Mori, M. H. Zahangir, A. Kishimura, T. Mori, Y. Katayama, *Medchemcomm* **2017**, *8*, 415.
257. A. D. Wong, M. Ye, M. B. Ulmschneider, P. C. Searson, *PLoS One* **2015**, *10*, e0123461.
258. H. Maeda, *Adv. Drug Deliv. Rev.* **2015**, *91*, 3.
259. Y. Du, X. Liu, Q. Liang, X.-J. Liang, J. Tian, *Nano Lett.* **2019**, *19*, 3618.
260. J. E. Lemaster, F. Chen, T. Kim, A. Hariri, J. V. Jokerst, ACS Appl. *Nano Mater.* **2018**, *1*, 1321.
261. Q. Wang, X. Ma, H. Liao, Z. Liang, F. Li, J. Tian, D. Ling, *ACS Nano* **2020**, *14*, 2053.
262. G. Song, M. Chen, Y. Zhang, L. Cui, H. Qu, X. Zheng, M. Wintermark, Z. Liu, J. Rao, *Nano Lett.* **2018**, *18*, 182.
263. X. Y. Zhou, K. E. Jeffris, E. Y. Yu, B. Zheng, P. W. Goodwill, P. Nahid, S. M. Conolly, *Phys. Med. Biol.* **2017**, *62*, 3510.
264. P. Ludewig, N. Gdaniec, J. Sedlacik, N. D. Forkert, P. Szwargulski, M. Graeser, G. Adam, M. G. Kaul, K. M. Krishnan, R. M. Ferguson, A. P. Khandhar, P. Walczak, J. Fiehler, G. Thomalla, C. Gerloff, T. Knopp, T. Magnus, *ACS Nano* **2017**, *11*, 10480.
265. E. Y. Yu, P. Chandrasekharan, R. Berzon, Z. W. Tay, X. Y. Zhou, A. P. Khandhar, R. M. Ferguson, S. J. Kemp, B. Zheng, P. W. Goodwill, M. F. Wendland, K. M. Krishnan, S. Behr, J. Carter, S. M. Conolly, *ACS Nano* **2017**, *11*, 12067.
266. P. Vogel, J. Markert, M. A. Rückert, S. Herz, B. Keßler, K. Dremel, D. Althoff, M. Weber, T. M. Buzug, T. A. Bley, W. H. Kullmann, R. Hanke, S. Zabler, V. C. Behr, *Sci. Rep.* **2019**, *9*, 1.
267. X. Zhu, J. Li, P. Peng, N. Hosseini Nassab, B. R. Smith, *Nano Lett.* **2019**, *19*, 6725.
268. R. Thomas, I.-K. Park, Y. Jeong, *Int. J. Mol. Sci.* **2013**, *14*, 15910.
269. L. M. Sanchez, V. A. Alvarez, *Bioengineering* **2019**, *6*, 75.
270. G. Wang, W. Gao, X. Zhang, X. Mei, *Sci. Rep.* **2016**, *6*, 28258.
271. J. Li, L. Zheng, H. Cai, W. Sun, M. Shen, G. Zhang, X. Shi, *ACS Appl. Mater. Interfaces* **2013**, *5*, 10357.
272. J. Zhu, Y. Lu, Y. Li, J. Jiang, L. Cheng, Z. Liu, L. Guo, Y. Pan, H. Gu, *Nanoscale* **2014**, *6*, 199.
273. H. Y. Zhao, S. Liu, J. He, C. C. Pan, H. Li, Z. Y. Zhou, Y. Ding, D. Huo, Y. Hu, *Biomaterials* **2015**, *51*, 194.
274. D. Kim, M. K. Yu, T. S. Lee, J. J. Park, Y. Y. Jeong, S. Jon, *Nanotechnology* **2011**, *22*, 155101.
275. E. Li, X. Cheng, Y. Deng, J. Zhu, X. Xu, P. E. Saw, H. Gu, C. Ge, Y. Pan, *Biomater. Sci.* **2018**, *6*, 1892.
276. P. Padmanabhan, A. M. Nedumaran, S. Mishra, G. Pandarinathan, G. Archunan, B. Gulyás, *Adv. Biosyst.* **2017**, *1*, 1700019.
277. N. V. S. Vallabani, S. Singh, *3 Biotech* **2018**, *8*, 279.
278. D. L. J. Thorek, D. Ulmert, N.-F. M. Diop, M. E. Lupu, M. G. Doran, R. Huang, D. S. Abou, S. M. Larson, J. Grimm, *Nat. Commun.* **2014**, *5*, 3097.
279. R. Torres Martin de Rosales, R. Tavaré, R. L. Paul, M. Jauregui-Osoro, A. Protti, A. Glaria, G. Varma, I. Szanda, P. J. Blower, *Angew. Chemie Int. Ed.* **2011**, *50*, 5509.
280. J. Xie, K. Chen, J. Huang, S. Lee, J. Wang, J. Gao, X. Li, X. Chen, *Biomaterials* **2010**, *31*, 3016.
281. H.-Y. Lee, Z. Li, K. Chen, A. R. Hsu, C. Xu, J. Xie, S. Sun, X. Chen, *J. Nucl. Med.* **2008**, *49*, 1371.
282. R. Madru, M. Budassi, H. Benveniste, H. Lee, S. D. Smith, D. J. Schlyer, P. Vaska, L. Knutsson, S.-E. Strand, *Cancer Biother. Radiopharm.* **2018**, *33*, 213.
283. G. Thomas, J. Boudon, L. Maurizi, M. Moreau, P. Walker, I. Severin, A. Oudot, C. Goze, S. Poty, J.-M. Vrigneaud, F. Demoisson, F. Denat, F. Brunotte, N. Millot, *ACS Omega* **2019**, *4*, 2637.
284. S. Kim, M. K. Chae, M. S. Yim, I. H. Jeong, J. Cho, C. Lee, E. K. Ryu, *Biomaterials* **2013**, *34*, 8114.
285. E. Forte, D. Fiorenza, E. Torino, A. Costagliola di Polidoro, C. Cavaliere, P. A. Netti, M. Salvatore, M. Aiello, *J. Clin. Med.* **2019**, *9*, 89.

286. C.-H. Weng, C.-C. Huang, C.-S. Yeh, H.-Y. Lei, G.-B. Lee, *Microfluid. Nanofluidics* **2009**, *7*, 841.
287. D. K. Hwang, D. Dendukuri, P. S. Doyle, *Lab Chip* **2008**, *8*, 1640.
288. Y.-S. Lin, K.-S. Huang, C.-H. Yang, C.-Y. Wang, Y.-S. Yang, H.-C. Hsu, Y.-J. Liao, C.-W. Tsai, *PLoS One* **2012**, *7*, e33184.
289. H. Xu, B. Dong, S. Xu, S. Xu, X. Sun, J. Sun, Y. Yang, L. Xu, X. Bai, S. Zhang, Z. Yin, H. Song, *Biomaterials* **2017**, *138*, 69.
290. T. Fook Kong, W. Ye, W. K. Peng, H. Wei Hou, Marcos, P. R. Preiser, N.-T. Nguyen, J. Han, *Sci. Rep.* **2015**, *5*, 11425.
291. J. Sheng, L. Zhang, J. Lei, H. Ju, *Anal. Chim. Acta* **2012**, *709*, 41.
292. D. Issadore, H. J. Chung, J. Chung, G. Budin, R. Weissleder, H. Lee, *Adv. Healthc. Mater.* **2013**, *2*, 1224.
293. Y.-H. Lin, C.-H. Chiang, M.-H. Wu, T.-M. Pan, J.-D. Luo, C.-C. Chiou, *Appl. Phys. Lett.* **2011**, *99*, 253704.
294. H. Markides, M. Rotherham, A. J. El Haj, *J. Nanomater.* **2012**, *2012*, 1.
295. Z. Jiang, K. Shan, J. Song, J. Liu, S. Rajendran, A. Pugazhendhi, J. A. Jacob, B. Chen, *Life Sci*. **2019**, *220*, 156.
296. F. Ahmad, X. Liu, Y. Zhou, H. Yao, *Aquat. Toxicol.* **2015**, *166*, 21.
297. A. Nemmar, S. Beegam, P. Yuvaraju, J. Yasin, S. Tariq, S. Attoub, B. H. Ali, *Part. Fibre Toxicol.* **2015**, *13*, 22.
298. F. Pacchierotti, M. Bellusci, A. La Barbera, F. Padella, M. Mancuso, A. Pasquo, M. G. Grollino, G. Leter, E. Nardi, C. Cremisini, P. Giardullo, *Int. J. Nanomedicine* **2014**, *9*, 1919.
299. Q. Feng, Y. Liu, J. Huang, K. Chen, J. Huang, K. Xiao, *Sci. Rep.* **2018**, *8*, 2082.
300. L. Sadeghi, V. Y. Babadi, H. R. Espanani, *Bratislava Med. J.* **2015**, *116*, 373.
301. D.-E. Coricovac, E.-A. Moacă, I. Pinzaru, C. Cîtu, C. Soica, C.-V. Mihali, C. Păcurariu, V. A. Tutelyan, A. Tsatsakis, C.-A. Dehelean, *Front. Pharmacol.* **2017**, *8*, 154.
302. T. Revathy, M. A. Jayasri, K. Suthindhiran, *3 Biotech* **2017**, *7*, 126.
303. R. K. Kermanshahi, V. Hojati, A. Shiravi, *Zinc Oxide Nanoparticles Absorption Rate in the Heart Tissue of Female Mice*, Islamic Azad University, Damghan Branch, Islamic Republic Of Iran, **2015**.
304. Z. Mozaffari, K. Parivar, N. H. Roodbari, S. Irani, *Adv. Stud. Biol.* **2015**, *7*, 275.
305. S. Saranya, K. Vijayaranai, S. Pavithra, N. Raihana, K. Kumanan, *Toxicol. Rep.* **2017**, *4*, 427.
306. J. Zhao, R. R. Magaya, B. Zou, H. Shi, H. Yu, X. Yue, K. Liu, X. Lin, J. Xu, C. Yang, A. Wu, *Int. J. Nanomedicine* **2014**, *9*, 1393.
307. L. Kong, M. Tang, T. Zhang, D. Wang, K. Hu, W. Lu, C. Wei, G. Liang, Y. Pu, *Int. J. Mol. Sci.* **2014**, *15*, 21253.
308. M. Abudayyak, T. Altinçekiç Gürkaynak, G. Özhan Turkish, *J. Pharm. Sci.* **2017**, *14*, 169.
309. Y. Nguyen, C. Celerier, R. Pszczolinski, J. Claver, U. Blank, E. Ferrary, O. Sterkers, *Acta Otolaryngol*. **2016**, *136*, 402.
310. J. Xu, H. Shi, M. Ruth, H. Yu, L. Lazar, B. Zou, C. Yang, A. Wu, J. Zhao, *PLoS One* **2013**, *8*, e70618.
311. F. M. Fartkhooni, A. Noori, A. Mohammadi, *Int. J. Life Sci.* **2016**, *10*, 65.
312. Z. Arefian, F. Pishbin, M. Negahdary, M. Ajdary, *Biomed. Res.* **2015**, *26*, 89.
313. M. Mauro, M. Crosera, M. Pelin, C. Florio, F. Bellomo, G. Adami, P. Apostoli, G. De Palma, M. Bovenzi, M. Campanini, F. Filon, *Int. J. Environ. Res. Public Health* **2015**, *12*, 8263.
314. A. Awaad, *J. Basic Appl. Zool.* **2015**, *71*, 32.
315. M. Ajdary, M. Negahdary, Z. Arefian, H. Dastjerdi, *J. Nat. Sci. Biol. Med.* **2015**, *6*, 335.
316. X. Cai, A. Lee, Z. Ji, C. Huang, C. H. Chang, X. Wang, Y.-P. Liao, T. Xia, R. Li, *Part. Fibre Toxicol.* **2017**, *14*, 13.
317. Search of: magnetic nanoparticles - List Results - ClinicalTrials.gov n.d.
318. N. Tran, T. J. Webster, *J. Mater. Chem.* **2010**, *20*, 8760.
319. D. Bobo, K. J. Robinson, J. Islam, K. J. Thurecht, S. R. Corrie, *Pharm. Res.* **2016**, *33*, 2373.
320. J. M. Caster, A. N. Patel, T. Zhang, A. Wang, Wiley Interdiscip. *Rev. Nanomedicine Nanobiotechnology* **2017**, *9*, e1416.
321. D. Chen, Q. Tang, X. Li, X. Zhou, J. Zang, J. Xiang, C. Guo Xue, *Int. J. Nanomedicine* **2012**, *7*, 4973.
322. J. Kolosnjaj-Tabi, Y. Javed, L. Lartigue, J. Volatron, D. Elgrabli, I. Marangon, G. Pugliese, B. Caron, A. Figuerola, N. Luciani, T. Pellegrino, D. Alloyeau, F. Gazeau, *ACS Nano* **2015**, *9*, 7925.
323. P. Khanna, C. Ong, B. Bay, G. Baeg, *Nanomaterials* **2015**, *5*, 1163.
324. E. J. Furlani, E. P. Furlani, *J. Magn. Magn. Mater.* **2007**, *312*, 187.
325. B. Shapiro, *J. Magn. Magn. Mater.* **2009**, *321*, 1594.
326. M. Giannaccini, M. Giannini, M. Calatayud, G. Goya, A. Cuschieri, L. Dente, V. Raffa, *Int. J. Mol. Sci.* **2014**, *15*, 1590.

AUTHOR BIOGRAPHIES

Muzahidul I. Anik has completed B.Sc. (Eng.) in Chemical Engineering from Bangladesh University of Engineering and Technology (BUET) in 2017. Mr. Anik has worked as a lecturer in the Department of Chemical Engineering of Jashore University of Science and Technology in 2018. He is currently a Ph.D. candidate in the Chemical Engineering department at the University of Rhode Island, USA. He is working on developing engineered nanoplatforms for in-situ oxidative stress monitoring in mammalian cells. His research interest is focused on nanotechnology and biochemical engineering. One of his recent book chapters, titled '*Biomedical applications of magnetic nanoparticles*' is accepted by the Elsevier publisher.

M. Khalid Hossain is presently engaged in research as a MEXT fellow at the Kyushu University, Japan. He has worked as a Research Scientist at the Bangladesh Atomic Energy Commission since 2012. In his M.Sc. thesis work, he mainly focused on the development of the nanostructured ultra-soft magnetic materials by a rapid quenching method. M. Khalid Hossain is a Member of the American Ceramic Society, a Life Member of the Bangladesh Physical Society, and Bangladesh Electronic Society among others. He is also a member

of the Bangladesh Atomic Energy Scientist Association. His research interests include magnetic materials, functional materials, oxides materials among others. He has authored and co-authored 35 SCI(E) articles that have been published in reputable peer-reviewed journals. One of his recent book chapters, titled '*Biomedical applications of magnetic nanoparticles*' is accepted by the Elsevier publisher.

Dr. Imran Hossain received his Ph.D. in micro-/nano-systems engineering from Louisiana Tech in August 2020. Earlier he received his B.Eng. in Electrical Engineering in 2013 from Bangladesh University of Engineering and Technology and his MSc. In Engineering (major: Electrical Engineering) from Louisiana Tech in 2019. His doctoral research focus is to develop electrochemical biosensors to measure neurochemicals like GABA and Glutamate in-vitro as well as ex-vivo to understand brain diseases e.g., epilepsy. He also specializes in cleanroom microfabrication techniques. Currently, he is working to develop nanoparticle-based chemical sensors for water quality monitoring. He is a member of the IEEE and Electrochemical Society. He has published peer-reviewed papers and has reviewed publications for journals. One of his recent book chapters, titled '*Biomedical applications of magnetic nanoparticles*' is accepted by the Elsevier publisher.

A M U B Mahfuz obtained his MBBS from Sher-E-Bangla Medical College of University of Dhaka in 2018 and M.Sc. in Biotechnology & Genetic Engineering from University of Development Alternative (UODA), Dhaka in 2020. He is currently working as a Research Assistant in the Pharmaceutical Biotechnology Lab in UODA. His current research is focused on precision medicine and liposomal drug delivery. One of his recent articles is published in the *Journal of Biomolecular Structure and Dynamics* on '*drug targeting enzyme*'.

M. Tayebur Rahman received his B.Sc. (Eng.) and M.Sc. (Eng.) degrees in Materials Science and Engineering from the University of Rajshahi, Bangladesh in 2014 and 2015, respectively. During his B.Sc. program, he explored the area of nanotechnology in medicine sectors, and, during his M.Sc. program, he fabricated ceramic nanoparticles dispersed in HDPE and UPR polymer matrix as novel nanocomposites to evaluate the mechanical, thermal, optical, and electrical properties. Currently, he is working as a Senior Assistant Director at Walton Hi-Tech Industries Ltd. in the research and development department. Previously he was a research fellow in the Bangladesh Atomic Energy Commission (BAEC) and Bangladesh Council of Scientific and Industrial Research (BCSIR). His research interest mainly focuses on nanocomposite and nanomaterials for biomedical applications.

Isteaque Ahmed is a Ph.D. student in his second year at the Department of Chemical Engineering, University of Cincinnati, USA. He completed his bachelor's in Chemical Engineering from Bangladesh University of Engineering & Technology (BUET) in 2017. He is currently working on developing and optimizing fabrication techniques in microfluidics and incorporating PCR applications with it. One of his recent book chapters, titled '*Biomedical applications of magnetic nanoparticles*' is accepted by the Elsevier publisher.

How to cite this article: Anik MI, Hossain MK, Hossain I, Mahfuz AMUB, Rahman MT, Ahmed I. Recent progress of magnetic nanoparticles in biomedical applications: A review. *Nano Select*. **2021**;*2*:1146–1186.
https://doi.org/10.1002/nano.202000162